CHEMICAL REVIEWS

Review

pubs.acs.org/CR

Single-Molecule Studies of Intrinsically Disordered Proteins

Marco Brucale,*[,†] Benjamin Schuler,*[,‡] and Bruno Samorì*[,§]

[†]Institute for the Study of Nanostructured Materials (ISMN), Italian National Council of Research (CNR), Area della Ricerca Roma1, Via Salaria km 29.3 00015 Monterotondo (Rome), Italy

[‡]Department of Biochemistry, University of Zurich, Winterthurerstrasse 190, 8057 Zurich, Switzerland

[§]Department of Pharmacy and Biotechnology, University of Bologna, Via S. Giacomo 11, 40126 Bologna, Italy

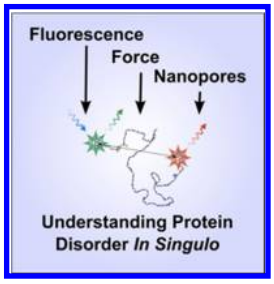

CONTENTS

1. Introduction 3281
- 1.1. Purpose and Scope of the Review 3281
- 1.2. On the Challenging Characterization of Intrinsically Disordered Proteins 3281
- 1.3. Added Value of Single-Molecule Studies on IDPs 3283

2. Literature Review 3285
- 2.1. Single-Molecule Fluorescence Techniques 3285
  - 2.1.1. Single-Molecule Fluorescence Instrumentation and Methods 3285
  - 2.1.2. Single-Molecule Fluorescence Spectroscopy of IDPs 3289
- 2.2. Single-Molecule Force Spectroscopy Techniques 3294
  - 2.2.1. Single-Molecule Force Spectroscopy Instrumentation and Methods 3295
  - 2.2.2. Single-Molecule Force Spectroscopy Spectroscopy of IDPs 3298
- 2.3. Single-Nanopore Techniques 3303
  - 2.3.1. Single-Nanopore-Sensing Instrumentation and Methods 3303
  - 2.3.2. Single-Nanopore Sensing of IDPs 3305

3. Conclusions and Perspectives 3308
- Foreseeable Future Developments of Single-Molecule Methodologies Applied to the Study of IDPs 3308
- On the Prospective Integration of Single-Molecule Techniques 3309

Author Information 3310
- Corresponding Authors 3310
- Notes 3310
- Biographies 3310

Acknowledgments 3311

References 3311

1. INTRODUCTION

1.1. Purpose and Scope of the Review

The last 15 years saw a dramatic increase in the number of published papers exposing research related to the concept of protein disorder and a concomitant increase in the number of papers reporting the results of single-molecule experiments. Even though, when taken separately, both sets of recent papers on protein disorder and single-molecule experiments are numerous, their intersection at the time of writing is limited to a group of around 200 published works, including particularly relevant theoretical works and reviews (see Figure 1). We will herein attempt a comprehensive review of the past decade of scientific literature concerning the subject of protein disorder investigated by single-molecule techniques.

1.2. On the Challenging Characterization of Intrinsically Disordered Proteins

Although a small number of papers touching on the concept of protein disorder can be found in the literature throughout the last three decades,[1] the interest shown by the scientific community in IDPs and in the concept of protein disorder in general has begun to rapidly and steadily increase only in the

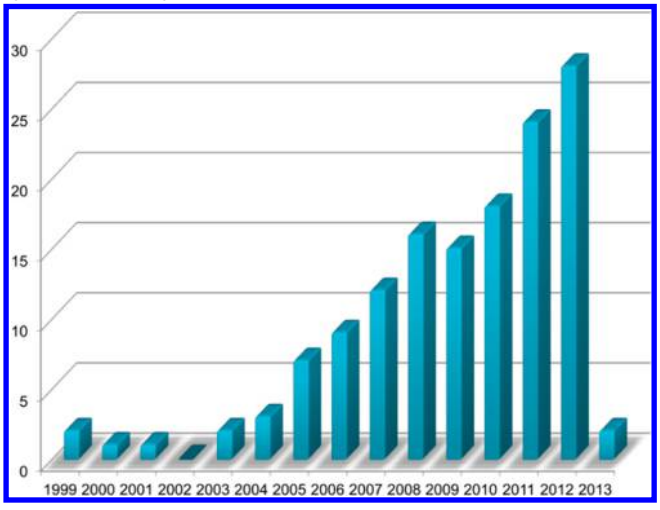

Figure 1. Number of works cited in this review, tallied by year, excluding reviews and methodological papers. Only reports of single-molecule level experiments giving access to information on a disordered protein or protein region were included.

Special Issue: 2014 Single Molecule Mechanisms and Imaging

Received: May 31, 2013
Published: January 17, 2014

   dx.doi.org/10.1021/cr400297g | *Chem. Rev.* 2014, 114, 3281−3317

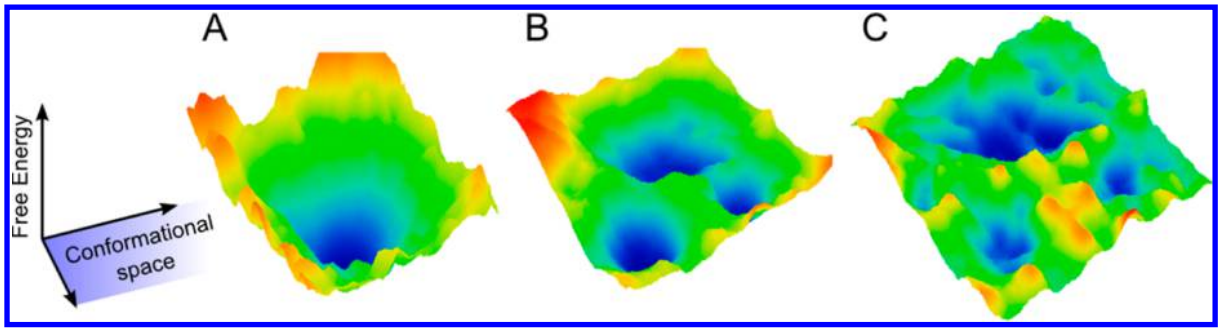

Figure 2. Pictorial representation of the free energy landscapes of proteins with an increasing degree of intrinsic disorder. Free energy landscapes of structured proteins characterized by a stable three-dimensional structure are dominated by a single deep funnel (A), while those corresponding to proteins able to adopt a limited number of structures show a small number of basins of similar depth separated by substantial barriers (B). Disordered proteins are instead characterized by shallow energy landscapes (C) with several local minima of comparable free energy, separated by low barriers allowing fast interconversion kinetics between conformations.

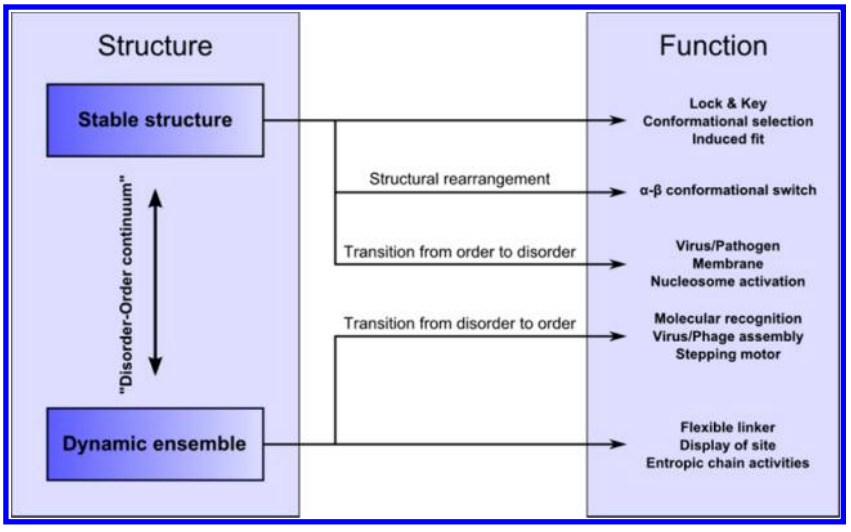

Figure 3. Schematization of the relationship between intrinsic disorder and protein function, as proposed in Figure 8 of ref 8. The concept of "structure" as implied by the classical structure–function paradigm needs to be substituted with the "disorder–order continuum" concept in order to describe many documented protein functions. Adapted with permission from ref 8. Copyright 2010 Elsevier.

last 15 years. As early as 2006, the distribution of papers per year published included in the database of protein disorder (DisProt)[2] clearly showed exponential growth. However, the IDP field was almost nonexistent a mere 15 years ago.[3] As suggested by Dyson,[4] during the last years of the 20th century two key factors concurred to weave a pattern that prompted the scientific community to reassess its understanding of the long-standing "structure–function paradigm".[5] The first was the rapid increase in the availability of gene sequences and the consequent observation that they often code for unstructured proteins.[6] The second factor was a rapid succession of papers independently reporting that several proteins linked to transcriptional/translational control or signaling failed to acquire a stable fold even in the most structure-inducing conditions.[7] The emerging picture was that a large number of proteins existed whose functional forms were not necessarily folded into a well-defined three-dimensional structure. The idea that a large class of those "flexible" proteins (as opposed to sporadic cases) existed and needed to be systematically studied in the context of a revised structure–function model began to take hold.[8] As noted by Uversky,[1] the late recognition of IDPs as a broad but coherent class of proteins as described above allowed them to be rediscovered several times from the 1970s onward, each time with a different name (examples include "pliable", "floppy", "rheomorphic", "mobile", "natively unfolded", "vulnerable", and "dancing" proteins).[1] Even though a few of these names are still used today, in recent years a consensus is emerging on using "IDP" almost exclusively.

Following a largely accepted definition, an IDP is a protein that populates a broad ensemble of different conformational states in at least one of its biologically active forms.[1,3−5,8−10] Under physiological conditions, IDPs do not assume a single, geometrically well-defined structure. In contrast, either their entire length or specific subregions dynamically interconvert among multiple conformations with similar free energies. Their structural parameters (e.g., their backbone dihedral angles) undergo ample and rapid fluctuations in time, clustering around several "most probable" values corresponding to those conformations having comparatively longer dwell times. Many IDPs are far from being ideal random coils, as their conformational behavior can be often portrayed by the combination of relatively few distinct structures,[1,11,12] but in other cases, the persistence of residual structure is so low that the fully disordered polymeric properties dominate.[13−18] These peculiar characteristics of IDPs are easily visualized in terms of their equally peculiar free energy landscapes.

Broadly speaking, free energy landscapes characterized by a single prominent minimum and a funnel-like topography

dx.doi.org/10.1021/cr400297g | Chem. Rev. 2014, 114, 3281−3317

correspond to proteins which fold into a single native conformation by progressively driving partially folded intermediates toward the bottom of the funnel.[19] The energy landscapes of IDPs are in contrast characterized by the lack of a single dominant global minimum and the presence of multiple, shallow local minima corresponding to the comparatively more stable conformations.[20,21] IDPs can thus be considered to lie in a "disorder−order continuum"[4,16] whose extremes are fully folded proteins on one end and excluded volume chains devoid of residual structure on the other (see Figure 2).

The biological functional repertoire of IDPs is highly complementary to that of ordered proteins[1,8] and focused on regulation, recognition, signaling, and control[17−19] (see Figure 3). Far from being a mere coincidence, the shallow energy landscape and consequent conformational flexibility typically shown by IDPs may in fact be an advantage for the fulfillment of their most common biological roles, just as a geometrically well-defined, robust three-dimensional structure is a prerequisite for most enzymes.[9,22,23]

For example, IDPs are often involved in pathways where the ability to interact with multiple partners with high specificity but low affinity could be crucial. Although the issue is quite complex and summarizing it in one sentence hides many of its subtle and intriguing aspects, in general terms the binding of an IDP to a specific partner often entails acquisition of structure by the disordered ensemble.[24] Consequently, complex formation implies a high entropic cost which balances the enthalpic gain, thus enabling low-affinity/high-specificity interactions.[25] It may be also due to this effect that intrinsic protein disorder has a prominent role in the functional mechanisms of the so-called protein hubs.[17,22] While the majority of nodes found in interactome graphs[26] have few connections,[27] a small number of highly connected hub nodes are observed, corresponding to proteins able to interact with multiple partners. Both structured and disordered proteins can act as a hub; often hub IDPs bind different partners via their disordered regions, and structured hubs bind their several partners' disordered regions.[28] These two specular behaviors are often referred to as "one-to-many" and "many-to-one" signaling, respectively.[23,29]

Another example of the peculiar modes of interaction with folded molecular partners available by intrinsic disorder is the comparatively fast kinetics of the coupled folding−binding processes observed in some instances by complexes involving IDPs.[30−33] A possible explanation for this feature is given by the "fly-casting"[34] model, according to which an unstructured protein is able to weakly bind to targets found within an unusually large capture radius then optimize the binding interaction via a concurrent acquisition of structure. As in the previous example, this short description neglects many fascinating facets of the phenomenon. For instance, even if the capture radii of IDPs are generally large due to higher flexibility, their capture rates may not be greater than those of folded proteins due to the slower translational diffusion caused by the extended conformations. However, based on simulations, it has been suggested that a smaller number of molecular encounters may be required for the successful interaction of an IDP with its target, resulting in enhanced binding rates with respect to an interaction between structured proteins.[35]

Although the biological function of IDPs frequently involve disorder-to-order transitions and partner binding as mentioned above, some of the activities ascribed to them fall under the so-called "entropic chain" functional category.[36] These activities directly depend on the flexibility, pliability, and plasticity of the backbone[1] and rely exclusively on the high conformational freedom of extended random-coil-like regions. Specific mechanisms of action employed by members of the entropic chain functional category identified so far include flexible linkers and spacers, "entropic bristles", "entropic springs", and "entropic clocks".[37]

As briefly exemplified in the above paragraphs, almost every aspect of IDPs—from their nonstructured state to the mechanisms of interaction with their molecular partners to their functional activities—is inadequately portrayed by static structural descriptions. The same characteristics making IDPs so interesting and unique from the biological and biophysical perspective renders them elusive to characterization by many traditional techniques. A fully quantitative characterization of the IDP's conformational energy landscape is needed, since the relative populations and mutual interconversion kinetics of the most stable conformations at equilibrium are determined by the depths, positions, and profiles of the basins found therein.

In practice, however, even an approximate quantitative reconstruction of a complex energy landscape relies on the ability to experimentally discern between multiple conformations of a protein in a given condition. This is not a trivial task since the conformations to be resolved typically have submicrosecond interconversion rates, and each of them could be present in the examined ensemble only as a small fraction of the entire population. Moreover, the picture is further complicated by the fact that several extrinsic factors such as pH, temperature, ionic strength, molecular crowding, and small-molecule binding can reshape the energy landscape, biasing the result by favoring one or more conformations with respect to others.

1.3. Added Value of Single-Molecule Studies on IDPs

Dozens of different biophysical and biochemical methods[8] have been applied to the study of unstructured protein regions and IDPs, each one giving different and potentially complementary information about the disordered state.[38−42] In particular, single-molecule techniques[43−46] have proven to be very successful in overcoming the limitations brought by the ensemble and time averaging of signals in classical methodologies.[47] While those limitations are often not as consequential when studying reasonably homogeneous populations such as those of structured proteins, they definitely render the meaningful characterization of heterogeneous ensembles such as those of IDPs challenging or even impossible. In contrast, the ability to individually discern signals originating from single molecules within a population at the maximum possible temporal resolution is particularly suited to study disordered protein regions for the reasons we outline in the following paragraphs.

All single-molecule experiments are by definition able to avoid ensemble averaging since they give information on the smallest possible subensembles of a population, i.e., individual molecules. This allows detection of rare individuals within a population whose contribution to the average signal could get lost in ensemble measurements. However, in the case of IDPs, the time scale of the measurement (in terms of both temporal resolution and maximum duration of the observation) is also crucial, since the dynamic heterogeneity of each individual molecule could be lost to time averaging. In very general terms, the relevant dynamics for interconversion between different

dx.doi.org/10.1021/cr400297g | Chem. Rev. 2014, 114, 3281−3317

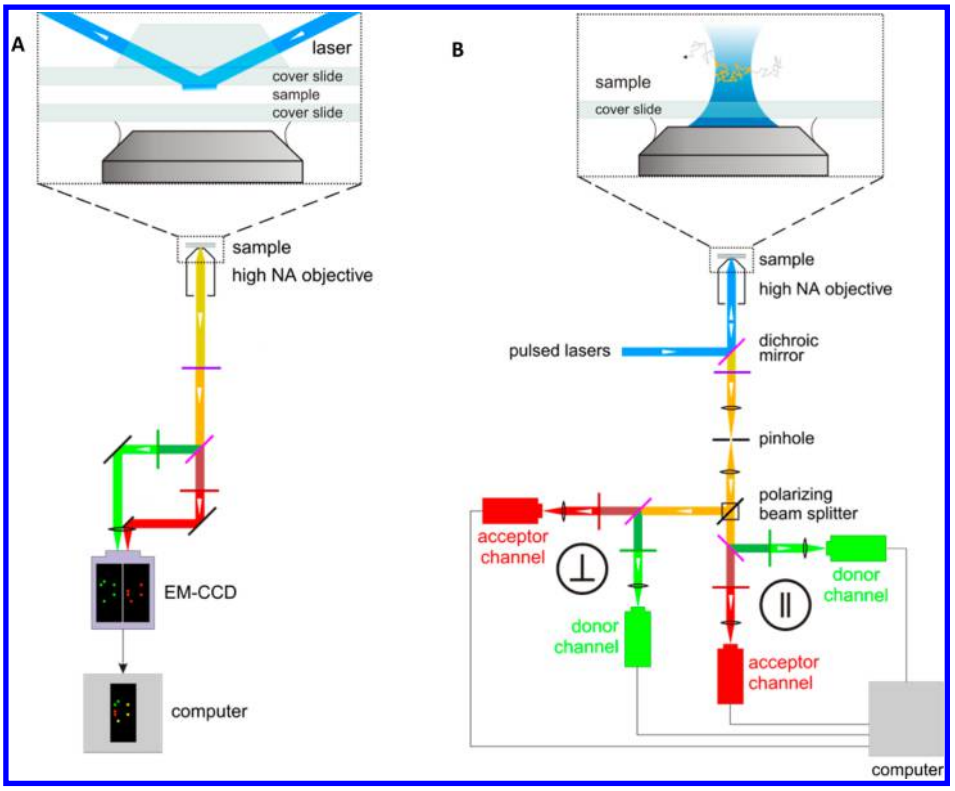

Figure 4. Schematic drawings of single-molecule fluorescence detection methods. (A) Prism-based total internal reflection fluorescence (TIRF) setup. A laser beam (blue) is reflected at the interface of the sample solution and the top of the sample cell, forming an evanescent field that can be used to selectively excite molecules in close proximity (typically <100 nm) to the surface of the cover slide. Molecules are usually immobilized to the surface. Fluorescence is collected with a high numerical aperture objective lens and focused onto a sensitive CCD camera. An image splitter can be used to direct emission of different wavelengths (e.g., donor and acceptor emission in a FRET experiment) to different areas of the CCD chip, which can then be superimposed for the analysis to quantify donor and acceptor intensities from the same molecule. (B) Confocal single-molecule experiment on freely diffusing molecules. In this example of a four-channel instrument, the fluorescence signal is first separated by polarization and then by wavelength into the detection channels corresponding to emission from donor and acceptor chromophores. Data can either be taken on molecules freely diffusing in solution at very low concentration and observed while they diffuse through the confocal detection volume, or data on immobilized molecules can be recorded by sample or laser scanning.

conformations range from the submicrosecond time scale for fully unstructured regions to increasingly longer times as the contribution of specific and cooperative interactions increases, resulting in a continuous transition into the seconds, minutes, and hours processes observed in protein folding and misfolding reactions.[48] Removal of ensemble and time averaging from measurements performed on protein ensembles gives potential access to several unique pieces of information.

(i) The complete distribution of an observable within a population rather than only the first moment available from most ensemble measurements.

(ii) Discrimination between static and dynamic heterogeneity.

(iii) Direct measurement of equilibrium or nonequilibrium kinetics without the need for ensemble synchronization.

(iv) Detection of rare individuals of a population and/or rare states of single individuals.

(v) Observation of cause and effect relationships between events and intermediate states found along a reaction pathway.[44]

While all the points above are generally pertinent to studies performed on all types of proteins, single-molecule measurements of IDPs bring forward a few more specific additional advantages. First, the ability to discern causal relationships mentioned in point v above is potentially particularly suited to explore sequences of events occurring after, or concurrently with, the formation of encounter complexes[49] such as those formed by IDPs upon binding with molecular partners.[50] Another advantage is related to the fact that several IDPs are prone to aggregate into multimeric structures[51] and that the molecular details of their aggregation are of particular interest since many of them are involved in neurodegenerative diseases.[52,53] Single-molecule experiments can be designed to discern between signals of IDP monomers and oligomers, thus giving access to information, e.g., about the first events in an amyloidogenic cascade.[54,55] However, the ability to discriminate between the signal of a monomer and that of superior multimers can be also exploited to rule out the possibility that observables ascribed to the monomer are not biased by the erroneous inclusion of signals generated by dimeric or oligomeric aggregates.[56−58]

Three broad families of single-molecule experiments have been successfully applied to the study of IDPs: (i) fluorescence-based techniques, (ii) force spectroscopy, and (iii) single-nanopore analysis. In the following section, we give a survey of existing literature on single-molecule experiments performed on IDPs.

dx.doi.org/10.1021/cr400297g | Chem. Rev. 2014, 114, 3281−3317

2. LITERATURE REVIEW

2.1. Single-Molecule Fluorescence Techniques

Single-molecule fluorescence methods have started to take an important place in the study of IDPs and protein conformations and conformational dynamics in general.[48,59,60] Even though the range of methods employed often share common principles, a variety of different approaches have proven to be particularly useful. In the following section, we will briefly introduce these techniques and summarize the underlying physical principles and the kind of information they can provide.

2.1.1. Single-Molecule Fluorescence Instrumentation and Methods.

2.1.1.1. Single-Molecule Fluorescence Detection. The instrumentation used for optical single-molecule detection[61−66] typically involves either confocal excitation and detection using pulsed or continuous wave lasers and avalanche photodiodes (APDs) or wide-field microscopy with two-dimensional detectors such as sensitive CCD cameras, often in combination with total internal reflection fluorescence (TIRF) (Figure 4).[67,68] Wide-field imaging allows the collection of data from many single molecules in parallel, albeit at much lower time resolution than in a confocal experiment using APDs. In confocal epifluorescence detection, a laser beam is focused with a high numerical aperture objective to a diffraction-limited focal spot that serves to excite the labeled molecules. In the simplest experiment, the sample molecules are freely diffusing in solution at very low concentration (typically 10−100 pM), ensuring that the probability of two or more molecules residing in the confocal volume at the same time is negligible. When a molecule diffuses through the laser beam, the fluorophore attached to the sample molecules is excited; fluorescence emission is collected through the objective and gets focused onto the pinhole, a small aperture serving as a spatial filter. Depending on the specific type of experiment, dichroic mirrors, polarizing beam splitters, or similar optical elements are used to direct emission to the corresponding detectors, from where the data are collected with suitable counting electronics. Modern electronics allow the arrival time of every individual detected photon to be stored with picosecond time resolution and completely synchronized for all detection channels.[69−71] This mode of data collection provides maximum flexibility and versatility for data processing. The setup can be extended to sorting photons by several colors, e.g., if more than two chromophores are used,[72,73] or by both color and polarization.[74] The advantage of observing freely diffusing molecules is that perturbations from surface interactions can largely be excluded, but the observation time is limited by the diffusion times of the molecules through the confocal volume. Typically, every molecule is observed for no more than a few milliseconds. The resulting fluorescence bursts can be identified by applying an intensity threshold[75] or more advanced algorithms.[76−78] From the identified bursts, transfer efficiency histograms or other signal distributions can be constructed. Alternatively, the molecules can be immobilized on the surface and then observed for a more extended period of time, typically a few seconds, until one of the chromophores undergoes photodestruction. A potential complication in this case is interactions with the surface that can easily perturb the sensitive conformational distribution and dynamics of IDPs. The details of single-molecule instrumentation can be found in several sources.[62,68,79,80] An important development for the wide application of single-molecule fluorescence methods is the recent availability of comprehensive commercial instrumentation.[81]

2.1.1.2. Single-Molecule Förster Resonance Energy Transfer (FRET). A goal of many single-molecule studies is the observation of conformations, conformational transitions, or molecular interactions, which requires methods for probing intra- and intermolecular distances on the nanometer length scale. The most popular method is single-molecule FRET,[68,82] which is based on the nonradiative transfer of excited-state energy from a suitable donor to an acceptor chromophore.[83] With the known dependence of the rate of energy transfer on the inverse sixth power of the distance,[84] the fluorescence emission of donor and acceptor can be related quantitatively to the separation of the chromophores (Figure 5). In this way, distances, distance distributions, and the underlying dynamics can be monitored in single molecules on length scales of ∼2−10 nm and on time scales from nanoseconds to days.[48,68]

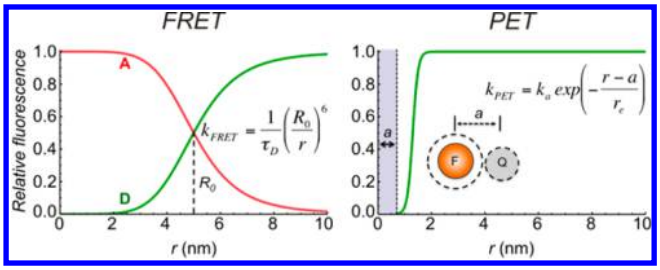

Figure 5. Comparison of FRET and PET. In its classical description, Förster resonance energy transfer (FRET) originates from the resonance of the transition dipole moments of donor (D) and acceptor (A) fluorophores. The rate constant of the resulting energy transfer (k_{FRET}) from D to A depends on the inverse 6th power of the D−A distance (r), the fluorescence lifetime of the donor (τ_D), and the characteristic distance R_0 that can be calculated from the spectroscopic properties of D and A. Typical values of R_0 make single-molecule FRET suitable for obtaining distance information in the range from ∼2 to ∼10 nm. In contrast, photoinduced electron transfer (PET) requires much closer contact between fluorophore (F) and quencher (Q, typically tryptophan). The rate constant of quenching (k_{PET}) depends on the contact radius (a), a characteristic distance (r_e) in the subnanometer range, and the quenching rate constant at the distance of closest approach (k_a). The on/off behavior resulting from the steep distance dependence of the fluorescence emission in PET can in principle be used to probe any process that leads to a change in quenching dynamics, but it does not afford direct distance information. As an example, both PET and FRET, when combined with ns-FCS, can provide information on the dynamics of unfolded and disordered proteins in the nanosecond to microsecond time regime. FRET-FCS can be used to determine the reconfiguration time of the chain; in addition, the distance or distance distribution between D and A can be obtained from the analysis of transfer efficiencies and/or fluorescence lifetimes. PET-FCS allows the determination of loop-closure rates between two points within a polypeptide chain. Complementarity of the two methods is expected to be increasingly useful for probing IDP dynamics over a wide range of distances and times. Reprinted with permission from ref 48. Copyright 2013 Elsevier.

A key strength of this type of experiment is the possibility to separate the signals from various subpopulations, such as different conformational states of an IDP, which allows a variety of subpopulation-specific parameters to be measured[85] that are difficult to determine otherwise. In a confocal experiment with pulsed excitation and four detection channels, for example, the emission wavelength range (i.e., whether it is a donor or an

dx.doi.org/10.1021/cr400297g | Chem. Rev. 2014, 114, 3281−3317

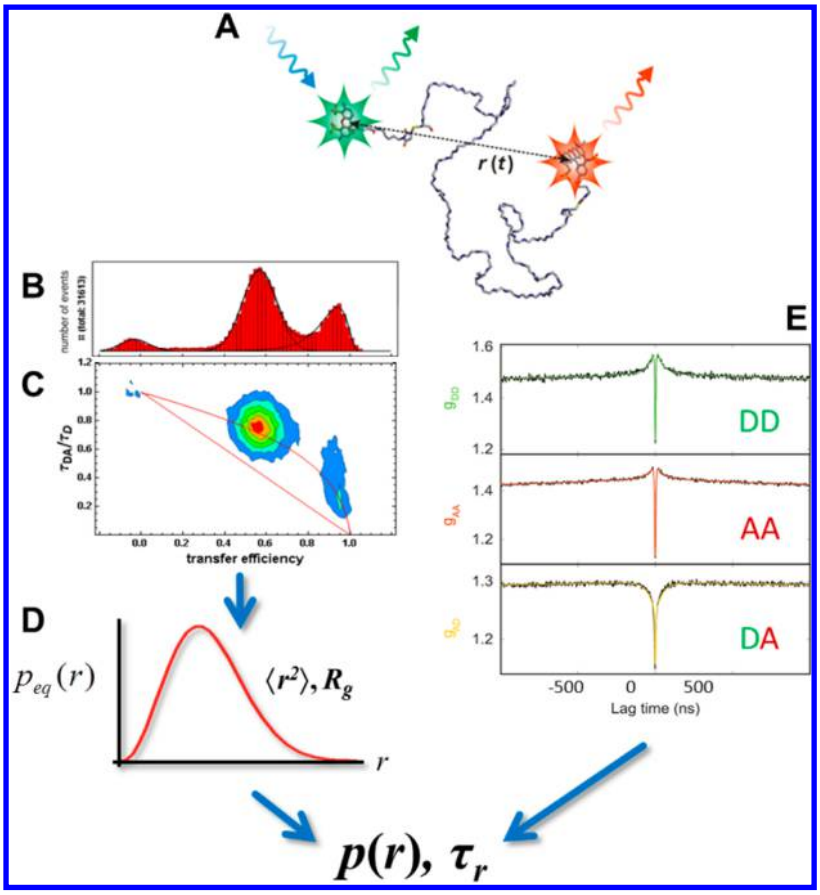

Figure 6. Combining single-molecule transfer efficiency and fluorescence lifetime measurements with nanosecond correlation spectroscopy for quantifying distance distributions and dynamics in IDPs and unfolded proteins. (A) Illustration of a disordered protein labeled with donor and acceptor fluorophores with a fluctuating intramolecular distance, $r(t)$. (B) Example of a transfer efficiency histogram illustrating the separation of a disordered and a folded population at transfer efficiencies of ~0.6 and ~0.9, respectively, a key prerequisite for distinguishing changes in intramolecular distances in the unfolded state from those caused by folding. The small population at $E \approx 0$ is caused by molecules with bleached or inactive acceptor fluorophore. (C) 2D histogram of relative fluorescence lifetime of the donor versus transfer efficiency. The straight line would be expected for a situation with a fixed intramolecular distance[74] and the curved line for a broad distance distribution, here approximated by a Gaussian chain.[17] (D) The combined analysis of transfer efficiencies and fluorescence lifetime distributions can be used to quantify intramolecular distances in terms of a distance distribution characterized, e.g., by the mean squared end-to-end distance, $\langle r^2 \rangle$, or the radius of gyration, R_g. (e) Examples of nanosecond FCS measurements showing the donor (DD, correlated) and acceptor (AA, correlated) autocorrelations and the donor−acceptor (DA, anticorrelated) cross-correlations with the common decay on the 100 ns time scale characteristic of the long-range dynamics in unfolded proteins and IDPs.[17,92−94] The pronounced correlation component below ~10 ns is caused by photon antibunching.[95] Global analysis of correlation functions, transfer efficiencies, and lifetimes can be used to quantify intramolecular distance distributions, $p(r)$, and chain reconfiguration times, τ_r, of IDPs and unfolded proteins.

acceptor photon), the polarization, and the time of emission relative to the excitation pulse become available for every detected photon. Consequently, we can calculate for each burst of photons from a single molecule the transfer efficiency, the donor and acceptor fluorescence lifetimes, the fluorescence anisotropy, and a number of other parameters that aid the interpretation of the results and allow accurate distance information to be extracted (Figure 6).[74,86] In a second step, the bursts from subpopulations can be grouped, e.g., to obtain fluorescence decays of an individual subpopulation, devoid of signal contributions from other molecules. Whereas, e.g., the fluorescence lifetime from an individual burst can only be estimated with relatively large uncertainty, the combination of all photons from a subpopulation can result in decays that are suitable for more detailed analysis. In this way, additional information becomes available and experimental complications, such as limited rotational mobility of the chromophores[87] or fluorescence quenching,[74] can be identified and taken into account for the analysis. Such complications are comparatively rare in unstructured polypeptides. However, care needs to be taken in the folded form of corresponding IDPs or in the context of complex formation with ligands or other biological macromolecules, where the local environment of the fluorophores can lead to steric constraints or fluorescence quenching. A very useful extension of single-molecule FRET experiments is the alternating excitation of donor and acceptor, which allows molecules to be sorted by fluorophore stoichiometry, and donor-only populations to be separated from species with very low transfer efficiencies.[88,89] For obtaining information on more than one distance simultaneously, three-[72,73,88] and four-color[90] FRET have been demonstrated and are starting to be used for IDPs.[91]

A particularly important point we have to take into account for the quantitative investigation of IDPs with FRET is the presence of broad intramolecular distance distributions, $P(r)$. A common misconception is that such broad distance distribu-

dx.doi.org/10.1021/cr400297g | Chem. Rev. 2014, 114, 3281−3317

tions will invariably lead to broad distributions of transfer efficiency histograms. However, the width of the observed efficiency distribution strongly depends on the dynamics of the system relative to the observation time scale (more precisely, the interphoton times[96]). As shown by Gopich and Szabo,[96,97] the observation time must be approximately an order of magnitude smaller than the relaxation time of the donor−acceptor distance to obtain physically meaningful distance distributions or corresponding potentials of mean force from the transfer efficiency histograms. In contrast, systems with very rapid dynamics sample all distances during the observation time, and even for a broad distance distribution, a narrow FRET efficiency histogram is observed as a consequence of this averaging. In this case, only the mean value of the transfer efficiency of the respective subpopulation can be used to extract information about the distance distribution, and an independent model for the shape of $P(r)$ is needed. Commonly employed distance distributions from polymer physics that have been used as approximations for unfolded or disordered proteins are the Gaussian chain,[15,98−100] the wormlike chain,[15,101] or a (weighted) Flory−Fisk distribution (Figure 6).[16,102] In practice, this means that distance distributions can be determined directly from transfer efficiency distributions obtained in free diffusion experiments on IDPs only if the underlying intramolecular dynamics are on a time scale greater than about 1 ms, given the photon count rates of $\sim 10^5$ s^{-1} typically obtained during fluorescence bursts.[96] A noticeable influence of dynamics on the width of the efficiency histograms, however, is already expected for fluctuations in the 10−100 μs time scale.[96,103] Three physically plausible and useful limits for the possible averaging regimes and the resulting mean transfer efficiencies $\langle E \rangle$ are as follows.[104]

(1) If the rotational correlation time τ_c of the chromophores is small relative to the fluorescence lifetime τ_f of the donor (i.e., the orientational factor $\kappa^2 = 2/3$) and the dynamics of the peptide chain (with relaxation time τ_r) are slow relative to τ_f, i.e., $\tau_c \ll \tau_f$ and $\tau_r \gg \tau_f$

$$\langle E \rangle = \int_a^{l_c} E(r)P(r)\mathrm{d}r \text{ with } E(r) = (1 + (r/R_0)^6)^{-1} \tag{12}$$

where $P(r)$ is the normalized interdye distance distribution, a is the distance of closest approach of the dyes, and l_c is the contour length of the polypeptide chain.

(2) If $\tau_c \ll \tau_f$ and $\tau_r \ll \tau_f$

$$\langle E \rangle = \frac{\int_a^{l_c} (R_0/r)^6 P(r)\mathrm{d}r}{1 + \int_a^{l_c} (R_0/r)^6 P(r)\mathrm{d}r} \tag{13}$$

(3) If $\tau_c \gg \tau_f$ and $\tau_r \gg \tau_f$

$$\langle E \rangle = \int_0^4 \int_a^{l_c} E(r, \kappa^2)P(r)p(\kappa^2)\mathrm{d}r\ \mathrm{d}\kappa^2$$
$$\text{with } E(r, \kappa^2) = \left(1 + \frac{2}{3\kappa^2}(r/R_0)^6\right)^{-1} \tag{14}$$

The theoretical isotropic probability density $p(\kappa^2)$ for the case in which all orientations of the donor and acceptor transition dipoles are equally probable[83,105] is

$$p(\kappa^2) = \begin{cases} \dfrac{1}{2\sqrt{3\kappa^2}} \ln(2 + \sqrt{3}) & 0 \le \kappa^2 \le 1 \\ \dfrac{1}{2\sqrt{3\kappa^2}} \ln\left(\dfrac{2 + \sqrt{3}}{\sqrt{\kappa^2} + \sqrt{\kappa^2 - 1}}\right) & 1 \le \kappa^2 \le 4 \end{cases} \tag{15}$$

with $\kappa^2 = (\cos\theta_T - 3\cos\theta_D \cos\theta_A)^2$, where θ_T is the angle between the donor and acceptor transition dipoles and θ_D and θ_A are the angles between the transition moments and the line connecting the centers of the donor and acceptor, respectively.

It is important to recognize that even for a molecule with a single fixed distance or very rapid conformational averaging, the resulting FRET efficiency histograms are still broadened. A fundamental source of broadening is shot noise, the variation in count rates about fixed means due to the discrete nature of the signals (i.e., only small numbers of photons observed from an individual molecule). In practice, histograms broader than expected from shot noise alone are commonly observed. The specific origin of this excess width is often unclear,[98,106] but there are common factors other than slow distance fluctuations that can contribute, such as variations in fluorescence quantum efficiencies caused by quenching or photochemical processes, imperfect alignment or size differences of the observation volumes for donor and acceptor channels, restricted mobility of the fluorophores, or chemical heterogeneity, e.g., from labeling permutations. Consequently, without additional information it is difficult to unequivocally assign a width in excess of shot noise to slow conformational dynamics. In these cases, it is thus essential to complement FRET efficiency distributions with additional information from fluorescence lifetimes, anisotropies, and correlation functions.[17,87,99] In many cases, much of this information can be obtained from a single measurement where multiple parameters are recorded simultaneously (Figures 4 and 6).[74,86]

Let us illustrate these aspects for a specific example, the case of a protein under conditions where both the folded and the disordered state are populated, as shown in Figure 6b. In the folded state, we expect a rather well-defined distance between donor and acceptor, whereas in the unfolded state, a broad distance distribution will be present. However, this pronounced difference in the widths of the underlying distance distributions is not obvious from the two peaks in the transfer efficiency histogram, because the reconfiguration time in the unfolded state is faster than the average interphoton time.[92] In other words, the disordered state rapidly samples its intramolecular distance distribution while the molecule diffuses through the confocal volume, which leads to complete averaging of transfer efficiencies during the observation time for a single fluorescence burst. As a result, the distance distribution does not contribute to the width of the transfer efficiency distribution significantly, and both the peaks from the folded and the unfolded molecules are dominated by shot noise and thus exhibit similar widths. (Note, however, that the shot noise width depends on the mean transfer efficiency of the peak; it exhibits a maximum at $E = 0.5$ and decreases toward $E = 0$ and $E = 1$.)[75] In such a case, information about the distance distribution in the disordered state can then be extracted using eq 12 in combination with a realistic $P(r)$, which can, e.g., be obtained from molecular simulations or based on suitable polymer models. Additional information about the shape of $P(r)$ is available from the analysis of fluorescence lifetimes in the unfolded subpopula-

dx.doi.org/10.1021/cr400297g | Chem. Rev. 2014, 114, 3281−3317

tion[17,99,107] (Figure 6c): since the chain dynamics for disordered states are typically much slower than the fluorescence lifetimes of the dyes, the distance distribution is reflected by a distribution of fluorescence intensity decay rates.[108]

2.1.1.3. Photoinduced Electron Transfer (PET) and Dexter Exchange Quenching. An approach complementary to FRET for the investigation of macromolecular dynamics is PET, which is based on the static quenching of a fluorophore by another group, frequently a tryptophan residue (Figure 5).[109] The rate constant of quenching decreases exponentially with the separation of the groups and has a characteristic distance in the subnanometer range. Since PET requires very close contact of dye and quencher, dynamics over a shorter distance range can be probed than with single-molecule FRET, but usually no distance information can be extracted. In combination with correlation analysis, time scales down to the nanosecond range are accessible. Closely related from a conceptual point of view is Dexter exchange[110] between two fluorophores. As in PET, the dyes need to come into close contact and form a complex that leads to fluorescence quenching. The resulting fluorescence intensity fluctuations can be used to characterize the dynamics of the system, e.g., with correlation methods. In practice, usually two identical fluorophores have been used,[111] which simplifies sample preparation, but the same effect can also occur between different dyes.

2.1.1.4. Fluorescence Correlation Methods. Any process that leads to fluctuations in fluorescence intensity can in principle be quantified by correlation analysis.[65,112,113] This type of analysis can provide access to a wide range of times, for short times only limited by the photon count rate (typically in the picosecond to nanosecond range), and for long times by the observation time of the molecules before photobleaching. While correlation analysis is also applied to measurements of immobilized samples, the most common application is in confocal measurements on freely diffusing molecules. The accessible concentration range of fluorescently labeled molecules is much greater than in typical single-molecule experiments, from picomolar to low micromolar (with an optimal contrast in the nanomolar range), which facilitates many applications both in vitro and in vivo. A process very commonly investigated by fluorescence correlation spectroscopy (FCS) is translational diffusion, but correlation analysis can equally be used to study conformational changes probed by FRET[48,92,114] (Figure 6), PET,[109] or Dexter exchange,[111] rotational diffusion,[71,115] fluid flow,[116−119] and a large range of photophysical and photochemical reactions.[65]

2.1.1.5. Fluorescence Colocalization. A useful method to quantify intermolecular interactions without the requirement of FRET or related processes is fluorescence colocalization, typically used in combination with confocal detection. Several variants of the technique are used,[120,121] but the basic idea is to label the binding partners with two different fluorophores and illuminate the same observation volume with corresponding lasers of two different wavelengths. Analysis of the fluorescence emission from the confocal volume allows the amount and stoichiometries of the associated molecules to be determined. Such analysis can be performed either in terms of coincidence between individual fluorescence bursts[121] or by cross-correlation spectroscopy.[120] Even small fractions of associated molecules in the low percent range can be detected in this way,[121] and fluorescence labeling is often simplified compared to methods that require a more stringent distance range, such as FRET.

2.1.1.6. Microfluidic Mixing. Even though kinetic information can often be obtained from equilibrium single-molecule experiments, in many cases it is still essential to probe nonequilibrium dynamics, especially if the reaction of interest is essentially irreversible during the observation time accessible at equilibrium. A method that lends itself very well to the combination with single-molecule detection optics is microfluidic mixing, and several different implementations have been reported.[122−126] The basic idea of these devices is to mix solutions in continuous laminar flow by reducing the dimensions such that the components of the solutions that are combined exchange very quickly, solely by diffusion.[127] After mixing, the confocal observation volume is placed at different points in the observation channel, corresponding to different times after the start of the reaction, with a dead time in the millisecond range[119,124] and even below.[125] Microfluidic mixing can be used, e.g., to rapidly change solution conditions or investigate the kinetics of protein−protein interactions.[122−125,128]

2.1.1.7. Fluorescence Labeling. Since even tryptophan, the natural amino acid with the highest fluorescence quantum yield (~0.13), is not suitable for single-molecule detection, and since fluorescent proteins[129] are typically of limited use for the investigation of IDPs because of their relatively large size and their inferior photophysical properties for single-molecule detection, labeling with extrinsic fluorophores is usually unavoidable for single-molecule spectroscopy. For FRET, two (or more) chromophores are needed, and their specific placement in the protein ideally requires groups with orthogonal chemistries. A wide range of labeling strategies exist, ranging from nonspecific labeling of amino or thiol groups present in the natural polypeptide to the incorporation of non-natural amino acids[130] or advanced chemical ligation[131] and intein-based approaches.[132] We refer the reader to reviews of the topic for a detailed treatment.[59,133] Currently, the simplest and most common approach is to rely on cysteine derivatization using maleimide chemistry. Increased specificity can be achieved by removing unwanted natural cysteines by site-directed mutagenesis or introducing cysteines with different reactivity due to different molecular environments within the protein.[134] Labeling is usually combined with multiple chromatography steps to purify the desired adducts. If even higher specificity is required, e.g., for FRET with more than two fluorophores,[135] cysteine labeling can be combined with orthogonal chemistries, such as non-natural amino acid incorporation.[91] A wide variety of suitable organic dyes with various functional groups for protein labeling have become commercially available. Examples of particularly popular chromophores for single-molecule FRET are the cyanine dyes[136] or the Alexa Fluor series.[137]

Note that interactions of the fluorophore with the protein can interfere with both the photophysics of the chromophores and the stability of the protein. This aspect needs to be taken into account for the design of the labeled variants. The use of hydrophobic dyes can reduce the solubility of the protein, or interactions with the protein can cause a reduction in fluorescence quantum yield, a problem that has been minimized by the introduction of charged groups in many of the popular dyes.[136,137] Important control experiments are equilibrium or time-resolved fluorescence anisotropy measurements,[87,98,104,138] which are sensitive to the rotational flexibility

of the dyes and can therefore provide indications for undesirable interactions with the protein. It is also essential to ensure by direct comparison with unmodified protein that labeling has not substantially altered the protein's biophysical properties or function.

2.1.2. Single-Molecule Fluorescence Spectroscopy of IDPs. A wide range of questions regarding IDPs have started to be addressed with the growing arsenal of single-molecule fluorescence techniques and analysis methods.[48,59,60] A particular focus has of course been to capture as directly as possible the conformational heterogeneity, dynamics, and interactions characteristic of IDPs and to relate them to their functional properties. In the following sections, we will summarize the recent developments and conceptual advances in this area.

2.1.2.1. Conformational Equilibrium Distributions. Förster radii of ~5 nm for the dye pairs currently available for single-molecule FRET allow the measurement of long-range intramolecular distances and dynamics and thus make the method ideal for investigating unfolded and disordered proteins, many aspects of which have been difficult to study in detail with ensemble methods because of the large structural heterogeneity of IDPs. An important advantage that has been exploited in single-molecule FRET experiments is the separation of structured and disordered subpopulations[98,138] (Figure 6), which allows changes of the conformational distribution within the disordered ensemble to be disentangled from possible transitions between disordered and structured states, e.g., in the presence of a ligand or binding partner.[15,139] Much of the single-molecule fluorescence methodology now applied to IDPs has been developed in the context of protein folding[75,86,140,141] and in particular for studying unfolded states, which for stably folded proteins often are populated only on addition of denaturants or at high temperature. The separation of subpopulations in single-molecule FRET experiments allows the properties of the unfolded state to be quantified accurately even under conditions where the majority of molecules are folded and would thus dominate the signal in an ensemble experiment, e.g., under near-native conditions, where the denatured state population is very small. As a result, processes such as the cooperative transition between folded and unfolded states can be distinguished from more gradual changes in unfolded state dimensions, and the properties of IDPs can be compared to those of denatured "regular" proteins under near-physiological conditions. For instance, this separation of subpopulations led to the identification of the continuous compaction, or collapse, of the unfolded state with decreasing concentration of denaturant,[98] a rather generic behavior[86,142] that reflects the change in solvent quality for the polypeptide chain[143,144] and is thus also observed for IDPs[15,16,114,145] (Figure 7). The denaturant-induced expansion of IDPs can be counteracted by osmolytes, such as trimethylamine-*N*-oxide (TMAO), which has been shown to lead to a collapse of α-synuclein without inducing a cooperative transition to a folded state.[146] One example of a cooperative folding transition in an IDP observed with single-molecule spectroscopy is the binding of Zn^{2+} to the intrinsically disordered N-terminal domain of HIV integrase, which leads to the formation of a folded state that coexists with the unfolded state at low Zn^{2+} concentrations.[15]

Single-molecule FRET experiments can also be used to investigate the effect of other changes in conditions on unfolded proteins and IDPs. In response to an increase in temperature, Nettels et al.[101] observed a compaction of the intrinsically disordered protein prothymosin α and an unfolded cold shock protein, suggesting an increase in effective intramolecular interactions upon heating. Molecular dynamics simulations indicated an important role of solvation and the possible involvement of secondary structure formation in this process.[101,147] For IDPs, which frequently contain a large fraction of charged amino acids, a contribution of particular importance is the interaction between charges in the polypeptide chain. Single-molecule FRET experiments in combination with an analysis based on polyampholyte theory showed that charge repulsion can in fact dominate the chain dimensions of IDPs and lead to a pronounced chain expansion at low ionic strength[15,148] (Figure 7), in agreement with results from simulations.[149] More surprisingly, however, attraction between charges of opposite sign within polypeptide chains with low net charge can lead to an additional compaction,[15] as

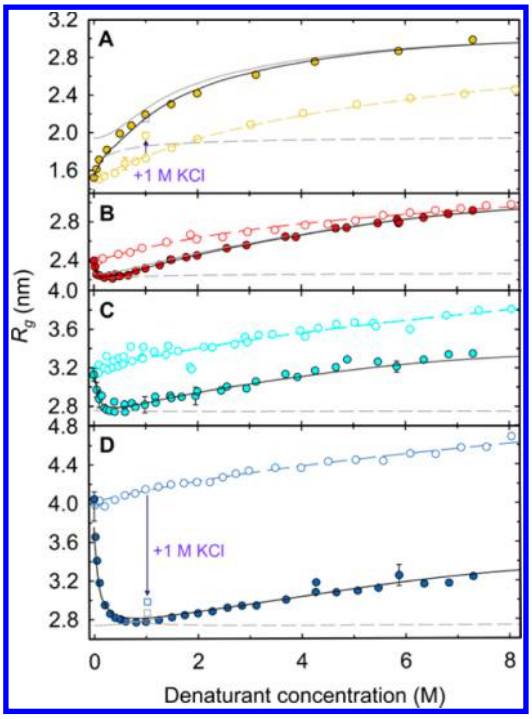

Figure 7. Effect of electrostatics and denaturant on unfolded and intrinsically disordered proteins.[15] Dependence of the apparent radii of gyration (R_g) of the labeled protein segments on the concentration of GdmCl (filled circles) and urea (open circles) with (A) CspTm, (b) the N-terminal domain of HIV integrase, (C) prothymosin α (ProTα) N-terminal domain, and (D) ProTα C-terminal domain. CspTm exhibits the monotonic unfolded state compaction at low denaturant concentrations frequently observed for unfolded proteins.[86,142] IDPs in A–D show a more complex behavior owing to the role of electrostatic repulsion within the chain and the role of charge screening by the ionic denaturant GdmCl. Fits to a binding model for the urea dependence and to polyampholyte theory for the GdmCl dependence (black solid lines) are shown. The two components of polyampholyte theory corresponding to the contributions of GdmCl binding and electrostatic repulsion are indicated as continuous and dashed gray lines, respectively. The addition of 1 M KCl illustrates the opposite effect of charge interactions in CspTm and ProTα: screening of the polyelectrolytic charge repulsion within ProTα with its large net charge leads to chain compaction (D); screening of polyampholytic charge attraction within CspTm with its net charge close to zero leads to chain expansion (A). Reprinted with permission from ref 15. Copyright 2010 National Academy of Sciences.

dx.doi.org/10.1021/cr400297g | *Chem. Rev.* 2014, 114, 3281–3317

predicted by polyampholyte theory.[150] Similar effects may play a role in the interesting effects of charge screening on the transfer efficiencies reported for tau protein[151] (Figure 8).

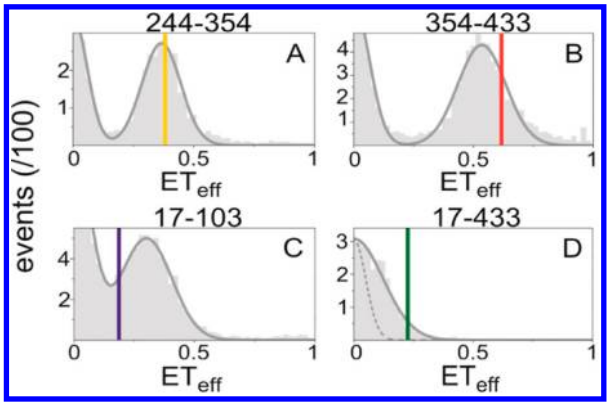

Figure 8. Effect of charge screening on the transfer efficiencies of tau protein labeled with FRET dyes at different positions within the chain. Transfer efficiency (ET_{eff}) histograms in 500 mM NaCl are shown for the intramolecular pairs 244−354 (A), 354−433 (B), 17−103 (C), and 17−433 (D), with colored vertical lines indicating the peak position for each construct at 50 mM NaCl. Note that the constructs respond to charge screening very differently, in some cases leading to expansion and in others to collapse. Reprinted with permission from ref 151. Copyright 2012 American Chemical Society.

Interestingly, single-molecule FRET experiments on the intrinsically disordered intracellular domain of an NMDA receptor subunit indicate that phosphorylation by Src kinase leads to pronounced chain expansion,[152] which may be relevant for its interaction with downstream signaling partners. Similarly, nitration of tyrosine residues in α-synuclein leads to changes in the conformational distribution of free protein and reduces its membrane affinity, presumably via the pronounced decrease in the pK_a of tyrosine caused by nitration and the resulting charge repulsion.[153] These results indicate that post-translational modifications can modify the molecular behavior of IDPs substantially by changes in charge interactions. Such modulations of the dimensions of IDPs may be of importance for their functional properties, such as the interaction with binding partners, e.g., in the fly-casting paradigm.[34]

If a separation of subpopulations is not required (i.e., if the population under investigation is known to be homogeneous on the observation time scale), information about the overall size of IDPs can also be obtained from translational diffusivity measured by FCS. Conceptually, such measurements are closely related to light scattering or small-angle X-ray scattering experiments, but they can be performed at much lower protein concentration, which can be crucial to avoid intermolecular interactions or aggregation. An example is the study of polyglutamine peptides by Crick et al.[154] (Figure 9A). The authors investigated the scaling of the hydrodynamic radii with chain length by FCS and found a surprisingly low scaling

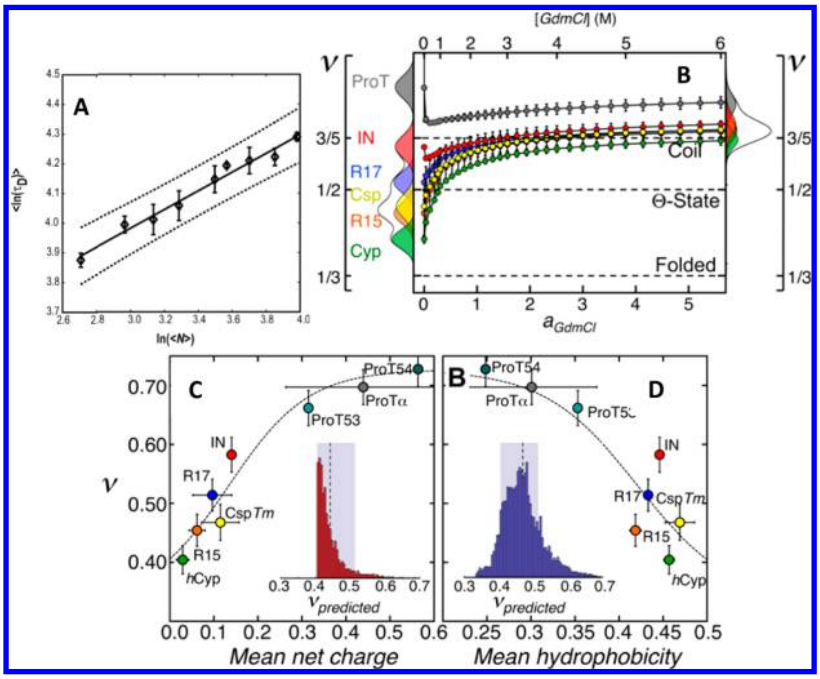

Figure 9. Scaling behavior of IDPs and unfolded proteins from single-molecule experiments. (A) Average translational diffusion time, τ_D (measured in microseconds), as obtained from FCS measurements as a function of the average chain length, $\langle N \rangle$, for the peptide series Gly-$(Gln)_{\langle N \rangle}$-Cys-$Lys_2$, with a fluorophore attached to the cysteine side chain.[154] The solid line is the line of best fit to the FCS data, and the dotted lines represent the 95% confidence intervals. Since τ_D is proportional to the Stokes radius of the chain, the resulting length scaling exponent of 0.32 ± 0.02 can be taken to indicate that the polyglutamine peptides are rather compact globules. (B) Scaling exponents, ν, for a range of unfolded and intrinsically disordered proteins extracted from single-molecule FRET spectroscopy over a wide range of GdmCl activities.[16] Scaling exponents expected for folded proteins, chains at the Θ state, and excluded volume chains (coils) are indicated as dashed lines. The distributions of ν in water (left) and 6 M GdmCl (right) reflect the variance in ν. The broad range of scaling exponents observed illustrates the different degrees of compaction of the polypeptides. The IDPs in this study (ProTα, IN) exhibited the largest scaling exponents. (C) Scaling exponents in the absence of denaturant exhibit a pronounced correlation with the net charge and an anticorrelation with the hydrophobicity of the chain, illustrating the connection between length scaling, i.e., chain compactness, and sequence composition over a broad and continuous range. Reprinted with permission from refs 154 and 16. Copyright 2006 and 2012 National Academy of Sciences.

exponent of $\nu = 0.32 \pm 0.02$, the value expected for a maximally collapsed polymer chain (such as folded globular proteins[155]) and significantly lower than the values expected for an ideal polymer ($\nu = 0.5$) or an excluded volume chain in good solvent ($\nu \approx 0.588$).

In general, the recent application of relatively simple polymer models and mean-field theories in analysis of single-molecule fluorescence experiments has been very successful for quantitatively describing global properties of IDPs and unfolded proteins.[48] Polymer concepts have thus emerged as a powerful framework for the conformational properties of IDPs.[13,14,18] Given the predominance of relatively weak and nonspecific intramolecular interactions, this may not be entirely surprising, but the quantitative success and predictive power go beyond a simple qualitative picture and now allow the properties of unstructured polypeptides to be classified more rigorously than previously possible. This point can be illustrated by recent work where eight IDPs and unfolded proteins were investigated in terms of the scaling of their unfolded state dimensions with chain length[16] (Figure 9B). The resulting scaling exponents exhibit a broad distribution from ∼0.4 to ∼0.7 and show a correlation with the mean net charge and an anticorrelation with the average hydrophobicity of the sequences (Figure 9C). The IDPs in the study showed larger scaling exponents than the unfolded states of "foldable" proteins; the scaling exponent is thus a useful quantity for classifying unfolded state properties in a continuous manner that provides an extension of the grouping into distinct categories such as "molten globules" or "premolten globules".[156] In general, even though trends are often obvious, a clear distinction between IDPs and the unfolded states of foldable proteins cannot be made; rather, a continuum of sequence compositions is observed that leads to a continuum of molecular behaviors, including the chain dimensions and the presence of specific secondary and tertiary structure.

Of course, not all conformational properties of IDPs will be amenable to a description in terms of simple mean field polymer models, and it will be interesting to quantify the role of more specific interactions and heteropolymer effects such as charge patterning in the sequence,[14,157] e.g., by direct complementation with the residue-specific local information accessible with methods such as NMR[158] or segmental mapping of distance distributions by single-molecule FRET[99,159] and the combination with molecular simulations.[101,104,106,159] The structural properties of more complex IDPs are already starting to be investigated with single-molecule spectroscopy. For example, Huang et al.[160] identified a large degree of structural heterogeneity in the intrinsically disordered N-terminal domain of tumor suppressor p53, indicating that single-molecule FRET can provide useful information even for large multimeric protein complexes.

2.1.2.2. Conformational Dynamics. As described above, distance information from single-molecule fluorescence measurements can provide important information regarding the conformational properties of IDPs. However, single-molecule fluorescence can also provide information on dynamics over a wide range of time scales.[48] A key benefit of single-molecule experiments is the possibility to extract dynamic information even from equilibrium measurements, which avoids the necessity for a synchronization of the system by perturbation methods, as frequently employed in ensemble experiments. For proteins, equilibrium dynamics have been investigated based on correlation functions,[17,92,161−163] the analysis of broadening and exchange between subpopulations in FRET efficiency histograms,[98,164−166] and from fluorescence trajectories of immobilized molecules.[163,166−172] In this way, both the equilibrium distributions and the kinetics can sometimes be obtained from the same measurement. An important extension of such equilibrium dynamics is the combination with perturbation methods, such as microfluidic mixing, if the reaction of interest is essentially irreversible during the observation time accessible at equilibrium. In the following sections, we will summarize single-molecule fluorescence results on IDP dynamics ranging from the shortest to the longest time scales that have been investigated.

The fastest accessible dynamics can be probed with nanosecond correlation spectroscopy (ns-FCS),[92−94] which can be readily implemented in confocal instruments with the latest generation of counting electronics.[71] In ns-FCS experiments based on FRET, the long-range distance fluctuations between the donor and the acceptor fluorophores report on the characteristic time scale of interconversion between different configurations of the polypeptide chain (Figure 7). The resulting relaxation times are in the range from tens of nanoseconds to ∼200 ns for the segment lengths from ∼30 to ∼200 amino acid residues investigated to date.[17,92−94,139] These times are remarkably close to the reconfiguration times expected for ideal polymers,[173] indicating that the underlying dynamics approach chain diffusion in the absence of persistent interactions within the polypeptide.

However, these rapid dynamics do depend on sequence composition and solution conditions. For unfolded proteins at low denaturant concentrations, the reconfiguration time can increase substantially above the values expected for an ideal chain.[17,92] This behavior has been attributed to "internal friction" caused by dissipative mechanisms within the polypeptide, such as dihedral angle rotations or transient side chain or backbone interactions,[92] but it eluded a quantitative description. The recent work of Soranno et al.[17] illustrates the use of concepts from polymer physics in combination with single-molecule FRET and ns-FCS for quantifying internal friction in unfolded proteins and IDPs. Polymer dynamics models, such as the Rouse model with internal friction,[174,175] show that the reconfiguration time, τ_r, of a polymer can be decomposed into a sum of two relaxation times, that of the ideal chain, τ_0, and a contribution due to internal friction, τ_i, i.e., $\tau_r = \tau_0 + \tau_i$. On the basis of this relationship and solvent viscosity- and position-dependent measurements of unfolded state dynamics, Soranno et al.[17] showed for a number of proteins that internal friction is close to zero at very high concentrations of denaturant, where the chains are very expanded and thus behave similar to an ideal polymer. For very compact chains, however, τ_i can dominate the chain dynamics and lead to an increase in τ_r of up to an order of magnitude above the value expected for an ideal chain (Figure 10). Highly charged IDPs do not exhibit this compaction and are expanded due to charge repulsion,[15,149,176,177] which reduces internal friction. The correspondingly faster dynamics may affect their interactions with cellular binding partners.[17,34] In summary, single-molecule FRET in combination with ns-FCS provides an opportunity to quantify the properties of unfolded and disordered proteins even on submicrosecond time scales and to rationalize them in terms of polymer-physical concepts.

Single-molecule fluorescence methods complementary to FRET that have already provided important dynamic

dx.doi.org/10.1021/cr400297g | Chem. Rev. 2014, 114, 3281−3317

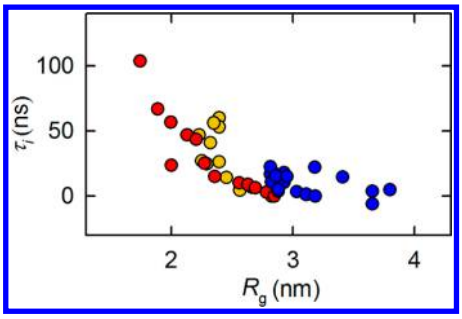

Figure 10. Role of internal friction in IDP dynamics from single-molecule FRET and correlation spectroscopy. The dependence of the internal friction time, τ_i, on the radius of gyration, R_g, for CspTm (red), the N-terminal domain of HIV integrase (yellow), and ProTα (blue) over a broad range of solution conditions shows a correlation between the contribution of internal friction to chain dynamics with the expansion of the chain.[17] Data from ref 17.

information on the time scale of fundamental chain dynamics are photoinduced electron transfer (PET)[109] and Dexter exchange quenching (or self-quenching) of fluorophores[111] combined with FCS. In one of the earliest studies, Chattopadhyay et al.[111] used the self-quenching of tetramethyl rhodamine incorporated in two positions of intestinal fatty acid binding protein unfolded at high denaturant concentration or low pH and observed relaxation times of about 2 μs. This time scale is still expected to result from rapid polymer-type dynamics of the unfolded protein but slower than the reconfiguration times observed by FRET for polypeptide segments of similar length (see above) because Dexter exchange probes contact formation, and only a small part of the distance distribution contributes to the observed signal. In other words, the observed relaxation time depends both on the intrinsic reconfiguration dynamics of the chain (as probed by FRET) and on the equilibrium probability of the two fluorophores being in sufficiently close contact for quenching to occur (essentially van der Waals contact), as in some ensemble quenching methods.[178−180] The same is true in the case of PET,[109] where static quenching of a fluorophore by tryptophan has been exploited for obtaining dynamics based on contact formation. The feasibility of measuring submicrosecond loop formation times was demonstrated in unstructured peptide segments of p53[181] and model peptides.[109,182−184] Neuweiler et al. used PET to monitor the submicrosecond loop-closure kinetics in the denatured state of small, fast-folding proteins.[161,185] The same method was applied to study microsecond and submicrosecond loop closure kinetics of four consecutive segments within the intrinsically disordered N-terminal domain of p53 and their response to protein binding and phosphorylation[186] (Figure 11). The authors found that, upon binding and phosphorylation, chain motions were altered not only within the targeted segments but also in more remote regions, indicating that long-range interactions are of importance for IDP interactions. Mukhopadhyay et al.[114] reported that not only tryptophan but also the unusually abundant tyrosine residues in the disordered domain of the prion protein Sup35 lead to PET quenching of an extrinsic fluorophore and can thus be used to monitor intramolecular IDP dynamics in the submicrosecond range. (Note that the quenching of FRET dyes by Trp and Tyr needs to be excluded[17,92,93] or taken into account explicitly[187] if intramolecular dynamics are monitored by FRET on the same time scale.)

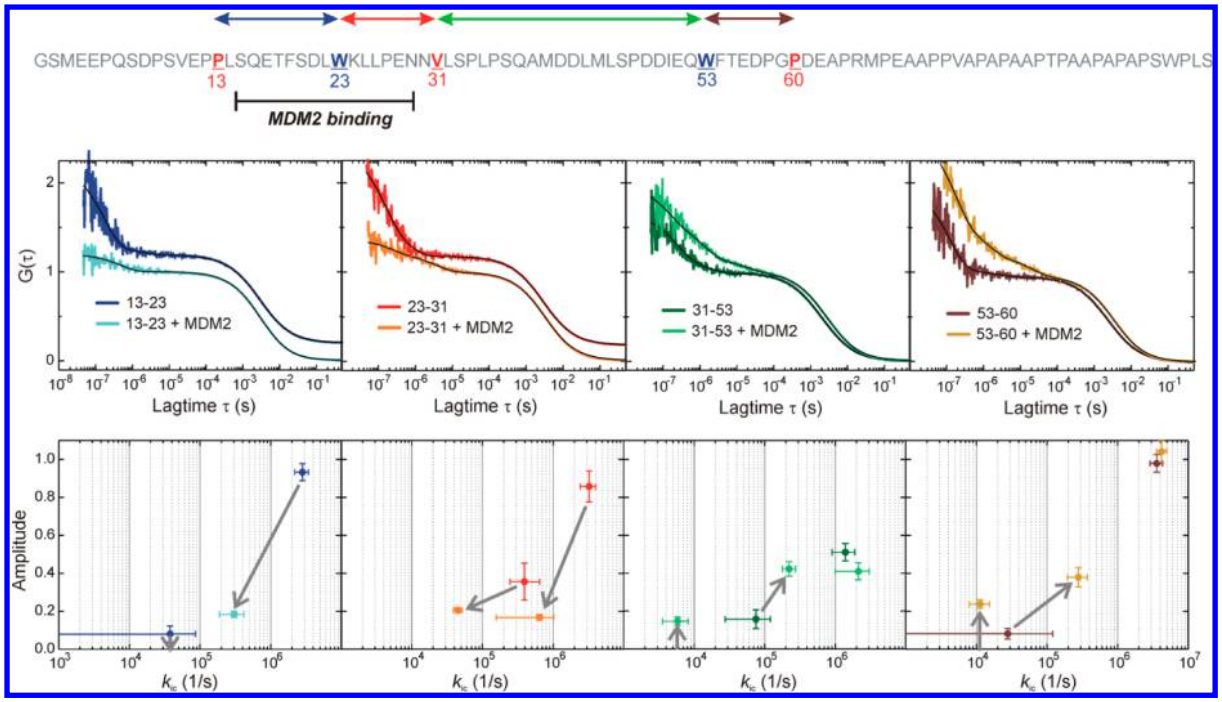

Figure 11. Segmental chain motions in p53-TAD(1−93) and influence of phosphorylation investigated by PET.[186] (Top) Polypeptide sequence with the sites of enzymatic phosphorylation indicated in bold and as black dots. (Middle) Autocorrelation functions (ACFs) recorded from modified p53-TAD(1−93) with and without side chains S33, S46, and T81 phosphorylated. Chain segments probed are color coded as illustrated in the top sequence and shown in each panel (phosphorylation is indicated as P). (Bottom) Plots of the amplitudes of each of the single-exponential submillisecond decays versus the corresponding rate constant of loop closure, k_{ic}. The arrows indicate the observed changes in amplitude and rate constant of the individual relaxations upon phosphorylation. Reprinted with permission from ref 186. Copyright 2012 American Chemical Society.

dx.doi.org/10.1021/cr400297g | *Chem. Rev.* 2014, 114, 3281−3317

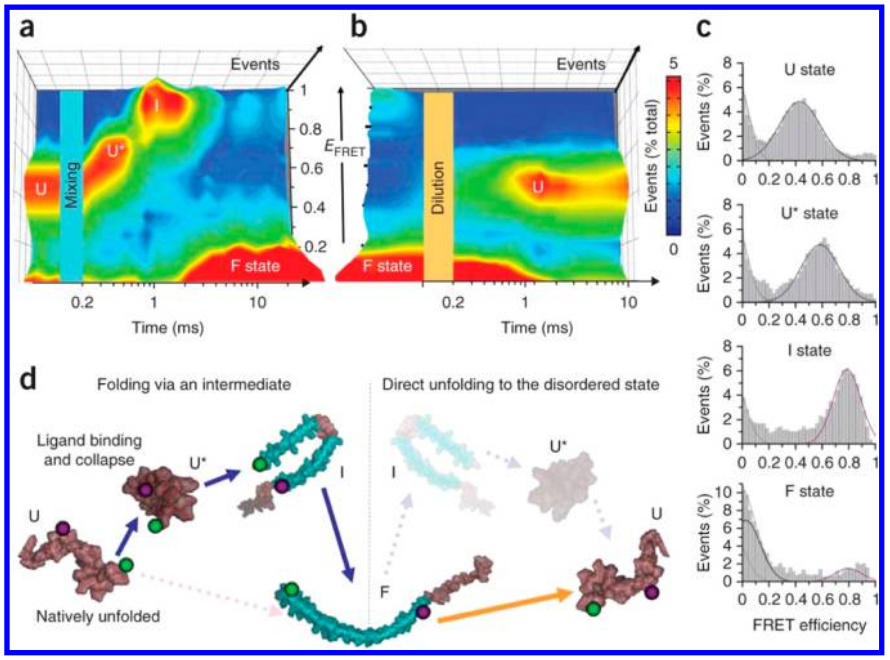

Figure 12. Microfluidic mixing employed for the investigation of the kinetics of conformational changes in α-synuclein upon interaction with SDS using single-molecule FRET.[50] (a and b) Histograms of the transfer efficiency, E_{FRET}, for the folding (a) and unfolding (b) reactions of α-synuclein, obtained at different time points after mixing with SDS, with the percentage of total events color coded as indicated. (c) Representative E_{FRET} histograms for various states: intrinsically disordered (U state, obtained before mixing), collapsed unfolded (U* state, 490 μs after mixing), intermediate (I state, 1.2 ms after mixing), and extended structures (F state, >10 ms after mixing). (d) Illustration of the suggested conformational transitions of α-synuclein. Shown are random coil (brown), α-helix (turquoise), and donor (green sphere) and acceptor (purple sphere) dye molecules. Reprinted with permission from ref 50. Copyright 2011 Nature Publishing Group.

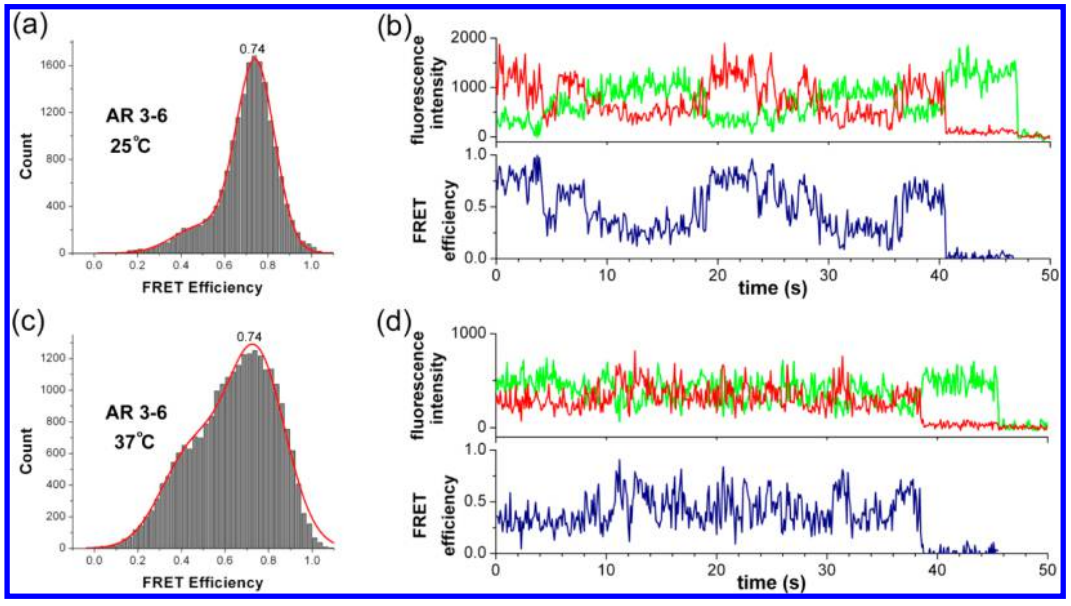

Figure 13. Slow processes in partially disordered proteins studied with single-molecule FRET on surface-immobilized molecules.[191] Transfer efficiency histograms (a and c) and corresponding fluorescence intensity traces (b and d) of immobilized IκBα molecules showing fluctuating high FRET efficiencies followed by photobleaching. Histograms show a major population centered at 0.74 and a broad shoulder at lower transfer efficiency. Change in temperature from 25 (A and B) to 37 °C (c and d) leads to a shift in populations and changes in FRET fluctuations. Reprinted with permission from ref 191. Copyright 2013 Elsevier.

An increasingly popular extension of such methods to investigate rapid dynamics by single-molecule measurements is microfluidic mixing, with dead times comparable to established ensemble methods based on turbulent mixing, such as stopped flow. In a recent mixer design, Gambin et al.[125] even achieved a dead time of ~200 μs, very close to the limits of time resolution dictated by the minimum residence time that is required to observe a sufficient number of photons from a single molecule flowing through the confocal volume (Figure 12). They used the device to investigate the kinetics of the structural transitions of α-synuclein upon interaction with sodium dodecyl sulfate (SDS) and were able to resolve the formation of an intermediate that they assigned to a helix−turn−helix structure preceding the final extended helix bound to micelles.[125]

dx.doi.org/10.1021/cr400297g | Chem. Rev. 2014, 114, 3281−3317

Another mixer design optimized for single-molecule fluorescence experiments[124,188] has recently been employed to investigate internal friction in unfolded and intrinsically disordered proteins.[17,189] Soranno et al.[17] and Borgia et al.[189] used the device in combination with ns-FCS to quantify internal friction in unfolded and disordered proteins. The microfluidic mixer allows the unfolded state of a protein to be transiently populated at low denaturant concentrations (where it is folded at equilibrium); in this way, the reconfiguration time can be determined under conditions where the unfolded state is most compact and can then be directly compared to IDPs. Due to the continuous-flow mixing employed, even correlation experiments with long acquisition times can thus be performed on such nonequilibrium populations.[17,189]

However, not only fast dynamics in the microsecond range and below have been reported for IDPs. Using camera-based single-molecule FRET imaging approaches on immobilized samples, slower dynamics have been observed. Lamboy et al.[190,191] identified partially unfolded states of the ankyrin repeat protein IκBα, a regulator of the transcription factor NFκB, under native conditions. By varying the position of the dye pair systematically within the protein, fraying of the terminal repeats was identified as the underlying cause. In the partially unfolded states, IκBα exhibited heterogeneous FRET dynamics (Figure 13) on time scales ranging from ∼0.1 s (the time resolution of the experiment) to a few seconds, as shown by cross-correlation analysis. The folded structure could be stabilized by NFκB binding, reduction in temperature, or suitable mutations, with a concomitant change in FRET fluctuations. Choi et al.[192] made a related observation on some proteins previously categorized as intrinsically disordered. For three of them, the transfer efficiency values were observed to be constant on the millisecond integration time of the camera, as expected from the rapid conformational dynamics of IDPs (see above). Neuroligin and the NMDAR-2B glutamate receptor, however, exhibited slow transitions between different FRET efficiency values on the time scale of seconds, indicating the presence of unexpectedly large free energy barriers, which are usually only found for conformational transitions involving specific and cooperative interactions, e.g., in protein folding or unfolding. This behavior is reminiscent of a previous report of unexpectedly slow unfolded state dynamics in denatured ribonuclease H.[172] The origin of such slow transitions and the structural identity of the transient states are currently unclear, but future experiments with multiple dye pairs, complementary methods, or trapping techniques that do not require surface attachment and can thus exclude the influence of surface interactions[193,194] may help to answer this question.

2.1.2.3. Intermolecular Interactions, Oligomerization, and Aggregation of IDPs. Single-molecule fluorescence spectroscopy can also be employed for probing intermolecular interactions, an important aspect for the functional repertoire of IDPs. To date, single-molecule FRET is the dominant method of choice, but FCS and PET are also used for studying the interactions of IDPs with binding partners.[186] Because of its role in neurodegenerative disorders, one of the IDPs most widely investigated with single-molecule methods is α-synuclein and its interactions with detergents and lipids.[59,195,196] α-Synuclein has been known to be unstructured free in solution[197] but adopts α-helical structure upon binding to negatively charged lipid vesicles[198,199] and SDS,[200] which has frequently been used as a membrane mimic. Single-molecule FRET has been employed to characterize the structure and dynamics of α-synuclein under these different conditions. Already at SDS concentrations below the critical micelle concentration (CMC) the transition between the unstructured (U) and a flexible α-helical conformation (I) was observed by a cooperative change in transfer efficiency.[139,201] Ferreon et al.[139] observed several additional SDS-induced transitions in the presence of unlabeled α-synuclein. At slightly higher SDS concentrations, an extended conformation assigned to a long α-helix is formed (F); at SDS concentrations above the CMC, α-synuclein binds to the SDS micelles in a kinked conformation (I_m); at even higher SDS concentrations, where cylindrical micelles or extended bilayers are formed, an extended conformation is formed again (F_m), which resembles the signature of α-synuclein bound to vesicles[139,202] or nanodiscs.[203] FCS experiments indicate that the affinity of α-synuclein (and other synucleins[204]) strongly depends on vesicle curvature and lipid composition.[205] Owing to the lack of stable tertiary interactions within α-synuclein, the concentration and assembly state of the interaction partner SDS thus dominate the conformational distribution of the IDP. An interesting observation was made for the interaction of tau protein with heparin.[151] Depending on the labeling positions used for FRET, either an expansion or a compaction of the corresponding chain segments was observed, with indications for the presence of both high (tens of nanomolar) and low (micromolar) affinity binding sites. Even though a detailed structural interpretation is still open, these results indicate that systematic repositioning of FRET pairs can be used to map the intermolecular interactions of IDPs and assess their conformational promiscuity.

Many IDPs, even if they are largely unstructured as monomers, can self-associate efficiently at higher concentrations, and some of them aggregate or form amyloid, e.g., α-synuclein, tau, Aβ, prion proteins, or polyglutamine-containing sequences.[206] While the concentration of labeled IDP in single-molecule experiments is extremely low, which allows aggregation to be excluded and the properties of the monomeric protein to be investigated,[151,207] oligomerization and aggregation can still be monitored by adding the same protein in its unlabeled form. A range of techniques have been employed successfully to investigate such processes, including FCS,[58,208−210] FRET,[55,58] fluorescence colocalization,[121,128] imaging,[208,211] and stepwise photobleaching.[212,213] A particularly promising aspect of single-molecule fluorescence studies is that relatively small oligomeric species involved in the aggregation process can become detectable,[55,212,213] which may lead to a more quantitative understanding of amyloid formation.

2.2. Single-Molecule Force Spectroscopy Techniques

During the last two decades, single-molecule force spectroscopy (SMFS) gradually established itself as a powerful tool for studying the mechanical behavior of biopolymers such as DNA, RNA, and proteins.[214−222] SMFS instruments, irrespective of their specific technical implementation, are in essence nanoscale manipulators and dynamometers able to exert and measure forces on individual molecules. In a typical SMFS experiment, the analyte molecule is subjected to a controlled mechanical stress prompting some form of structural transition; depending on the time derivate of applied force, the observed event can occur in quasi-equilibrium conditions or in out-of-equilibrium conditions.[46,223] Structural, thermodynamic, and kinetic information about the transition can be inferred from the amount of force needed to induce it and/or from the

observed geometrical changes it caused.[46,223−236] Even though the general SMFS strategy outlined above can be practically implemented with several different experimental techniques on biopolymers, to the best of our knowledge only two of these techniques were applied to the study of IDPs: atomic force microscopy (AFM)[237] and laser optical tweezers (OT)[238] (Figures 14 and 15).

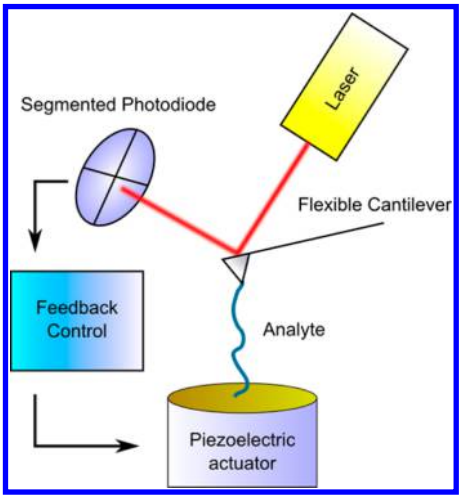

Figure 14. Schematic representation of the main components of a typical AFM apparatus. The analyte is tethered to a surface that can be precisely positioned via a piezo electric actuator and to a sharp tip mounted on a flexible cantilever with a known spring constant. The distance between the surface and the probe tip coincides with the end-to-end distance imposed to the analyte, which in turn corresponds to a specific force exerted on it. Force-induced deformation of the flexible cantilever is usually monitored by measuring the movements of a laser beam reflected on its reflective surface via a segmented photodiode. The real-time measurement of the applied force is in some cases (e.g., in force clamp mode, see main text) used to control the position of the surface via a negative feedback loop.

2.2.1. Single-Molecule Force Spectroscopy Instrumentation and Methods. In AFM-based SMFS experiments a molecule of the analyte needs to be positioned so that it can act as a mechanical connection between a micrometer-sized cantilever and a surface. There are several strategies to obtain this arrangement, the most straightforward (but least controllable) of which being simply the random dispersion of the analyte on the surface by drop casting followed by pressure-induced random physisorption on the cantilever. It is usually convenient to employ solutions containing very low analyte concentrations to optimize the separation between individual molecules and avoid the simultaneous interaction of the probe with multiple molecules. Additional control on the orientation, position, and area density of the analyte molecules either on the surface or the cantilever can be obtained at the cost of having to resort to more involved functionalization chemistry.[239,240] During the AFM-SMFS experiment, the relative position of the cantilever tip and the surface is controlled via a piezo electric actuator while the analyte molecule bridges the gap and distributes the mechanical stress between the two. The force applied on the analyte can be continuously monitored by measuring the deflection induced on a flexible cantilever with known mechanical characteristics. The behavior of the cantilever is usually approximated to that of a single Hookean spring, and its single elastic constant parameter can be measured, e.g., with the thermal noise method.[241,242]

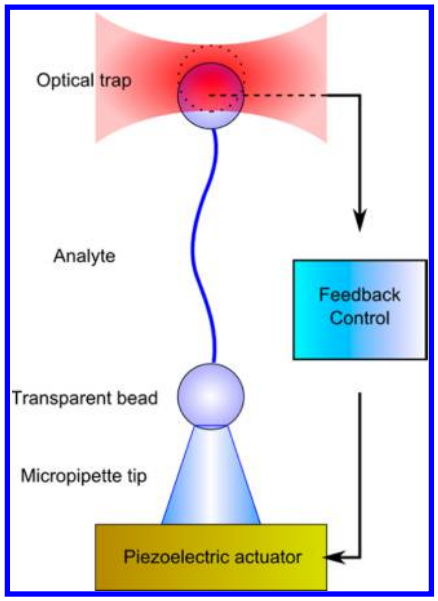

Figure 15. Main components of a typical OT apparatus. The analyte is tethered to two microsized transparent beads whose relative position determines the applied force. At least one of the beads is optically trapped via a focused laser beam, while the other is usually attached by suction to a micropipette tip. The pipette is sometimes substituted with a glass slide or a second optical trap. In any case, the force-induced displacement of the optically trapped beads from the center of the beam waist can be used to determine the force applied on the analyte and concurrently drive a piezo electric actuator via a negative feedback loop to adjust the relative position of the beads. In some apparatuses, the active feedback loop is dispensed with and substituted via an all-optical passive force clamp (see main text).

The applied force can be used in principle either to compress[243] or to stretch the analyte.[244] One of the very few examples of an experimental strategy relevant to the study of protein disorder based on the compression of the analyte is represented by the works of J. H. Hoh and colleagues during late 1990s. They employed AFM-based SMFS to probe the mechanical behavior of individual neurofilaments immobilized on a mica surface.[245,246] The side arms of neurofilaments are constituted by a mixture of highly disordered polypeptides[247] exerting entropically and electrostatically driven repulsion forces that play a role in modulating interfilament spacing.[248] Force−distance curves recorded while applying pressure on native neurofilaments revealed a weak, long-range repulsive force extending 50−100 nm from the core of the filament, while homopolymeric filaments reconstructed from purified NF-L polypeptides and filaments lacking the long disordered tails did not show the repulsive behavior.[245,246] The same group applied a similar approach to the study of microtubule-associating proteins (MAPs) electrostatically anchored to mica with their projection domains extending away from the surface.[249] Similarly to what was observed in neurofilaments, the MAP-functionalized surface exerted long-range (>100 nm) repulsive forces that were found to be influenced by ionic strength, as expected for a polyelectrolyte polymer brush. Excluding the rare examples of experiments based on analyte compression like those mentioned above, reported studies on single, flexible polypeptide chains such as those of IDPs only involve stretching.

Given that piezo electric actuators in modern commercial AFMs allow a spatial resolution of less than 0.1 nm and that

dx.doi.org/10.1021/cr400297g | Chem. Rev. 2014, 114, 3281−3317

with modern electronics analog to digital data conversion and storage can occur at MHz speed, in practice the spatial and temporal operative ranges as well as the force resolution of AFM apparatuses are mostly influenced by the mechanical characteristics of the cantilever. The softest commercial cantilevers have elastic constant values falling in the 50−150 pN nm^{-1} range, which for $k_BT \approx 4$ pN nm correspond to thermal force fluctuations of around 15−25 pN. This makes the measurement of mechanical events occurring at few tens of pN problematic due to a low signal-to-noise (SN) ratio. Moreover, virtually all AFM setups show signal drift in the second time scale, making it almost impossible to use long acquisition times to overcome the low SN ratio. An advantage of the relative stiffness of AFM cantilevers is that it allows the instrument to respond rapidly to signal variations, making it possible to observe transient intermediates such as those encountered during folding and unfolding, especially when special instrumental strategies are employed.[250] Taken together, these instrumental characteristics imply that even optimally adjusted commercial SMFS AFM setups are suited to measure forces above 15 pN[45,215] with a temporal resolution of around 10^{-3} s.[214] However, the group of M. Rief demonstrated that a force resolution of around 1−2 pN can be reached with special procedures and instrumentation, although at the cost of a lower temporal resolution.[251]

One of the main advantages of AFM in the context of this review is its relative accessibility: there are nowadays many commercial systems that can be used for performing SMFS even without hardware modifications. Of all the instruments that can be used for SMFS, AFMs are perhaps the quickest and easiest while also offering a quite ample flexibility in terms of experimental conditions such as temperature, solvent, and type of surface/cantilever functionalization chemistry. Its main disadvantages instead are represented by its comparatively high force range and temporal resolution, which make AFM SMFS most suitable for measuring events occurring at high applied forces, such as the mechanical unfolding of structured protein domains.[214] Moreover, obtaining clear AFM SMFS data on single-protein domains is often arduous due to a series of practical considerations such as the occurrence of nonspecific surface/probe interactions, while measurements are easier on larger polydomain artificial constructs[252,253] containing multiple tandem repeats of the analyte region. While not strictly necessary in theory, the artificial polyprotein strategy proved to be so advantageous that several different sample preparation methods[254−257] were developed and are often employed in AFM SMFS experiments.

SMFS experiments performed with laser optical tweezers (OT) apparatuses are conceptually identical to those performed with AFM instruments; however, the analyte is not manipulated with a piezo-controlled surface and a flexible cantilever but via transparent dielectric particles whose exact position in the three-dimensional space can be controlled via laser optical traps.[258,259] Optical trapping in OT apparatuses is performed by focusing a laser beam with Gaussian profile intensity on a diffraction-limited spot via an objective with a high numerical aperture. When the spherical particles become subject to radiation pressure from the beam, their trajectories are modified due to conservation of momentum in different ways depending on the position of their centers relative to the beam waist. Particles happening to be exactly at the center of the three-dimensional potential well located near[259] the focal point will diffract light with equal intensity toward all lateral directions, resulting in a null net lateral force, while those at outer regions of the focus area will diffract with radially anisotropic intensity, resulting in a net restoring force driving the particle back toward the center of the beam. This allows the controlled movement of the average equilibrium position of individual particles in solution with subnanometer resolution. Particles with sizes varying from several tens of nanometers to micrometers can be stably trapped for comparatively long times. The optical trap also works as a nanodynamometer, since the restoring force exerted on the particles is proportional to their displacements from the beam waist. For small displacements occurring around the flattest region of the beam intensity profile, the restoring force has an approximately linear dependence on displacement and the optical trap can be thus modeled as a Hookean spring.

To translate the above concepts into practice, most OT SMFS experimental setups employ near-infrared lasers as they minimize damage to biopolymers.[260,261] The power of the laser traps needs to satisfy the two opposite requirements of being high enough to effectively trap particles for experimentally reasonable times and low enough to minimize local heating at the focal point and oxidative damage to samples.[262] While most OT apparatuses originally employed a single optical trap to modulate the relative position of two spherical particles, one of which was instead kept in position by a micropipette, recently the group of Bustamante demonstrated that a dual-trap setup can significantly improve instrumental performance.[263,264] In both cases, one single-analyte molecule needs to be immobilized by selectively anchoring it to both particles in order to make the experiment possible, which is not a trivial task. Moreover, the use of long "molecular handles" linking the analyte to both beads but at the same time acting as a spacer to minimize unwanted analyte/bead interactions is practically almost always necessary.[265] The spring constant of the trap in typical OT apparatuses depends on a variety of factors[214] but usually falls in the range of 0.01−0.2 pN nm^{-1}, thus making the signal-to-noise ratio due to thermal fluctuations extremely high and allowing the clear detection of mechanical events occurring at tenths of pN. Particle displacement is usually detected with subnanometer resolution via back-focal plane interferometry.[266,267] The most commonly used particles are micrometer-sized polystyrene beads, which are highly polarizable, largely transparent to near-infrared, and easy to produce with relatively uniform diameters.

The main advantages of OT in the context of SMFS of IDPs are its excellent force resolution, low susceptibility to thermal drifts, and easy access to long observation times. These features make OT well suited to study processes occurring in near-equilibrium conditions under very low applied loads.[268] Some of the drawbacks are represented by the fact that there are few commercially available apparatuses that could be used for performing SMFS on proteins, and even those would require careful hardware optimization. Sample preparation is also not trivial[265] and usually implies the functionalization of the analyte with dsDNA linkers which also sets an upper limit of 65 pN to the range of workable forces due to its well-known BS transition.[269]

Regardless of the specific combination of apparatus and experimental strategy employed, all SMFS experiments performed on proteins share the same conceptual foundation. A single-protein molecule is mechanically manipulated so that the distance between two points along its length (usually, but not necessarily, its termini)[270,271] is artificially altered from its

dx.doi.org/10.1021/cr400297g | Chem. Rev. 2014, 114, 3281−3317

equilibrium value. The SMFS apparatus must be able to constantly monitor the separation between the points of force application and the resulting applied force on the molecule. These are closely related values, since most SMFS experiments are conceived so that the dependence between applied force and displacement is well approximated by a linear function with a measurable slope. In this way, the mechanical work needed to stretch the protein for a given distance molecule can be experimentally measured. Even for proteins behaving as ideal random coils, this kind of manipulation requires nonzero mechanical work to overcome entropic pulling, which gives rise to a well-known force/distance profile given by the Kratky–Porod[272] (or "worm-like chain") model (WLC).[273] Proteins with residual structure, when subjected to force, will show deviations from the WLC model as part of the work done on the protein will be used to disrupt enthalpic interactions. These deviations originate mechanical events data that can be studied to obtain information on the structure, energy, and kinetics of the force-induced transition.

The simplest approach to the elaboration of SMFS data is to approximate the complex and multidimensional conformational energy landscape of the protein to its one-dimensional projection along a single, easily measurable reaction coordinate, i.e., the displacement distance measured along the vector of force application. This gives an additional advantage in the form of a "geometrically relevant" reaction coordinate, which can be used to obtain structural information on the transient structures encountered along the folding/unfolding pathway.[274,275] Since the force applied by nanomanipulators can be described in most cases by Hooke's law (i.e., applied force increases linearly along the reaction coordinate), the protein's energy landscape is modified at each point in a known way, basically being reduced by an amount equal to the mechanical work performed on the analyte. The net result is that the energy landscape is "tilted" by force to favor states occurring at high displacements more than those occurring near the equilibrium position (Figure 16) and high-energy states become increasingly populated (and thus more easily observable), allowing the approximate reconstruction of the complete unperturbed energy landscape at zero applied force employing methods based on Kramers theory.[227] Despite its simplicity, this approach is able to broadly capture the basic features of protein folding and unfolding,[226,276] even though subtler transitions occurring in near-equilibrium conditions such as those of IDPs are best discussed in terms of more sophisticated models.[277−279] Methods commonly employed for reconstructing the energy landscape starting from a series of mechanical measurements are slightly different for each specific SMFS protocol and will be broadly summarized in the next paragraphs.

Several different strategies to perform SMFS experiments on proteins with AFM and OT instruments, mostly differing in the specific protocol of force application to the sample, are described in the literature. The most common are by far the so-called force clamp (or constant force) and velocity clamp (or constant velocity) modes. Force clamp experiments are more commonly performed with OT instruments, but ad-hoc modified AFM apparatuses can be also used with excellent results.[280] Even though OT instruments would also be suited to perform velocity clamp experiments due to a number of practical considerations (such as the relatively high involved forces and loading rates) these are instead almost exclusively performed on AFM instruments.

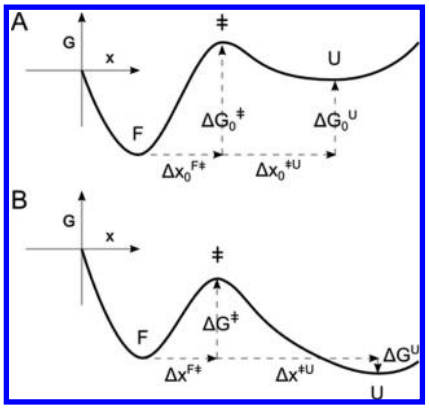

Figure 16. (A) Projection on the mechanical reaction coordinate (x) of the free energy (G) landscape of an unfolding protein, modeled as a two-state system. The folded (F) and the unfolded (U) states are separated by the transition state (‡). The height of the unfolding barrier at zero applied force $\Delta G_0^{\ddagger}$ determines the unfolding reaction rate, while the free energy difference between F and U in the absence of force ΔG_0^{U} determines the relative population of the two states. (B) Effect of an applied force on the energy landscape A. Each point is lowered by an amount which is linearly dependent on x. The resulting values for $\Delta G^{\ddagger}$ and ΔG^{U} are lower than their unperturbed counterparts $\Delta G_0^{\ddagger}$ and ΔG_0^{U}. Under an applied favorable force the unfolding rate and the population of the unfolded state are thus increased. It is important to note that the relative positions along x of the three states F, ‡, and U in the unperturbed energy landscape, described by $\Delta x_0^{F\ddagger}$ and $\Delta x_0^{\ddagger U}$, do not coincide with the corresponding values $\Delta x^{F\ddagger}$ and $\Delta x^{\ddagger U}$ under the effect of an applied force. The amounts of their shifts along x depend on the local curvature of the energy landscape.[268]

In force clamp experiments, the SMFS apparatus is used to exert on the analyte a force which is kept constant over time. The applied force can bring the energy of two selected states (e.g., a folded and an unfolded state) to similar values, so that continuous equilibrium transitions or "hopping" between the two states becomes detectable with sufficiently long observation times. The different states correspond to minima of the energy landscape occurring at different points along the reaction coordinate and correspond to different elongations of the analyte molecule. Hopping is thus recorded by the instrument as a series of repeated changes of analyte elongation. This allows a direct comparison of the dwell time distribution of each different state, which can be used to quantitatively infer equilibrium free energies and kinetic constants using several different methods[280] including hidden Markov models[281] and signal-pair correlation analysis.[282]

It is apparent from the above that force clamp SMFS ultimately rely on the ability of the chosen experimental apparatus to stably maintain a known value of the applied force with as little perturbation as feasible for relatively long times. While conceptually simple, this is not a trivial task at the single-molecule scale. The most common approach used with both OT and AFM systems is the so-called "active" clamp, in which a feedback loop adjusts the position of the optical trap (OT)[283,284] or the substrate (AFM)[251,280] based on real-time monitoring of the force effectively applied to the analyte. While active force clamp SMFS proved to be a powerful tool for investigating several biomechanical phenomena[46,47,250,268,273,280,285] its main drawback appears to be particularly limiting in the context of IDPs. This drawback stems from the fact that active feedback loops have a finite

dx.doi.org/10.1021/cr400297g | Chem. Rev. 2014, 114, 3281−3317

response time which hinder efficient force stabilization in the microsecond time scale and ultimately limits the measurement bandwidth to less than 1 kHz.[283] This limitation can be circumvented by careful optimization of the experimental setup, reaching feedback response times of a few microsecond.[286] Block and co-workers instead addressed this issue with the introduction of an all-optical "passive" force clamp strategy, which takes advantage of the flat anharmonic region of the optical trap and allows even higher bandwidths to be reached.[287]

In AFM velocity clamp SMFS experiments, the piezo electric actuator is retracted from the cantilever contact position at a constant speed, typically in the 10−5000 nm/s range. During the retraction the force exerted on the analyte is left free to vary without any feedback loop, while mechanical events are recorded in force/retraction plots. Since the values of piezo displacement and the effective separation between the points of force application on the analyte are not coincident due to varying cantilever deflection, the collected force/retraction plots must be first transformed into force/distance plots. These can be then used to infer information on the energy landscape of the induced transition. While technically much faster and simpler to perform than force clamp experiments, velocity clamp SMFS produces data sets that are considerably harder to interpret and even more importantly their interpretation crucially relies on a set of simplifications and assumptions made about the energy landscape under study.[46,236,288−291] The model derived from Kramers' theory[227] by Evans and co-workers[224,225] is still the most widely employed, and even though it entails radical simplifications its results are surprisingly close to those of more refined models.[224,226,236,281] Although special precautions can be taken,[215,292] the common AFM drift problems mentioned in section 2.2.1 limit the range of practicable retraction speeds to values which are most suited to study out-of-equilibrium unfolding transitions. The position of unfolding transition states along the reaction coordinate can be determined relatively easily with the "dynamic force spectroscopy" (DFS) approach,[236,289,291] while refolding can be studied using multipulse protocols.[252,274,275,293]

On the basis of the brief summary of SMFS apparatuses and techniques applicable to the study of protein energy landscapes provided above, some general considerations can be made regarding their suitability to IDPs. First and foremost, a comparison between the submicrosecond time scales revealed by other techniques for conformational changes of unstructured peptides[48] and the much longer experimentally accessible time scales of almost all SMFS experiments reveal a major discrepancy. Moreover, even the lowest currently achievable applied forces (few pNs) currently required by SMFS experiments, when acting on the very shallow energy landscapes of IDPs, arguably favor elongated states to the point of making transient compact states invisible, even though recent theoretical and experimental improvements promise to represent a solution of this problem in the future.[277,294] Taken together, these considerations imply the fact that at the current state of the art SMFS experiments cannot reliably observe the unperturbed conformational distribution of a mostly unstructured protein region as it is possible to do with, e.g., fluorescence methods. However, the same characteristics make SMFS methodologies very well suited to study processes which imply occasional acquisition of structure by largely disordered regions and to dissect complex reaction pathways by measuring quantitative parameters of its constituent processes, as exemplified in several of the works reviewed in the following section.

2.2.2. Single-Molecule Force Spectroscopy Spectroscopy of IDPs. A clear increase in the number of papers related to SMFS of IDPs is evident during the last 2 years, probably prompted by recent technical advances and increased attention to the concept of protein disorder in general. To the best of our knowledge, the first papers entirely devoted to the description of SMFS experiments performed on full-length IDPs appeared in 2008,[57,295] when the groups of Samori[57] and Lyubchenko[295] almost simultaneously applied AFM SMFS to the study of the same IDP, human alpha synuclein (αSyn). An experimental SMFS approach previously employed to characterize intermolecular interactions between fragments of αSyn[296] was modified by Lyubchenko and co-workers[295] and applied to the full-length protein. This approach required the covalent anchoring of αSyn molecules to both the AFM cantilever tip and the mica surface via their flexible C-termini through silane chemistry. The functionalization had be optimized so that the final αSyn surface density was low enough for bimolecular encounters to be the most probable when tip and surface are brought into close proximity. The velocity clamp SMFS data collected by repeating approach/retraction cycles revealed an occasionally enhanced interprotein interaction attributed by the authors to the acquisition of structure by the transiently formed αSyn dimers (Figure 17). DFS data collected at various loading rates allowed them to observe two different lifetimes for the transient interactions, both of which were measured to fall in the seconds time range. Since these values are much higher than characteristic for the dynamics of monomeric αSyn, one interpretation of these results could be that occasionally formed stable αSyn dimers might function as nuclei for amyloidogenic aggregation, even though the ranges of pH (2.7−5.1) at which the first measurements were performed limit their direct physiological applicability.[295] The authors then refined their observations in successive papers describing the impact of metal ions on the phenomenon.[297,298]

Rather than investigating intermolecular dimer formation, the experimental approach proposed by Sandal et al.[57] focused on elucidating the behavior of αSyn in its monomeric form. Inspired by the work of Fernandez and co-workers,[299] multidomain protein chimeras containing the full-length αSyn sequence were produced and their mechanical behavior was measured via velocity clamp AFM SMFS.[300] The inclusion in the chimeric polyprotein ensured that amyloidogenic aggregation was prevented during the measurement and that signals originating from αSyn monomers could be distinguished from spurious signals. The experiment revealed a surprisingly high proportion of compact states capable of offering significant resistance to mechanical unfolding (Figure 18). An extremely heterogeneous class of mechanically weak interactions was detected as well as a more homogeneous class of conformations having SMFS signals compatible with extensive acquisition of β structure. The authors proposed that this observation demonstrated the ability of the αSyn monomer to sporadically populate a β-containing form which could be relevant to the mechanism of accretion to fibrils. The same approach was used to show that factors linked to enhanced Parkinson pathogenicity, such as the presence of metal ions[57] or familial αSyn point mutations,[301] substantially increased the amount of observed compact structures.

Since neither the lifetimes of the occasionally acquired "β-compatible" structure nor its relative abundance with respect to

dx.doi.org/10.1021/cr400297g | Chem. Rev. 2014, 114, 3281−3317

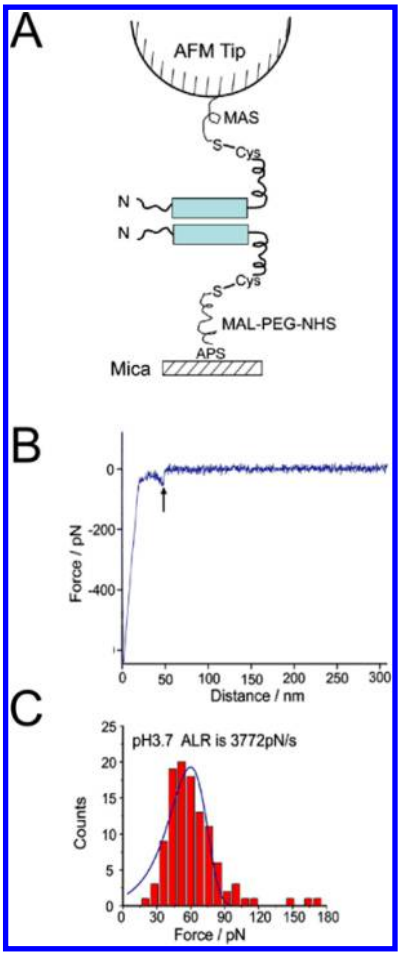

Figure 17. αSyn intermolecular interactions probed via AFM-based SMFS as reported by Yu et al.[295] (A) Schematization of the experimental setup: αSyn molecules are covalently anchored via silane chemistry to the AFM probe and a mica surface in a reciprocal orientation that should enhance contacts between the respective amyloidogenic N-terminal regions (gray boxes). (B) Force curve representative of those considered to contain the mechanical rupture signature of a bimolecular αSyn interaction at pH 3.7. (C) Rupture force distribution for the mechanical events exemplified in B. The continuous line is the fit of the experimental data collected at pH 3.7 with the probability density function (PDF). The maximum of the PDF was found to be at 61.6 ± 2.3 pN. Reprinted with permission from ref 295. Copyright 2008 Elsevier.

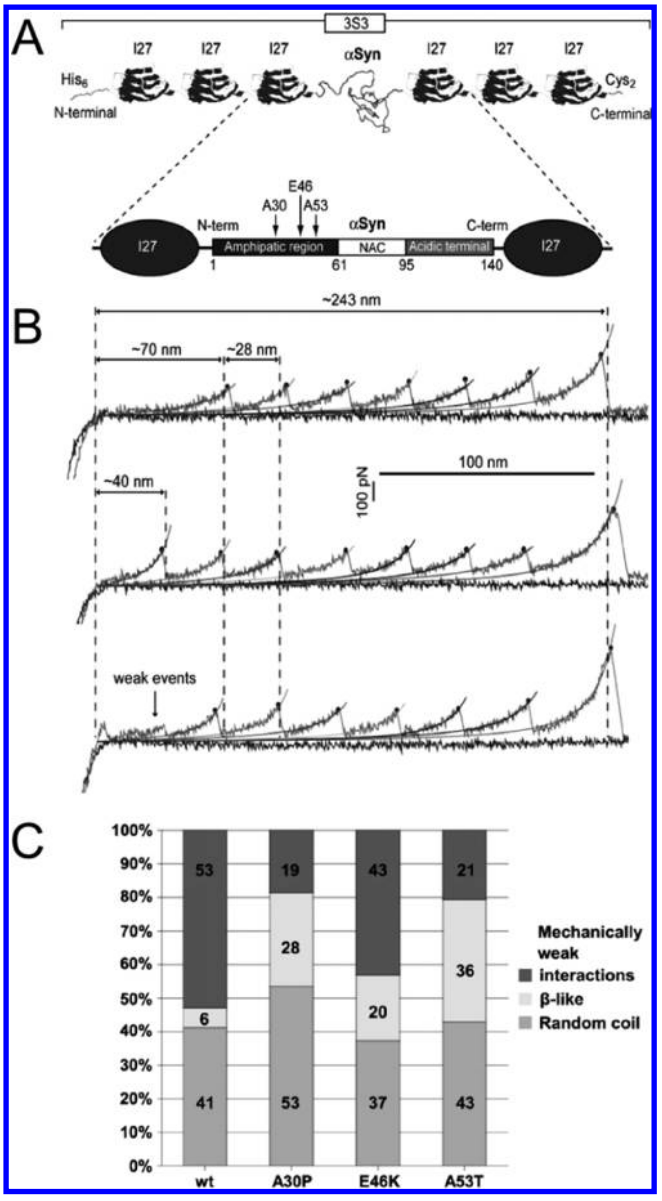

Figure 18. (A) Schematization of the chimeric polyprotein constructs employed in refs 57 and 301 for studying the mechanical unfolding behavior of monomeric αSyn. The analyte sequence is flanked on both sides by three I27 modules serving as internal force gauges and molecular handles. (B) Force curves representative of the three types of mechanical behavior shown by αSyn, compatible with the expected signals of three broad types of conformations (from top to bottom, mostly random coil, β-structured, and compact non-β conformations). (C) Relative abundance of the three classes of mechanical behavior shown by WT αSyn and its pathological mutants A30P, E46K, and A53T. Adapted with permission from ref 301. Copyright 2009 Wiley-VCH.

disordered and partially structured states were found to be compatible with observations performed on free monomeric αSyn in solution, it is quite probable that the inclusion of the IDP in the chimeric construct heavily modified its behavior. In a subsequent paper, the authors discussed some of the factors that could contribute to this conformational bias,[301] including electrostatic interactions and modification of the average end-to-end distance due to the presence of the "molecular handles", molecular crowding, vicinity to the surface, and others. However, the abundance of αSyn states showing substantial mechanical response in several AFM SMFS studies[56,57,255,300−302] suggests that states containing a high proportion of β structure, although not frequently visited by free monomeric αSyn, could become readily accessible after perturbation of the energy landscape via intramolecular interactions. As recently reported by Irbäck and co-workers,[303] all-atom Monte Carlo simulations[303] seem to support this view. Since the accretion of disordered monomers to growing amyloid fibrils entails a large entropic penalty, the free energy landscape of αSyn could be particularly prone to perturbations by intermolecular interactions morphing it into a funnel, progressively driving molecules toward fibril-like folds.[303]

An elegant refinement of the experimental strategy outlined above was recently introduced by Carrion-Vazquez and co-workers[56,255,302] via the development of cloning/expression vectors termed "pFS" (plasmids for force spectroscopy). The pFS-2 plasmid in particular was designed to express chimeric

dx.doi.org/10.1021/cr400297g | Chem. Rev. 2014, 114, 3281−3317

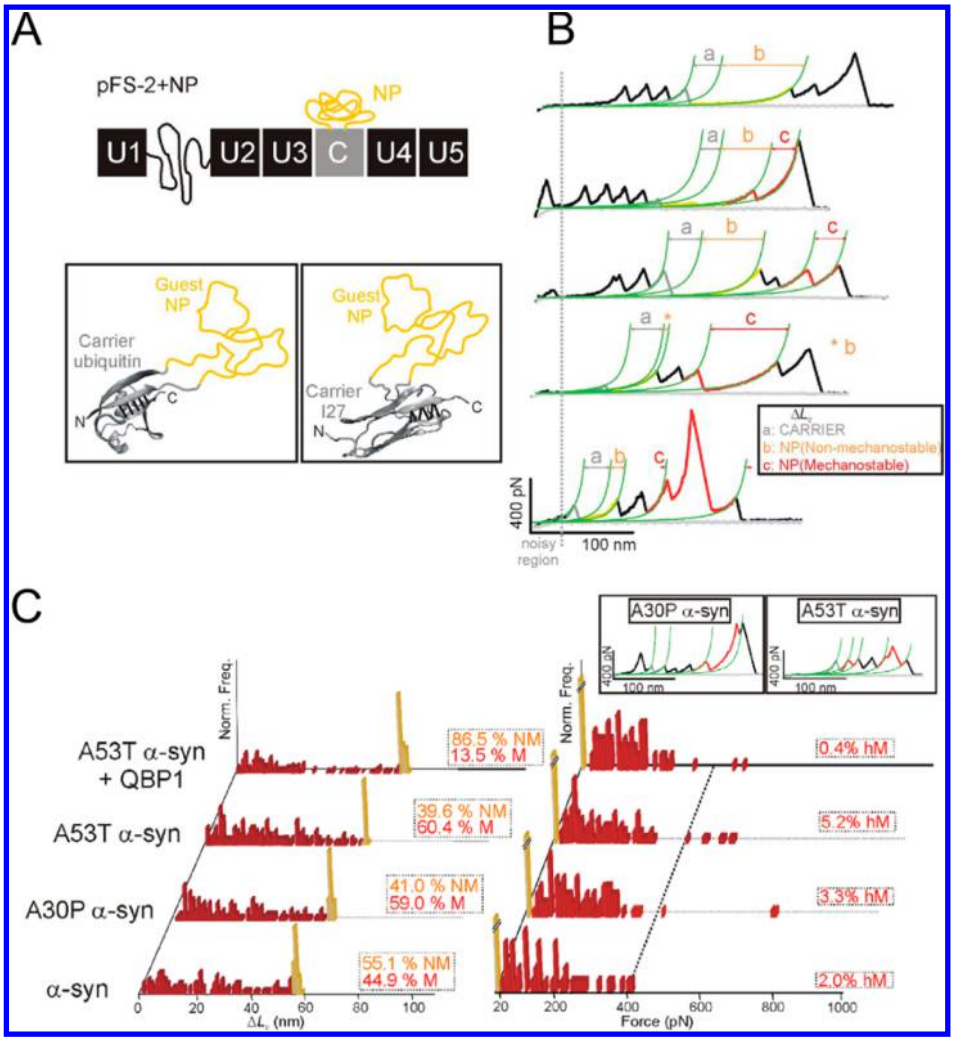

Figure 19. (A) (Top) Schematic representation of the pFS-2 polyprotein employed in refs 56, 255, and 302. Analyte neurotoxic protein (NP, in orange) is mechanically protected by the carrier module (C, in gray), flanked by ubiquitin repeats (U, in black) working as internal force and contour length gauges. (Bottom) Cartoon representation of the ubiquitin (left) and titin I27 (right) carrier–guest constructions used in the pFS-2 vector. (B)Representative mechanical unfolding traces of pFS-2+Sup35NM. Several different conformations adopted by the analyte Sup35NM region can be discerned, ranging from featureless random coil traces ("non-mechanostable", orange) to compact conformations with different degrees of mechanical stability ("mechanostable" and "hyper-mechanostable", red). (C) Contour length (left) and rupture force (right) distributions of the αSyn signals in pFS-2+αSyn mechanical unfolding traces. Mutants A30P and A53T are found to increase the abundance of mechanostable conformers with respect to W, while 20 mM QBP1 decreases the formation of compact conformers in A53T. The two insets show curves containing the mechanical signature of "hyper-mechanostable" A30P and A53T conformers. Adapted from ref 302.

protein constructs having a number of desirable features for AFM SMFS velocity clamp experiments performed on IDPs, i.e. a long unstructured chain acting as a spacer to bypass the typically noisy AFM proximal region, a homomeric polyprotein internal force gauge, and a carrier domain protecting the protein of interest from uncontrolled mechanical stress (Figure 19A). Taken together, these features should allow one to avoid the stringent data selection[57] required by AFM SMFS studies, especially when the protein under study has a weaker mechanical stability than those of the force marker as in case of IDPs. In turn, this should make it possible to experimentally measure subtler mechanical features of IDP behavior.

This "carrier/guest" approach was first tested by Oroz et al.[255] by grafting into the pFS-2 vector the nonfibrillogenic, intrinsically disordered cytoplasmic region of synaptobrevin (VAMP2) from *Rattus norvegicus*. The totally featureless stretching behavior of the IDP was unequivocally determined via AFM SMFS, confirming the validity of the approach. In a subsequent work,[302] the authors applied the same methodology to a representative selection of four conformationally polymorphic proteins involved in neurodegenerative diseases: polyglutamine (polyQ) stretches of three different lengths for Huntington's disease, β-amyloid$_{1-42}$ (Aβ42) for Alzheimer's, αSyn for Parkinson's, and a yeast prion extensively used as a human prion model (Sup35NM, Figure 19B). It is interesting to note that all these IDPs are found intracellularly and thus potentially subject to mechanical stresses exerted by protein processing machinery.[304] All the neurodegeneration-related proteins showed conformational polymorphism, and the possibility that the observed acquisition of structure was artifactually induced by the close proximity of the disordered region with the carrier domains was ruled out by several control experiments.

The same experimental approach, when applied to Aβ42,[302] revealed a high degree of polymorphism. The possibility that the observed perturbations of ideal WLC behavior were

dx.doi.org/10.1021/cr400297g | *Chem. Rev.* 2014, 114, 3281–3317

originated by intermolecular interactions occurring during the experiment due to the high aggregation propensity of the peptide was ruled out via preincubation of the pFS construct with the SV111 peptide,[305] a strong inhibitor of Aβ42 aggregation: experiments performed in the presence of SV111 yielded similar results to those executed in its absence. The familial-disease Arc Aβ42 (E22G) mutant was observed to assume "mechanostable" (MS) and even "hyper-mechanostable" (hMS) conformations more than its wild-type (WT) counterpart, while the double mutant F19S/L34P, known to be less prone to fibrillogenesis, behaved instead like an ideal random coil, remarkably showing complete absence of mechanical events. Hervas et al. also explored the mechanical behavior of αSyn via the pFS approach,[302] confirming that the WT IDP adopted a MS conformation in almost one-half (45%) of the recorded traces, while two pathogenic (and more fibrillogenic) mutants significantly increased the prevalence of hMS states (Figure 19), as previously found by Sandal et al.[57,301] Interestingly, the QBP1 peptide,[306] when present in micromolar amounts, was able to drastically depress the MS and hMS population in the A53T αSyn mutant. In the same paper, the degree of polymorphism of Sup35NM was shown to be even more prominent than those of polyQ, Aβ42, and αSyn, and also in this case the QBP1 peptide shifted the conformational equilibria toward the most unstructured conformers. On the basis of the above results, the authors proposed the concept of "proteinoscleroses" linking all the neurodegenerative cascades.[302]

AFM SMFS experiments performed on the polyQ-containing pFS construct[302] allowed the authors to show that the Q_{19} tract, which has a length considered to be subthreshold for the triggering of polyQ diseases, showed no detectable MS conformations. Conversely, the Q_{35} (near-threshold) and Q_{62} (superthreshold) tracts showed increasingly common MS and hMS conformations whose unfolding required the application of forces in excess of 400 pN. On the basis of these results, the authors propose that polyQ tracts with lengths of more than 35 amino acids can undergo a transient acquisition of structure that might correspond to β-sheet-containing conformations.

The behavior of polyQ tracts was also studied via force clamp AFM SMFS experiments by Dougan et al.[307] Multiple polyQ stretches of different lengths (Q_{15}, Q_{25}, Q_{50}, and Q_{75}) were inserted in chimeric polyprotein constructs in which titin I27 domains (whose role was mainly to act as force markers and spacers) flanked each disordered domain. Irrespective of their lengths, all polyQ tracts offered significant resistance to mechanical elongation under applied load (Figure 20). The authors suggest that polyQ peptides can form a heterogeneous ensemble of mechanically stable collapsed structures and show how the formation of compact conformations is disrupted by proline point mutations. The mechanical extensibility of polyQ residues was also shown to be a function of the exact position of the proline mutation along the chain.

According to the respective authors, the mechanical resistance to elongation of polyQ stretches with a length above 15[307] or 35–40[302] residues, as observed via force clamp[307] or velocity clamp[302] SMFS experiments, is caused by their ability to sporadically[302] or continuously[307] assume compact, globular-like conformations able to sustain extremely high mechanical loads. The observed unfolding forces of these compact conformations are extremely (and surprisingly) high, far exceeding those of β-sheet-rich globular proteins in their native fold: Hervas et al.[302] observed the rare (~1–3%)

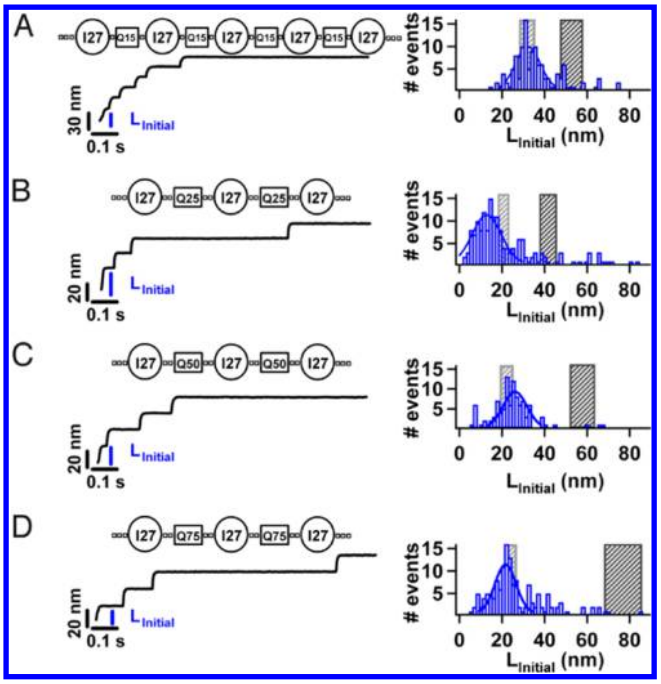

Figure 20. Mechanical properties of homopolypeptide chains as reported in Dougan et al.[307] Chimeras containing tandem repeats of the titin I27 module and polyglutamine chains of different length, namely, Q15 (A), Q25 (B) Q50 (C), and Q75 (D), were studied via force clamp AFM SMFS. (Left) Representative extension versus time plots of all constructs at an applied force of 180 pN. (Right) Distributions of the initial extension measured at the first mechanical event in traces containing the full mechanical signature of the marker I27 domains. For all constructs, significant mechanical resistance to unfolding was measured prior to reach elongations corresponding to the full extension of the construct with folded I27 domains (black shaded areas in right column histograms). Reprinted with permission from ref 307. Copyright 2009 National Academy of Sciences.

occurrence of HMS structures in Q_{35} and Q_{62} polyQ stretches, whose elongation required forces in the range of 400–800 pN, while Dougan et al.[307] reported the total inextensibility of Q_{50} tracts up to forces of 800 pN. The authors attribute those unusually high values to either the formation of extensive β-sheet structures[302] or the presence of an extensive network of intrachain interactions, which should cause the distribution of the applied force over several points simultaneously.[307] As noted by Dougan et al.,[307] the two hypotheses are mutually incompatible, as the distribution of construct lengths measured in their force clamp experiments at the onset of the first mechanical event is incompatible with the presence in the polyQ tracts of mechanically stable but geometrically elongated structures such as β-sheet. A further discrepancy also seems to exist between the two sets of experimental data mentioned above: in the force clamp experiment,[307] Q_{50} tracts show extreme mechanical resilience even to prolonged (~12 s) application of forces of several hundred pN, while in the velocity clamp experiment polyQ tracts of comparable length fail to yield a mechanical signal in the vast majority (>97%) of cases.[302]

It is not easy to give a definitive answer to the above issues recurring to available literature on polyQ stretches. Several independent measurements and simulations performed on monomeric polyQ homopeptides suggest that they are intrinsically disordered in aqueous solvents,[154,308–311] and FCS measurements show a distinct preference for collapsed

dx.doi.org/10.1021/cr400297g | Chem. Rev. 2014, 114, 3281–3317

structures in water.[154] The origin of this behavior may be that glutamine side chains contain primary amines that can compete with the solvent for backbone interactions, thus lowering the radius of gyration and favoring collapsed structures. However, this enhanced tendency to populate compact conformations does not imply an equally enhanced tendency to form ordered structures[309] since polyQ's augmented repertoire of intramolecular backbone interactions is not linked to specific backbone conformations; as a consequence, the entropic cost linked to structural transitions occurring at specific dihedral angles values is increased, making the formation of, e.g., β-sheets thermodynamically unfavorable.[308,310,311] No evidence for a differential, length-dependent propensity of polyQ to undergo substantial conformational changes (e.g., involving the acquisition of β structure) was evidenced by MD simulations[310,311] based on a continuum solvation model.[312]

The same velocity clamp AFM SMFS experimental strategy previously applied to the study of αSyn[57,300,301] was employed by Muller and co-workers to characterize the transient intramolecular interactions taking place in the 441 amino acid (aa) long, intrinsically disordered, monomeric human tau protein (hTau40).[313] Their data suggest that intramolecular interactions promote two different types of transient folding. Interactions localized in the repeat domain stabilize folds of ~19 aa and ~42 aa stretches which tend to promote aggregation, while those occurring at the unstructured N-terminus promote the folding of long (>100 aa) stretches of random length that prevent aggregation. The aggregation-promoting single-deletion mutant linked to frontotemporal dementia, hTau40/ΔK280, was observed to promote the folding occurring at the repeat domain and to suppress those taking place at the N-terminus. This observed trend was completely reversed in the antiaggregant mutant hTau40/ΔK280/PP. Moreover, the aggregation inducer heparin was found to promote strong intramolecular interactions in both hTau40 and hTau40/ΔK280, which favored aggregation-prone conformations.

In 2005, a pioneering investigation via force clamp OT SMFS of the folding/unfolding transitions of RNase H by Bustamante and co-workers[285] revealed the existence of a compact, on-pathway intermediate state that was suggested to be identical to the early folding state forming in the absence of applied force. Prompted by this result and similar indications from FRET measurements,[172,314] Ritort and co-workers posed the question whether it was possible to infer structural information on this type of unstructured intermediate state from the SMFS experiments.[315] They answered by proposing a phenomenological model that approximates the behavior of the analyte protein in SMFS experiments to that of an on-lattice heteropolymer under applied mechanical load,[315] choosing its end-to-end extension as the reaction coordinate. On the basis of the semiquantitative output provided by that model, it was possible to propose experimental SMFS protocols specifically conceived to help investigate transient intermediate states. They also suggest that the same protocols could be used to help unveiling local structure acquisition processes occurring in globally disordered proteins containing a mixture of structured and unstructured regions.

An ongoing series of excellent papers relevant to the force clamp OT SMFS investigation of disordered proteins and regions was published by Woodside and co-workers during the last years, a selection of which will be discussed here.[282,294,316,317] Gupta et al.[294] provided experimental validation to a theoretical work by Hummer and Szabo[223,229] in which the authors described a method that allows the reconstruction of energy landscapes from nonequilibrium SMFS data. This method, based on an extension of the Jarzinsky equality,[231−235] had been first applied by Bustamante and co-workers[303] and successively by Harris et al.[304] to SMFS experiments.[318,319] The results of force clamp and force ramp OT SMFS measurements performed on DNA hairpins with distinct, sequence-dependent folding landscapes were compared[294] showing quantitative agreement between the energy profiles given by the nonequilibrium reconstruction method and by the equilibrium probability distribution method.[277] The same approach was tested on the *add* adenine riboswitch aptamer, which visits three partially folded states, some of which have very low dwell times in physiological conditions. While the overall profile of the energy landscape could be successfully reconstructed, some of the states were found to be difficult to resolve due to low occupancy or potential well overlapping. The ability of reconstructing multistate energy landscapes through different compatible SMFS experimental methods, although technically challenging in some cases,[294] could represent an important tool for the study of IDPs.

A recent work by the same group[282] discusses the main drawbacks of the most common methods employed for extracting kinetic information from state-switching trajectories obtained via SMFS experiments. Briefly, kinetic analysis is performed via dwell time distributions,[320] which are in turn reconstructed by assigning discrete states to specific regions of the measured SMFS signal trajectories.[321] As often happens in other techniques sharing similar issues, this assignment is of crucial importance and can be performed via several different algorithms,[322] from simple thresholding, to maximum likelihood methods,[323] to hidden Markov modeling,[324] and correlation function fitting.[325,326] Application of all these methods to the study of multistate systems in particular is problematic. The method proposed by Hoffmann and Woodside[282] is a new type of correlation analysis particularly suited to multistate systems, similar to one previously applied to FRET measurements.[165] Briefly, the signal is divided into discrete ranges, and the time correlations between each pair of ranges are calculated. Different kinetic models are then tested by numerically fitting all the resulting cross-correlations with the functions derived for each of them in the kinetic scheme; this allows choosing the most probable scheme and calculating all the associated rates. As a practical demonstration of their approach, the authors performed force clamp OT SMFS on several model molecules, including the largely disordered protease-resistant fragment of the C179A/C214A mutant of the hamster prion protein. The signal-pair correlation analysis allowed the detection of a rarely occupied intermediate state and its univocal positioning in the overall folding/unfolding reaction scheme as an off-pathway intermediate reached from the unfolded state only. This remarkable achievement would not have been a trivial task using other, established methods. An extension of the same approach[317] was subsequently employed (Figure 21) to derive, from the full energy landscape of truncated WT hamster, SHaPrP(90−231), several crucial quantities which are notoriously very difficult to experimentally determine with any established method, such as the diffusion constants for barrier crossing and the transition path times across the barriers.

The ability of a truncated form of the WT syrian hamster prion protein, SHaPrP(90−232), to follow nonnative folding

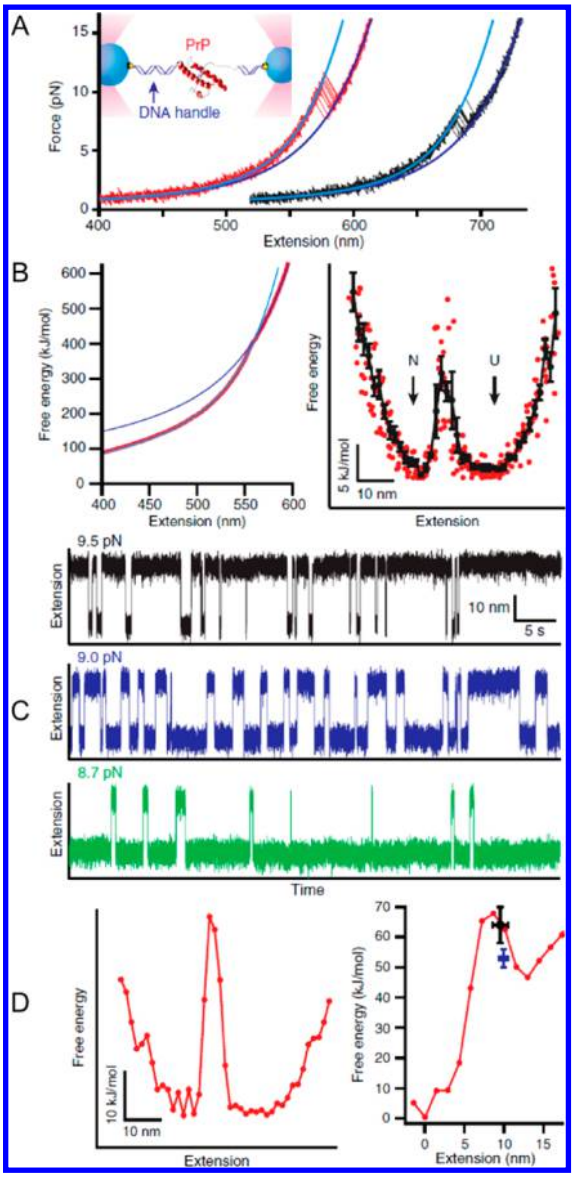

Figure 21. Characterization of the PrP unfolding energy landscape via passive force clamp OT experiments, as described in Yu et al.[317] (A) Unfolding (red) and refolding (black) force–extension curves obtained by ramping up the force applied on a PrP-containing DNA–protein construct (inset) prepared as described by Cecconi et al.[265,327] Continue lines are WLC fits of the folded and unfolded states. Abrupt contour length changes are observed at a force of ~9 pN, corresponding to folding and unfolding transitions (here occurring in a two-state process). (B) (Left) Free energy profile at zero force reconstructed from the force–extension traces exemplified in A via the Hummer–Szabo method,[226,276] mostly determined by the elastic behavior of the DNA handles. (Right) PrP energy landscape under an applied force of 9.1 pN displayed as the average (black line) of different sets of force–extension curves (red dots). (C) Extension vs time plots recorded at different constant forces, showing a clear two-state folding–unfolding behavior. The force $F_{1/2}$ at which the two folding states were observed to be identically populated was again ~9 pN. (D) (Left) Unfolding free energy profile at $F_{1/2}$ after deconvolution. (Right) Same energy landscape "tilted" to 0 pN applied force. The position and height of the energy barrier is shown to be in excellent agreement with the values (black, unfolding; blue, refolding) found via kinetic analysis of force–extension curves exemplified in A and B. Adapted with permission from ref 317. Copyright 2009 National Academy of Sciences.

pathways was explored by Yu et al.[316] via passive force clamp OT SMFS. No experimental support was found to the extensively discussed hypothesis that some form of partially folded intermediate visited by individual PrP molecules en route to their native state could mediate misfolding and subsequent prion pathogenicity. Instead, while the native folding pathway was found to involve no detectable intermediates, the unfolded state was observed to undergo frequent transitions into off-pathway, marginally stable intermediates. Three different misfolding pathways starting from the unfolded state were detected, and PrP was determined to visit these with a higher frequency than the native folding reaction. The combined calculated values for the formation rates of the off-pathway intermediates imply that around 90% of the structure acquisition attempts by unfolded PrP lead to non-native, transient conformations. Interestingly, no evidence for structure formation within the disordered N-terminus was recovered. A PrP double mutant (C179A/C214A), known to form oligomers rich in β structure, was also investigated with the same methodology, revealing an increased occupancy of the same off-pathway misfolded states with respect to WT PrP, suggesting that these could act as intermediates leading to oligomerization.

2.3. Single-Nanopore Techniques

Widespread discussion about the practical feasibility of nanopore sequencing[328,329] began during the early 1990s. Since then, the study of nanopore biophysics was propelled by substantial investments being steadily made in a potentially very remunerative technology which promised to give access to fast and inexpensive sequencing. While biosensors based on a general "particle through a hole" concept started to be patented as early as the 1950s,[330] constant refinement of fabrication and sensing methods was needed to reach the current technological level at which details of single molecules threading through a single nanopore can be detected. One of the most important advances toward nanopore biosensing was without doubt the patch clamp electrophysiological technique developed by Neher and Sakmann,[331,332] which demonstrated how it was possible to measure the ionic currents of single channels. As reported in Branton et al.,[333] during the early 1990s two groups independently proposed that individual bases of nucleic acid strands electrophoretically driven through a suitably sized nanopore could induce measurably different effects on the ionic current. Soon, one of those groups demonstrated how it was possible to force single-stranded DNA and RNA through an α-hemolysin nanopore and detect translocation events by monitoring the ionic current.[334] During the following years, nanopores gradually established themselves as a novel class of label-free, single-molecule biosensors mainly employed for nucleic acid sensing. Nanopore sensing started to be increasingly applied to the study of single-protein molecules in the recent past.[335] Issues in protein science investigated via nanopores include protein–DNA interaction,[336] protein–antibody interactions,[337] protein translocation,[338] and protein folding.[339] In particular, the exploration of proteins with disordered regions and IDPs using nanopore sensing seems to be accelerating in the past few years, as reported in several excellent reviews.[335,340−342]

2.3.1. Single-Nanopore-Sensing Instrumentation and Methods. The critical component of all nanopore-sensing apparatuses is a nanoscopic gap in an insulating barrier. The main types of pore used in this type of experiment can be

dx.doi.org/10.1021/cr400297g | Chem. Rev. 2014, 114, 3281−3317

divided into two classes, usually referred to as biological nanopores and solid-state nanopores. The first class refers to pores formed by proteins capable of self-assembling into complexes which puncture lipid bilayers. Thus far, most biological nanopore-sensing experiments were performed using the pore-forming toxins α-hemolysin and aerolysin, since they show continuous nongating conductance and a diameter that is well suited to the translocation of single-biopolymeric strands.[330] The second class refers to apertures[343,344] drilled with electron or ion beam in thin membranes of highly dielectric materials such as silicon nitride[340] with diameters in the 2−100 nm range.[340] Both types of nanopores were employed for the characterization of unfolded and disordered protein regions.

Irrespective of the details of its setup, a nanopore protein-sensing apparatus includes two reservoirs of aqueous solutions containing an electrolyte (usually KCl) and the analyte, separated by an insulating membrane pierced by a single hole. The reservoirs also contain nonpolarizable electrodes with fast kinetics (such as the Ag/AgCl electrode). The application of a constant voltage induces ion exchange across through the nanopore, thus closing an electrochemical circuit, resulting in a measurable steady-state ionic current (Figure 22). If the sole electrochemical reactions occurring are those related to the ion-exchange process, the system can exhibit ohmic response in specific bias windows, which has several practical advantages. Charged protein molecules are driven to, and through, the nanopore by a complex interplay of electrophoresis, electro-osmosis, and diffusion.[345] The nanopore interacts with translocating proteins, hindering their conformational freedom by temporarily confining them into a nanoscale volume. Single-molecule nanopore sensing is then obtained by real-time monitoring of some property during perturbations caused by the pore−protein interaction.

While several sensing strategies have been proposed for nanopores, the most commonly employed method remains ionic-current blockade sensing, sometimes called resistive pulse sensing[340] (Figure 23). Briefly, when the pore is free of any occlusion, a baseline ionic current usually referred as the open-pore current is measured. During nanopore−analyte interaction

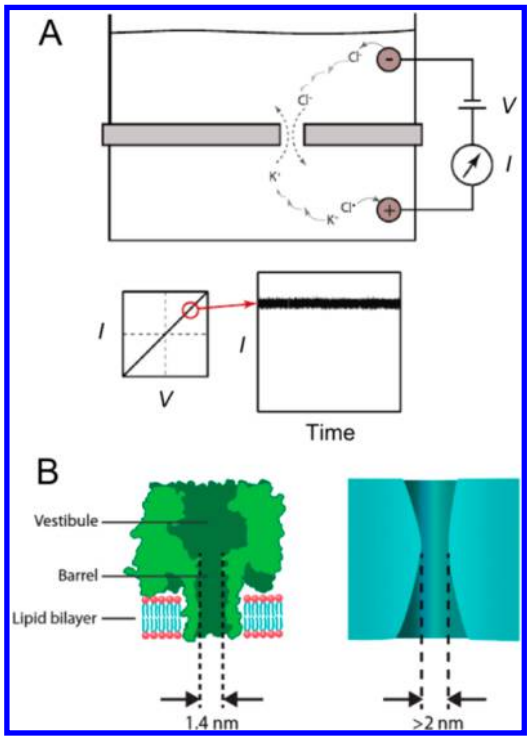

Figure 22. (A) (Top) General scheme of a single-nanopore-sensing apparatus. Voltage is applied across a single nanopore constituting the sole communication between two reservoirs, resulting in ion migration through the nanopore. (Bottom) Ion transport leads to a measurable steady-state current which is often linearly dependent on the applied voltage (see main text). (B) Examples of biological (alpha-hemolysin heptameric transmembrane complex embedded in a lipid bilayer, left) and solid-state (aperture in a silicon nitride membrane obtained by photolithographic methods, right) nanopores commonly employed in single-nanopore-sensing experiments. Adapted with permission from Wanunu[330] (Copyright 2012 Elsevier) and Miles et al.[340] (Copyright 2013 Royal Society of Chemistry).

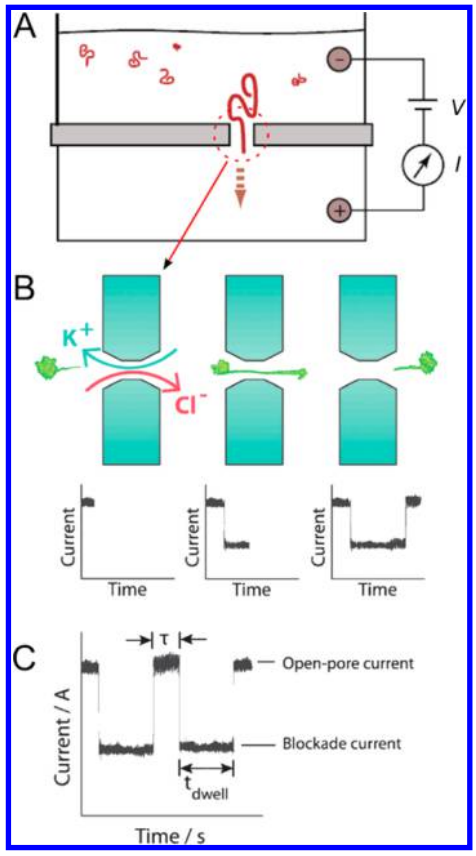

Figure 23. Sensing the translocation of single molecules through the nanopore via resistive pulse detection. (A) Applied voltage drives analyte molecules toward the nanopore through a complex interplay of different phenomena (see main text) resulting in multiple translocation events over time. (B) Details of a translocation event. (Left) When the pore is free from any obstruction by analyte molecules, the unhindered ionic transport is responsible for the steady-state baseline "open pore" current. (Middle) For the duration of each translocation event, ion transport is influenced by the analyte occupying the nanopore and the recorded current is different from the open pore current. (Right) After each ionic blockade event, the recorded ionic current reverts back to the open pore value. (C) Quantitative parameters of a translocation-induced resistive pulse: dwell time of the analyte in the nanopore, average amplitude recorded during the event, lag time between successive discrete events, shape of the current blockade. Adapted with permission from Wanunu[330] (Copyright 2012 Elsevier) and Miles et al.[340] (Copyright 2013 Royal Society of Chemistry).

dx.doi.org/10.1021/cr400297g | Chem. Rev. 2014, 114, 3281−3317

events, transient changes to the baseline current take place. These sudden changes are usually called blockades, since they often involve a reduction of ionic current due to partial or complete occupation of the aperture by the analyte. Quantitative parameters of the blockade, such as its duration, amplitude, and shape, depend on the type of pore−analyte interaction which caused it and can thus be ultimately mapped to specific properties of the analyte. In very general terms, blockade duration corresponds to the dwell time of the analyte in the pore, which for charged biopolymer molecules is a function of their length and of the amount of interactions occurring between them and the pore. The mean current amplitude recorded during a blockade can be considered a measure of the grade of pore occupancy during interaction, while the time elapsed between successive blockades is related to analyte concentration.[330,346,347]

As a more protein-specific example of the general considerations made in the previous paragraph, in Oukhaled et al.[348] a single α-hemolysin nanopore was employed to measure translocation events of proteins denatured to different extents using guanidinium chloride. The authors report three different classes of ionic blockades: long, short, and very short blockades (also called spikes or bumps). Bumps were ascribed to events in which folded molecules with diameters largely exceeding that of the nanopore simply collided with the pore and then diffused away. The short blockades were linked instead to the passage through the pore of unfolded molecules offering no resistance to translocation, and their frequency (but not their duration) was found to be a function of denaturant concentration. The longest blockades were instead caused by partially structured conformations able to thread through the pore but possessing residual structure capable of hindering their passage. The duration of these blockades was inversely proportional to denaturant concentration.

As recently discussed by Wanunu in an excellent review paper,[330] three different but related resolution limits are relevant to nanopore sensing: temporal, geometric, and current amplitude resolution. While the present current amplitude resolution is theoretically ∼1 pA, temporal resolution depends on measurement bandwidth, which in turn determines the fidelity of current recording, so these two resolution limits are inextricably related. The fastest reported nanopore-sensing measurements[349] can explore the submicrosecond range, an ability which could potentially be useful for inferring detailed information about disordered protein regions and IDPs. The geometrical resolution of a nanopore is instead related to its actual size and can cause problems when the analyte is small to the point of not being able to fully occupy the pore during translocation. For example, the geometrical depth of α-hemolysin nanopores constitutes a problem for the measurement of oligonucleotides with lengths of less than 12 bases,[350] suggesting that geometrical resolution should hardly be an issue for the nanopore sensing of full-length IDPs.

Interestingly, the publication of papers reporting biological or solid-state nanopore-sensing measurements of denatured or intrinsically disordered regions, including full-length IDPs, seems to be sharply accelerating in the early 2010s. In the next section, we will review a selection of the literature most relevant to the study of IDPs among the latest nanopore-sensing published works.

2.3.2. Single-Nanopore Sensing of IDPs. A series of papers discussing the nanopore translocation properties of structured proteins in partially or fully denaturing conditions appeared recently in the literature, shedding light on specific aspects of nanopore sensing which are potentially pertinent to the study of IDPs. Talaga et al.[351] measured the translocation events of single molecules of bovine β-lactoglobulin variant a (βLGa) and histidine-containing phosphocarrier protein (HPr) through a solid-state silicon nitride nanopore at different urea concentrations (0−8 M). The authors observed heterogeneous translocation event distributions, which they could quantitatively link to dwell times and excluded volumes of single molecules passing through the nanopore in folded, partially folded, or unfolded states. Specific details found in the signals were ascribed to translocation-stalling events, in turn influenced by the charge distribution pattern along the peptide chain. These details were demonstrated to be functional in defining which one of the two examined proteins originated a translocation signal and in which broad type of folding state. Moreover, the authors show how mechanical forces generated by physiologically relevant electrical potentials are able to unfold proteins. Oukhaled et al. studied the translocation through a solid-state silicon nitride nanopore of the recombinant maltose-binding protein (MalE) in folded and denatured states as a function of applied voltage,[352] revealing peculiar translocation dynamics they could associate to a specific free energy barrier. The unfolded conformations of the translocating proteins were found to be partially stretched by the electrical field. An analogous set of experiments on urea or thermally denatured bovine serum albumin (BSA) was reported by Freedman et al.[353] The authors discuss how it is possible to calculate the excluded volumes of various observed conformational states of BSA without the need for assumptions regarding the translocation times.

Experiments similar to those mentioned in the previous paragraph were also performed on biological nanopores. Pelta and co-workers utilized an aerolysin nanopore-sensing apparatus to analyze the entry and subsequent transport events generated by MalE in denaturing conditions,[354] quantitatively associating the durations of specific current blockades with the transport time of single molecules. The same results were compared and found to be in agreement with those obtained using an α-hemolysin pore.[355] In both cases, it was possible to distinguish between unfolded and partially folded states of transported proteins and between WT MalE and its destabilizing mutant MalE219[356] compared at the same denaturant concentration.

Literature reporting nanopore-sensing experiments performed on IDPs started to appear around 2010. Baran et al.[357] characterized via nanopore analysis the behavior of the recombinant murine myelin basic protein (rmMBP, an IDP involved in the development and stability of central nervous system myelin sheets) in the presence of Cu^{2+} and Zn^{2+} ions. The study was motivated by the fact that high amounts of Zn^{2+} are present in myelin and possibly stabilize it. The single-molecule nanopore translocation measurements allowed the authors to determine that both Cu^{2+} and Zn^{2+} induce folding or compaction of rmMBP into one or more conformations that are too large to pass through the pore (Figure 24). On the basis of their results, the authors also propose that the divalent metal ions could promote the acquisition of a specific tertiary structure which could reflect the (yet unknown) arrangement of MBP in myelin.

Madampage et al. employed an α-hemolysin nanopore-sensing apparatus to obtain conformational information on various forms of Aβ peptide, α-syn, and PrP.[342] Analysis yielded

dx.doi.org/10.1021/cr400297g | Chem. Rev. 2014, 114, 3281−3317

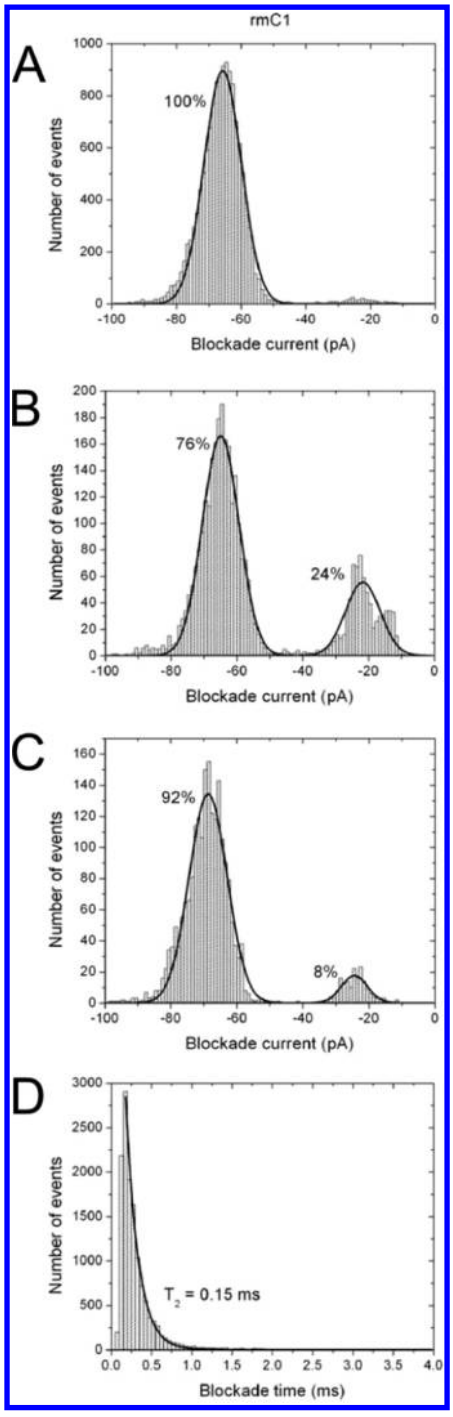

Figure 24. Ionic current blockade parameters measured for rmMBP translocation through an α-hemolysin nanopore at an applied voltage of 100 mV in 1 M KCl as reported in Baran et al.[357] (A–C) Blockade current distributions for (A) rmMBP, (B) rmMBP with 0.02 mM Cu^{2+}, and (C) rmMBP with 0.2 mM Zn^{2+}. (D) Blockade time distribution of the events included in A. The authors attribute the peak at −65 pA to translocation events and the one at −25 pA to transient protein–pore interactions termed "bumps". Both metal cations induce compact rmMBP conformations with enhanced tendency to bump against the pore rather than translocate through it. Reprinted with permission from ref 357. Copyright 2010 Elsevier.

quantitatively different translocation behaviors for Aβ40 and Aβ42 peptides. Interestingly, the familial mutant and Aβ40/D23N was found to have a translocation peak that could be ascribed to acquisition of a β-sheet-folded conformation in the monomer, which was observed to be less aggregation prone than the WT isoforms. WT α-Syn and its familial Parkinson-linked point mutants A30P, A53T, and E46K were also observed to behave differently when subject to nanopore translocation. While most interaction events between WT α-Syn and the nanopore were found to correspond to simple translocations as expected for such a highly charged IDP, the A30P and A53T mutants showed a lower frequency of translocation events and a much more heterogeneous repertoire of interactions. The same mutants produced bumping events of large oligomeric objects with a higher frequency compared to that of WT α-Syn and at least one further class of events possibly corresponding to specific folded intermediates. Interestingly, the E46K mutant showed instead comparatively more bumping events than WT α-Syn but no evidence of folded intermediates. Finally, the authors analyzed various PrP isoforms, evidencing different translocation behaviors for human PrP(23–231) and bovine PrP(25–242). Most recorded human PrP nanopore interaction events showed evidence for pore intercalation, i.e., transient occupation of the nanopore by unfolded portions of the protein, while a folded core could not easily translocate through the pore. The broader distribution of blockade currents generated by bovine PrP(25–242) suggests that the bovine protein has a larger range of possible interactions with the nanopore and thus a higher conformational flexibility than human PrP.

Japrung et al. studied the behavior shown upon translocation through a solid-state nanopore by two IDPs, a ligand-binding domain from an activator of thyroid hormone/retinoid receptors (ACTR) and the nuclear coactivator binding domain (NCBD) of the CREB binding protein, as well as their folded bimolecular complex.[358] Both IDP monomers were observed to translocate through the nanopore in different conformations, whereas their structured complex assumes only one stable conformation (Figure 25). A very interesting aspect of NCBD which could be measured with these experiments is that it undergoes charge reversal at higher than physiological salt concentrations, suggesting that local fluctuations in ionic strength or pH occurring in vivo could significantly impact the binding properties of NCBD.

Nanopore-sensing experiments are also suited for the detection of oligomerization and transient intermolecular complexation events, which are of particular relevance for the study of several IDPs. Lee and co-workers published a series of works discussing how the distribution of observed ionic current blockades induced by several different proteins containing disordered regions is significantly altered in the presence of potential binding partners.[359−362] The translocation behavior of the small Zn-finger module Zif268 through an α-hemolysin pore was observed by Stefureac et al.[359] in the presence of Zn^{2+} ions, revealing that the magnitude and duration of current blockades varied in response to the concentration of the divalent binding ion. In particular, increasing concentrations of Zn^{2+} ions corresponded to increasing amounts of bumping events, while the occurrence of translocation events correspondingly decreased. This result is in accord with the observation that the α-hemolysin pore is geometrically narrower than the Zn-induced fold of Zif268. Since several IDPs involved in neurodegenerative disorders are able to bind metal ions, this technique could be used to study the putative perturbations of their conformational ensembles induced by metals.

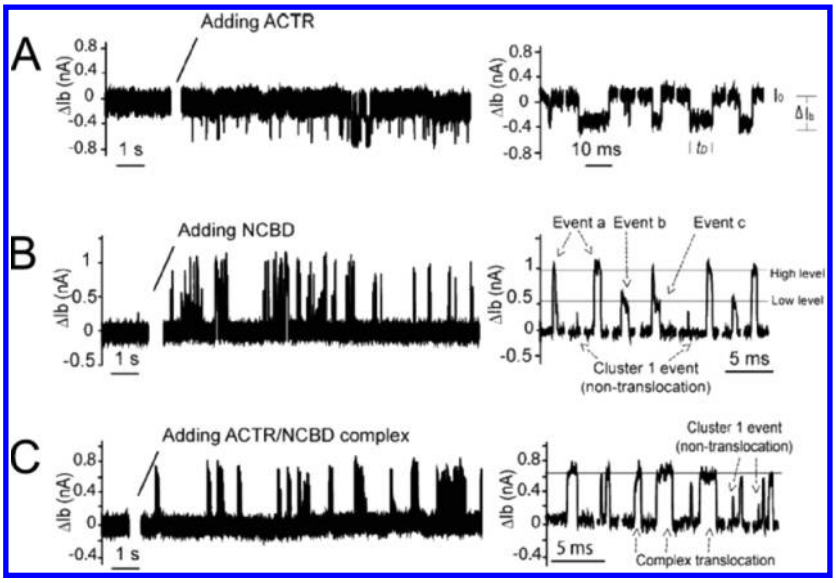

Figure 25. Translocation traces of (A) ACTR, (B) NCBD, and (C) the ACTR+NCBD complex through a solid-state nanopore in a silicon nitride membrane at an applied voltage of 300 mV as described in Japrung et al.[358] Both IDPs are observed to translocate establishing a variety of different interactions with the nanopore, while their structured complex only shows one type of event. Interestingly, both NCBD and the ACTR+NCBD complex show current enhancement during interaction with the pore, while ACTR induces resistive pulses. Reprinted with permission from ref 358. Copyright 2013 American Chemical Society.

The same approach was employed to study the interaction between two prion peptides chosen from the (143−178) region of recombinant bovine PrP and the monoclonal antibody M2188. The current blockade histograms recorded for PrP(143−169), which contains the M2188 epitope, changed considerably upon addition of the antibody, in particular showing a drastic reduction of translocation events and an increased preponderance of bumping events.[361] A control peptide not containing the epitope for M2188, PrP(168−178) was instead not effected to the same extent, although it was possible to detect a modest increase in its translocation time upon antibody addition, suggesting that transient intermolecular interactions could be possible. The experiment was also performed on full-length PrP. Upon addition of M2188, the ratio between translocation and bumping events decreased from 1:2 to 1:10 for the full-length protein, demonstrating that its interactions with the antibody can be detected by nanopore analysis. Interestingly, current blockade histograms of full-length PrP showed a broader translocation peak with respect to both peptides, suggesting that the full-length protein has access to a larger variety of translocation and unfolding mechanism than those available to its fragments and that this increased complexity is captured in some (quantitatively yet unexplored) way in the data.

The interaction between α-syn and methamphetamine was characterized via nanopore sensing by Tavassoly et al.,[362] revealing that their binding induces a conformational change which eludes detection by circular dichroism spectroscopy. The authors repeated the experiment on selected α-syn subdomains, including the 1−60 and 61−140 truncated forms and a Δ(61−95) isoform lacking the central hydrophobic NAC domain, demonstrating that drug binding occurs within the N-terminal region.

Nanopore analysis was also employed to characterize the relative in vitro oligomerization propensity of Aβ40 and Aβ42.[342] It should be noted that even if typical reported durations for each experiment are in the range of hours, the experimental conditions used by the authors apparently precluded aggregation of all the examined species during the collection of current blockade data, since none of the collected distributions varied significantly during their respective recordings. While the distribution of interactions between Aβ42 and the α-hemolysin pore captured by the recorded blockade histogram comprised an overwhelming preponderance of bumping events due to the presence of oligomeric aggregates, Aβ40 showed instead a prevalence of translocation events, suggesting a lesser aggregation propensity. Wang et al.[363] used the same experimental approach to assess the influences exerted on the translocation behavior of Aβ42 by two species (Congo red and β-cyclodextrin) which are known to have opposite effects on its aggregation. The current blockade distributions confirmed the macroscopic observation that β-cyclodextrin promotes aggregation and Congo red inhibits it at the single-particle level. Yusko et al. examined the Aβ40 aggregation issue with an experimental approach based on solid-state nanopores coated with lipid bilayers.[54] Through the analysis of the resistive pulse distribution resulting from oligomer−pore interaction events, the authors were able to calculate size and shape distributions of Aβ40 aggregates found in solution, substantiating their findings with a comparison with TEM analysis performed on the same aggregates.

2.3.2.1. Single-Molecule Studies of the Nuclear Pore Complex. In the following paragraphs, we offer a succinct review of the literature that recently appeared on the nuclear pore complex issue, a research field that seems to be drawing the attention of several groups employing a variety of single-molecule techniques for its exploration.

The exchange of molecules between the cytoplasm and the nucleoplasm of eukaryotic cells is mediated by large protein complexes called nuclear pore complexes (NPCs). Although no chemical energy expenditure is required to traverse a NPC, passive diffusion through it is hindered by a permeability barrier provided by a mesh of intrinsically disordered regions extending into the pore lumen.[364] The NPC includes 30

dx.doi.org/10.1021/cr400297g | Chem. Rev. 2014, 114, 3281−3317

nucleoporins (Nups), 13 of which contain numerous phenylalanine-glycine repeat motifs (FGs). The FG-rich disordered network hinders the passage of objects which are not bound to nuclear transport receptors (NTRs). The permeability of the barrier to a molecular cargo is ultimately determined by the interactions between its NTR and the FGs.[365−367] While originally considered structurally and chemically homogeneous, the disordered network barrier was found to contain two distinct types of FG domains: collapsed coils with low charge content and highly charged extended coils.[368] Single-molecule FRET experiments[369] have been used to probe related questions regarding the compaction of the human Nup153 FG-domain. Characterization of Nups is made difficult by the factors discussed in section 1.2 and germane to all IDPs, but their peculiar position and role within the NPC makes their observation even more challenging. Nevertheless, single-molecule studies of NPC-related issues are steadily appearing in the scientific literature during recent years.[370]

Yang et al. reported the use of single-molecule fluorescence microscopy (see section 2.1.1) to track individual model protein NLS-2xGFP molecules in the process of transit through the NPC of permeabilized cells with a temporal resolution of 2−3 ms and a spatial resolution of 15−30 nm.[371,372] Their results evidenced the unbiased bidirectional movement of the substrate molecules within the pore and the fact that the overall transport can be modeled as a single-rate-limited process.

The group of Hinterdorfer extensively studied several issues related to NPC gating and transport via dynamic SMFS (see section 2.2.1).[373−376] In a series of papers that appeared in the early 2000s, Nevo et al.[373−375] studied the interaction of Ran (a GTPase regulating the assembly and disassembly of the receptor−cargo complexes) with the nuclear import receptor importin at the single-molecule level. The molecular-recognition-based dynamic SMFS data allowed the authors to discriminate between two distinct conformational states characterized by different adhesion strength within the Ran-importin complex,[373] to characterize different modes of protein activation mechanism,[374] and to characterize the interaction energy landscape,[375] the roughness of which was found to be consistent with the ability of impbeta1 to adopt different conformations upon interaction with different ligands. Lim et al. employed the same general strategy to characterize the nanomechanical properties of FG-motif binding domains of importin, suggesting that they can reversibly collapse into compact conformations, thus freeing a portion of the permeability barrier.[377] Otsuka et al. similarly studied the effect of Ran on the importin FG-binding sites.[378] In Rangl et al., the authors describe the transient interactions occurring between importin and the two distinct classes of FG domains first described by Yamada et al.:[368] FG domains behaving as collapsed coils with a low content of charged residues prone to "stick" to each other and extended coils containing a high proportion of charged amino acids, resulting in electrostatic repulsion.[376] Most importantly, the energetics of interaction between importin and all the tested FG-repeat-containing proteins were revealed to be largely unaffected by the details of the sequences outside the FG domains, thus supporting the hypothesis that importins diffuse through the NPC by substituting intramolecular FG−repeat interactions occurring in Nups with energetically equivalent importin−FG repeat interactions.[376]

Biomimetic nanopore-sensing strategies were recently applied to the study of the NPC.[367,379] Dekker and co-workers recently demonstrated how a biomimetic artificial nanopore replicating the transport characteristics of the NPC can be obtained by decoration of a solid-state nanopore with a truncated version of the FG Nups Nup98 and Nup153.[379] Individual translocation events are sensed via ionic blockade measurements (see section 2.3.1) with submillisecond temporal resolution. Transport receptors were found to have dramatically lower dwell times with respect to nonspecific proteins.

The growing number of papers appearing in the literature describing single-molecule experiments performed on various NPC-related issues using all the techniques mentioned in this review seems to indicate that this particular field of research might represent in the near future an interesting conceptual meeting point for scientists with different kinds of single-molecule expertise, which may foster the integration of different single-molecule techniques (see section 3).

3. CONCLUSIONS AND PERSPECTIVES

Single-molecule techniques have started to provide important new types of information on the structural and dynamic behavior of IDPs. Two of the key strengths of the approaches described here are their ability to resolve structural and dynamic heterogeneity and to provide quantitative information that can be used for testing physical models. Single-molecule approaches will be essential for quantifying the broad spectrum of behaviors and conformational stabilities and for providing a link to elementary processes in protein folding. An essential contribution to these investigations will continue to come from a close link of experiment to theory and simulation. A wide range of approaches, from analytical theory and coarse-grained models all the way to atomistic simulations, can enable or inspire physical insight that would otherwise be inaccessible.[13,380,381,34,382−386] For atomistic simulations, a key aspect will be the availability of increasingly realistic force fields for unfolded and disordered proteins.[147,312] Information on chain dimensions, dynamics, mechanics, and residual structure from single-molecule results and other experimental techniques provide excellent benchmarks for the required optimization process. In return, simulations will help to guide experiments and ultimately allow us to develop a realistic molecular picture of the structural and functional properties of IDPs. For more complex scenarios, such as molecular crowding, folding upon binding, or large complexes containing unstructured regions, suitable coarse-grained models with realistic generalizable interactions are required.[383,385] Lastly, analytical theory and simple models adapted for the specific questions in the context of IDPs will be essential for the analysis of experimental data and testing the role of different physical concepts.

In spite of the advances over the past decade, single-molecule methods are still developing rapidly; many of the experimental techniques and analysis methods introduced only a few years ago are now an established part of the state-of-the-art toolbox, while new techniques keep emerging. In the following paragraphs, we will try to outline some of the foreseeable future developments for the different single-molecule methods, both individually and in their promising combination.

Foreseeable Future Developments of Single-Molecule Methodologies Applied to the Study of IDPs

The single-molecule fluorescence approaches available, ranging from FRET to PET and FCS, can provide information on intra- and intermolecular distances and, even more importantly, distance distributions, dynamics on time scales from nano-

dx.doi.org/10.1021/cr400297g | Chem. Rev. 2014, 114, 3281−3317

seconds to seconds, and changes in molecular size or dimensions, to name but a few. The available results to date suggest that single-molecule fluorescence techniques are very well suited for addressing key questions in the IDP field. These include the quantitation and structural and dynamic classification of IDPs within the continuous spectrum ranging from order to disorder (Figure 2), e.g., in terms of polymer models, and the relation of these properties to IDP functions. To complete the picture, a close combination and comparison with NMR[387] and small-angle scattering[312,388] results will be particularly valuable.

In the future, we expect a particularly strong impact on IDP dynamics, folding, and binding from several newly emerging methods. Three-color FRET is clearly one of them: monitoring up to three distances at a time allows correlations to be established between conformational changes in different parts of a protein or between folding and binding events in IDPs.[91,135] Related goals might be attainable with a direct combination of FRET and PET.[187] The biochemically very demanding specific labeling of proteins with three chromophores will benefit from new and improved labeling and chromophore incorporation strategies.[130,389] The continued development of methods for the analysis of single-molecule experiments and for the modeling of photon statistics[74,182,390−394] will play an important role for dissecting systems of increasing complexity. Technical developments that may have a major impact (in particular on experiments based on fluorescence trajectory analysis) include zero-mode waveguide arrays for increased throughput,[395] single-photon avalanche diode arrays[396] for the combined advantages of area detectors with time-correlated single-photon counting and full correlation analysis, or methods that allow individual molecules to be monitored for extended times without requiring tethering to a surface.[194,397] A key requirement for improving the time resolution of single-molecule fluorescence will be to increase the photon emission rate by further optimization of photoprotective additives[398] and other methods.[399] Single-molecule fluorescence measurements in vivo have started to be feasible,[400,401] which opens up the exciting possibility to investigate the effect of the cellular environment on the structure and dynamics of IDPs.

At first glance, force spectroscopy and IDPs might seem an unlikely combination. The practicalities of both AFM- and OT-based SMFS experiments imply that the analyte protein is observed under conditions that significantly alter its unperturbed state; the very notion of mechanically manipulating a protein entails its interaction with spurious elements. Due to this, SMFS seems best suited to study biological phenomena actually influenced by mechanical forces in vivo,[268] which are otherwise quite difficult to observe. Moreover, minima in a typical IDP's energy landscape have very similar energies, and the kinetic barriers separating them are as small, even at zero applied force, as to render their detection via SMFS challenging even when employing current state-of-the-art SMFS apparatuses. As exemplified in section 2.2, SMFS experiments often give information on protein disorder by focusing on more easily measurable phenomena which are directly influenced by it, such as the unfolding of transiently acquired stable structure by a mostly disordered protein[301,302,313] or the detection of occasionally visited misfolding pathways by a protein which has a large disordered region.[316,317]

Despite its inherent limitations, SMFS provides relatively straightforward access to the quantitative characterization of transition states and complex kinetic schemes, including notoriously elusive variables such as diffusion rates and transition times.[281,294,317] Moreover, the constant technical refinement of both AFM and OT apparatuses already allows one to observe conformational fluctuations of single-protein molecules.[251,294] Taken together, these two considerations suggest that, in the near future, SMFS studies will increasingly employ the energy landscape formalism as a quantitative tool to describe the behavior of proteins prone to rare misfolding events and/or visiting different conformations in native conditions, thus promising to give access to a fully quantitative characterization of the disorder−order continuum.

The increasing number of papers reporting the successful application of various nanopore-sensing strategies to the study of IDPs and denatured proteins published in the last 2−3 years testifies that nanopore analysis is ideally suited to the study of protein disorder. While nanopore sensing of single proteins is still an emergent field[335] and a fully quantitative understanding of the translocation behavior (as reflected, e.g., in current/time traces) is currently unavailable, tools are being developed which allow quantitative exploration of protein folding[339] and thus promise to find direct applicability in the study of IDPs. Nanopore sensing also seems particularly suited to the label-free detection of transiently formed protein oligomers,[54] an ability which does not give direct access to information on protein disorder but is nonetheless relevant to the study of several IDPs linked to amyloidogenesis.

On the Prospective Integration of Single-Molecule Techniques

An especially promising direction for studying protein disorder in singulo is represented by the design of experimental setups combining two or more single-molecule techniques. As early as 1999, the new opportunities offered by the combination of single-molecule fluorescence with force-based or patch clamp methodologies were fully foreseen by Weiss;[402] today they have become reality. Multitechnique prototype instruments have been developed, even if several technical challenges still need to be overcome for them to become of widespread use. By simultaneously monitoring different observables through a synergistic integration of techniques, these instruments allow some of the intrinsic limitations held by the single methods to be resolved or circumvented. As an example, the simultaneous readout of SMFS and SM-FRET observables can provide information on local conformational heterogeneity while probing the features of a folding/unfolding energy landscape. Several examples of single-molecule combined experiments already reported in the literature at the present date will be mentioned below.

The combination of AFM-based SMFS with optical spectroscopy has been explored since over a decade ago. Hugel et al.[403] reported an investigation of individual polymer molecules via SMFS in combination with optical excitation in total internal reflection (TIRF). Single-polymeric chains of bistable photosensitive azobenzenes were optically lengthened and contracted by switching the azo groups between their trans and cis conformations. The mechanical work delivered by successive contraction cycles was measured via AFM, demonstrating optomechanical energy conversion in a single-molecule device. AFM-SMFS and TIRF fluorescence spectroscopy were combined by Sarkar et al.[404] A constant pulling force of 100 pN was applied to a single polyubiquitin chain, triggering unfolding events recorded by the AFM apparatus as a

dx.doi.org/10.1021/cr400297g | Chem. Rev. 2014, 114, 3281−3317

series of stepwise elongations of the protein's end-to-end distance. Simultaneously recorded fluorescence intensity changes showed a staircase of diminishing amplitude that mirrored the unfolding events observed with the AFM, thus demonstrating the ability of a calibrated evanescent wave to track the variations in length of a single molecule with subnanometer resolution.

The combination of single-molecule fluorescence with optical trapping has an even longer history. The first pioneering experiment combining these two techniques, simultaneously detecting mechanical and ATP-binding events for single-myosin molecules, was reported by Ishijima and colleagues[405] in 1998. Hohng et al.[406] and Tarsa et al.[407] used optical traps to mechanically unzip DNA hairpins while simultaneously monitoring DNA conformational states using SM-FRET. Their approach of mapping two-dimensional reaction landscapes is readily applicable in the biologically important regime of weak forces to other nucleic acid systems and to their interactions with proteins and enzymes.

One of the main technical difficulties that were faced in the integration of single-molecule fluorescence and OT manipulation was their incompatibility in time scales. In a typical OT experiment, a single molecule can be manipulated and studied for minutes and even hours. In contrast, fluorophores can bleach in a few seconds under simultaneous exposure to both trapping and fluorescence excitation beams. The approach of using long DNA molecular handles, formerly introduced to separate protein analytes from the trap,[265,327] essentially also solved the bleaching problem through the spatial separation of trapping and excitation laser beams.[408] Since the mechanical behavior of DNA has been extensively characterized,[269,409−411] its contribution to the overall signal can be easily deconvoluted. However, this solution imposes a reduced force resolution due to the presence of long entropic chains in the form of the DNA handles. Brau et al. recently demonstrated how acousto-optical modulators can be used to rapidly switch between the trapping and the excitation lasers, thus preventing the simultaneous exposure of the fluorophores to both beams and reducing their bleaching.[412] This allows a substantial shortening of the tether−bead DNA linkers and a consequent increase in force resolution.[413] A second limitation of combined OT-SMFS and fluorescence spectroscopy is the spatial drift of the fluid chamber. This type of drift problem, mainly introduced by surface tethers or fixed micropipette tethers, has long been known in the optical tweezers field, and a dumbbell trap arrangement was proposed as a solution.[263,414] A stabilization system with a feedback loop may also be introduced to improve a surface-coupled optical trapping system.[415] The fluorophore bleaching issue can be completely avoided by substituting optical trapping with magnetic tweezers.[416] Electromagnetic tweezers and TIRF illumination were recently used to study folding/unfolding kinetics of protein L.[417]

While ionic current blockade monitoring is currently the most widely implemented method for the detection of single-molecule translocation events in nanopore analysis, several different detection methods of potential relevance to protein translocation studies are being tested.[335,340] Combination of single-molecule fluorescence and ionic current measurements in single-ion channels was developed[418] to monitor structural changes in single channels. Fluorescence spectroscopy can be also integrated with solid-state nanopore sensing giving simultaneous readouts.[419] One advantage of this approach is that fluorescence excitation can be localized to a very small volume surrounding the nanopore through the generation of an evanescent wave in the nanopore[420] or via TIRF spectroscopy.[421] Zwolak and Di Ventra[422] proposed the design of solid-state nanopores with integrated tunnelling electrodes, potentially offering unprecedented spatial resolution during translocation events; this approach was then independently pursued by several groups in the past few years.[340]

To the best of our knowledge, no experiments on IDPs using combined single-molecule technologies have been reported yet. In our opinion, these experiments will be well within technical feasibility in the next few years and are likely to yield novel insights into the dynamic heterogeneity of IDPs and an increasingly quantitative description of the disorder−order continuum.

AUTHOR INFORMATION

Corresponding Authors

*E-mail: marco.brucale@ismn.cnr.it.
*E-mail: schuler@bioc.uzh.ch.
*E-mail: bruno.samori@unibo.it.

Notes

The authors declare no competing financial interest.

Biographies

Marco Brucale received his Master's degree in Industrial Chemistry from Bologna University in 2002 with a thesis on the synthesis of ferrocene-based chiral catalysts under the supervision of Professor B. F. Bonini. He then obtained his Ph.D. degree in Chemical Sciences from the same institution in 2007 with a thesis on the design and synthesis of DNA supramolecular nanostructures under the supervision of Professor B. Samorì. His postdoctoral research work focused on single-molecule force spectroscopy techniques for investigation of protein folding and protein disorder. In 2011 he moved to the Institute for the Study of Nanostructured Materials of the Italian National Research Council (CNR-ISMN) in Rome, where he is currently a research fellow.

Ben Schuler employs and develops single-molecule fluorescence spectroscopy for the investigation of protein structure, folding, and dynamics, with a particular focus on disordered and non-native conformations. He studied Chemistry and Biochemistry at the University of Regensburg, Germany, and at the University of Kent, U.K., and received his Ph.D. degree in Physical Biochemistry from the University of Regensburg in 1998. After his postdoctoral research in Biophysics at the National Institutes of Health in Bethesda, USA, he headed an independent research group at the University of Potsdam in Germany, supported by the Emmy Noether Program of the Deutsche Forschungsgemeinschaft. He joined the faculty of the University of Zurich, Switzerland, in 2004, where he now is a full professor at the Biochemistry department.

During the last 15 years, the main research focus of Bruno Samorì gradually shifted from DNA nanoscience and nanotechnology to the study of AFM-based single-molecule methodologies applied to exploration of the conformational space and the aggregation processes of intrinsically disordered proteins. He studied Chemistry at the University of Bologna, where he was appointed Research Assistant and then Associate Professor over the 1970s and 1980s. He has been working also at the Department of Chemistry of the King's College, London, and the University of California, Berkeley. In 1990 he moved to Cosenza, where he became Full Professor at the University of Calabria, and after 5 years he returned to the University of Bologna, where in 2013 he was appointed the honorary title of Alma Mater Professor.

ACKNOWLEDGMENTS

We thank Alessandro Borgia, Hagen Hofmann, Andrea Soranno, and Massimo Sandal for helpful comments on the manuscript. M. B. and B. Samorì acknowledge the Human Frontier Science Program (ref RGP0010/2011). The work of B. Schuler has been supported by the Swiss National Science Foundation, the National Center of Competence in Research for Structural Biology, a Starting Investigator Grant of the European Research Council, and the Human Frontier Science Program.

REFERENCES

(1) Uversky, V. N. *Int. J. Biochem. Cell Biol.* **2011**, *43*, 1090.
(2) Sickmeier, M.; Hamilton, J. A.; LeGall, T.; Vacic, V.; Cortese, M. S.; Tantos, A.; Szabo, B.; Tompa, P.; Chen, J.; Uversky, V. N.; Obradovic, Z.; Dunker, A. K. *Nucleic Acids Res.* **2007**, *35*, D786.
(3) Tompa, P. *Trends Biochem. Sci.* **2012**, *37*, 509.
(4) Dyson, H. J. *Q. Rev. Biophys.* **2011**, *44*, 467.
(5) Gsponer, J.; Babu, M. M. *Prog. Biophys. Mol. Biol.* **2009**, *99*, 94.
(6) Romero, P.; Obradovic, Z.; Kissinger, C. R.; Villafranca, J. E.; Garner, E.; Guilliot, S.; Dunker, A. K. *Pac. Symp. Biocomput.* **1998**, *3*, 437.
(7) Wright, P. E.; Dyson, H. J. *J. Mol. Biol.* **1999**, *293*, 321.
(8) Uversky, V. N.; Dunker, A. K. *Biochim. Biophys. Acta* **2010**, *1804*, 1231.
(9) Dunker, A. K.; Silman, I.; Uversky, V. N.; Sussman, J. L. *Curr. Opin. Struct. Biol.* **2008**, *18*, 756.
(10) Tompa, P. *Trends Biochem. Sci.* **2002**, *27*, 527.
(11) Huang, A.; Stultz, C. M. *PLoS Comput. Biol.* **2008**, *4*, e1000155.
(12) Choy, W. Y.; Forman-Kay, J. D. *J. Mol. Biol.* **2001**, *308*, 1011.
(13) Babu, M. M.; Kriwacki, R. W.; Pappu, R. V. *Science* **2012**, *337*, 1460.
(14) Mao, A. H.; Lyle, N.; Pappu, R. V. *Biochem. J.* **2013**, *449*, 307.
(15) Müller-Späth, S.; Soranno, A.; Hirschfeld, V.; Hofmann, H.; Rüegger, S.; Reymond, L.; Nettels, D.; Schuler, B. *Proc. Natl. Acad. Sci. U.S.A.* **2010**, *107*, 14609.
(16) Hofmann, H.; Soranno, A.; Borgia, A.; Gast, K.; Nettels, D.; Schuler, B. *Proc. Natl. Acad. Sci. U.S.A.* **2012**, *109*, 16155.
(17) Soranno, A.; Buchli, B.; Nettels, D.; Müller-Späth, S.; Cheng, R. R.; Pfeil, S. H.; Hoffmann, A.; Lipman, E. A.; Makarov, D. E.; Schuler, B. *Proc. Natl. Acad. Sci. U.S.A.* **2012**, *109*, 17800.
(18) Ziv, G.; Thirumalai, D.; Haran, G. *Phys. Chem. Chem. Phys.* **2009**, *11*, 83.
(19) Onuchic, J. N.; Wolynes, P. G. *Curr. Opin. Struct. Biol.* **2004**, *14*, 70.
(20) Sandal, M.; Brucale, M.; Samorì, B. In *Instrumental Analysis of Intrinsically Disordered Proteins*; Wiley-VCH: Berlin, 2010; pp 391–430.
(21) Papoian, G. A. *Proc. Natl. Acad. Sci. U.S.A.* **2008**, *105*, 14237.
(22) Tompa, P.; Szasz, C.; Buday, L. *Trends Biochem. Sci.* **2005**, *30*, 484.
(23) Mittag, T.; Kay, L. E.; Forman-Kay, J. D. *J. Mol. Recognit.* **2010**, *23*, 105.
(24) Zhou, H. X. *Trends Biochem. Sci.* **2012**, *37*, 43.
(25) Huang, Y.; Liu, Z. *Chem.—Eur. J.* **2013**, *19*, 4462.
(26) Bonetta, L. *Nature* **2010**, *468*, 851.
(27) Barabasi, A.-L.; Oltvai, Z. N. *Nat. Rev. Genet.* **2004**, *5*, 101.
(28) Dunker, A. K.; Cortese, M. S.; Romero, P.; Iakoucheva, L. M.; Uversky, V. N. *FEBS J.* **2005**, *272*, 5129.
(29) Hsu, W. L.; Oldfield, C.; Meng, J.; Huang, F.; Xue, B.; Uversky, V. N.; Romero, P.; Dunker, A. K. *Pac. Symp. Biocomput.* **2012**, *17*, 116.
(30) Hoffman, R. M.; Blumenschein, T. M.; Sykes, B. D. *J. Mol. Biol.* **2006**, *361*, 625.
(31) Vamvaca, K.; Jelesarov, I.; Hilvert, D. *J. Mol. Biol.* **2008**, *382*, 971.
(32) Lengyel, C. S.; Willis, L. J.; Mann, P.; Baker, D.; Kortemme, T.; Strong, R. K.; McFarland, B. J. *J. Biol. Chem.* **2007**, *282*, 30658.
(33) Huang, Y.; Liu, Z. *PLoS One* **2010**, *5*, e15375.
(34) Shoemaker, B. A.; Portman, J. J.; Wolynes, P. G. *Proc. Natl. Acad. Sci. U.S.A.* **2000**, *97*, 8868.
(35) Huang, Y.; Liu, Z. *J. Mol. Biol.* **2009**, *393*, 1143.
(36) Dunker, A. K.; Brown, C. J.; Lawson, J. D.; Iakoucheva, L. M.; Obradovic, Z. *Biochemistry* **2002**, *41*, 6573.
(37) Tompa, P. *Comput. Theor. Chem.* **2003**, *666–667*, 361.

(38) Daughdrill, G. W.; Pielak, G. J.; Uversky, V. N.; Cortese, M. S.; Dunker, A. K. In *Protein Folding Handbook*; Wiley-VCH: Berlin, 2008; pp 275−357.
(39) Receveur-Bréchot, V.; Bourhis, J.-M.; Uversky, V. N.; Canard, B.; Longhi, S. *Proteins* **2006**, *62*, 24.
(40) In *Instrumental Analysis of Intrinsically Disordered Proteins: Assessing Structure And Conformation*; Uversky, V. N., Longhi, S., Eds.; Wiley-VCH: Berlin, 2010.
(41) In *Intrinsically Disordered Protein Analysis*; Uversky, V. N., Dunker, A. K., Eds.; Springer: New York, 2012; Vol. 1.
(42) In *Intrinsically Disordered Protein Analysis*; Uversky, V. N., Dunker, A. K., Eds.; Springer: New York, 2012; Vol. 2.
(43) Greenleaf, W. J.; Woodside, M. T.; Block, S. M. *Annu. Rev. Biophys. Biomol. Struct.* **2007**, *36*, 171.
(44) Deniz, A. A.; Mukhopadhyay, S.; Lemke, E. A. *J. R. Soc. Interface* **2008**, *5*, 15.
(45) Ritort, F. *J. Phys.: Condens. Matter* **2006**, *18*, R531.
(46) Borgia, A.; Williams, P. M.; Clarke, J. *Annu. Rev. Biochem.* **2008**, *77*, 101.
(47) Bustamante, C. *Annu. Rev. Biochem.* **2008**, *77*, 45.
(48) Schuler, B.; Hofmann, H. *Curr. Opin. Struct. Biol.* **2013**, *23*, 36.
(49) Ubbink, M. *FEBS Lett* **2009**, *583*, 1060.
(50) Gambin, Y.; VanDelinder, V.; Ferreon, A. C. M.; Lemke, E. A.; Groisman, A.; Deniz, A. A. *Nat. Methods* **2011**, *8*, 239.
(51) Turoverov, K. K.; Kuznetsova, I. M.; Uversky, V. N. *Prog. Biophys. Mol. Biol.* **2010**, *102*, 73.
(52) Ross, C. A.; Poirier, M. A. *Nat. Med.* **2004**, *10* (Suppl), S10.
(53) Ross, C. A.; Poirier, M. A. *Nat. Rev. Mol. Cell. Biol.* **2005**, *6*, 891.
(54) Yusko, E. C.; Prangkio, P.; Sept, D.; Rollings, R. C.; Li, J. L.; Mayer, M. *ACS Nano* **2012**, *6*, 5909.
(55) Cremades, N.; Cohen, S. I. A.; Deas, E.; Abramov, A. Y.; Chen, A. Y.; Orte, A.; Sandal, M.; Clarke, R. W.; Dunne, P.; Aprile, F. A.; Bertoncini, C. W.; Wood, N. W.; Knowles, T. P. J.; Dobson, C. M.; Klenerman, D. *Cell* **2012**, *149*, 1048.
(56) Oroz, J.; Hervas, R.; Valbuena, A.; Carrion-Vazquez, M. *Methods Mol. Biol.* **2012**, *896*, 71.
(57) Sandal, M.; Valle, F.; Tessari, I.; Mammi, S.; Bergantino, E.; Musiani, F.; Brucale, M.; Bubacco, L.; Samorì, B. *PLoS Biol.* **2008**, *6*, 99.
(58) Hillger, F.; Nettels, D.; Dorsch, S.; Schuler, B. *J. Fluoresc.* **2007**, *17*, 759.
(59) Ferreon, A. C.; Moran, C. R.; Gambin, Y.; Deniz, A. A. *Methods Enzymol.* **2010**, *472*, 179.
(60) Schuler, B.; Muller-Spath, S.; Soranno, A.; Nettels, D. *Methods Mol. Biol.* **2012**, *896*, 21.
(61) Moerner, W. E. *J. Phys. Chem. B* **2002**, *106*, 910.
(62) Böhmer, M.; Enderlein, J. *ChemPhysChem* **2003**, *4*, 793.
(63) Hess, S. T.; Huang, S.; Heikal, A. A.; Webb, W. W. *Biochemistry* **2002**, *41*, 697.
(64) Eigen, M.; Rigler, R. *Proc. Natl. Acad. Sci. U.S.A.* **1994**, *91*, 5740.
(65) Rigler, R.; Elson, E. S. *Flourescence Correlation Spectroscopy: Theory and Applications*; Springer: Berlin, 2001.
(66) Edman, L.; Mets, U.; Rigler, R. *Proc. Natl. Acad. Sci. U.S.A.* **1996**, *93*, 6710.
(67) Axelrod, D.; Burghardt, T. P.; Thompson, N. L. *Annu. Rev. Biophys. Bioeng.* **1984**, *13*, 247.
(68) Selvin, P. R.; Ha, T. *Single-Molecule Techniques: A Laboratory Manual*; Cold Spring Harbor Laboratory Press: New York, 2008.
(69) Wahl, M.; Rahn, H. J.; Gregor, I.; Erdmann, R.; Enderlein, J. *Rev. Sci. Instrum.* **2007**, *78*, 033106.
(70) Felekyan, S.; Kuhnemuth, R.; Kudryavtsev, V.; Sandhagen, C.; Becker, W.; Seidel, C. A. M. *Rev. Sci. Instrum.* **2005**, *76*, 083104.
(71) Wahl, M.; Rahn, H.-J.; Röhlicke, T.; Kell, G.; Nettels, D.; Hillger, F.; Schuler, B.; Erdmann, R. *Rev. Sci. Instrum.* **2008**, *79*, 123113.
(72) Clamme, J. P.; Deniz, A. A. *ChemPhysChem* **2005**, *6*, 74.
(73) Hohng, S.; Joo, C.; Ha, T. *Biophys. J.* **2004**, *87*, 1328.
(74) Sisamakis, E.; Valeri, A.; Kalinin, S.; Rothwell, P. J.; Seidel, C. A. M. *Methods Enzymol.* **2010**, *475*, 455.
(75) Deniz, A. A.; Laurence, T. A.; Dahan, M.; Chemla, D. S.; Schultz, P. G.; Weiss, S. *Annu. Rev. Phys. Chem.* **2001**, *52*, 233.
(76) Eggeling, C.; Berger, S.; Brand, L.; Fries, J. R.; Schaffer, J.; Volkmer, A.; Seidel, C. A. *J. Biotechnol.* **2001**, *86*, 163.
(77) Zhang, K.; Yang, H. *J. Phys. Chem. B* **2005**, *109*, 21930.
(78) Nir, E.; Michalet, X.; Hamadani, K. M.; Laurence, T. A.; Neuhauser, D.; Kovchegov, Y.; Weiss, S. *J. Phys. Chem. B* **2006**, *110*, 22103.
(79) Ha, T. *Methods* **2001**, *25*, 78.
(80) Michalet, X.; Kapanidis, A. N.; Laurence, T.; Pinaud, F.; Doose, S.; Pflughoefft, M.; Weiss, S. *Annu. Rev. Biophys. Biomol. Struct.* **2003**, *32*, 161.
(81) Wahl, M.; Koberling, F.; Patting, M.; Rahn, H.; Erdmann, R. *Curr. Pharm. Biotechnol.* **2004**, *5*, 299.
(82) Ha, T.; Enderle, T.; Ogletree, D. F.; Chemla, D. S.; Selvin, P. R.; Weiss, S. *Proc. Natl. Acad. Sci. U.S.A.* **1996**, *93*, 6264.
(83) Van Der Meer, B. W., Coker, G. III, Chen, S. Y. S. *Resonance energy transfer: theory and data*; Wiley-VCH: Berlin, 1994.
(84) Förster, T. *Ann. Phys.* **1948**, *6*, 55.
(85) Widengren, J.; Kudryavtsev, V.; Antonik, M.; Berger, S.; Gerken, M.; Seidel, C. A. M. *Anal. Chem.* **2006**, *78*, 2039.
(86) Schuler, B.; Eaton, W. A. *Curr. Opin. Struct. Biol.* **2008**, *18*, 16.
(87) Hillger, F.; Hänni, D.; Nettels, D.; Geister, S.; Grandin, M.; Textor, M.; Schuler, B. *Angew. Chem., Int. Ed.* **2008**, *47*, 6184.
(88) Kapanidis, A. N.; Laurence, T. A.; Lee, N. K.; Margeat, E.; Kong, X.; Weiss, S. *Acc. Chem. Res.* **2005**, *38*, 523.
(89) Müller, B. K.; Zaychikov, E.; Bräuchle, C.; Lamb, D. C. *Biophys. J.* **2005**, *89*, 3508.
(90) Lee, J.; Lee, S.; Ragunathan, K.; Joo, C.; Ha, T.; Hohng, S. *Angew. Chem., Int. Ed.* **2010**, *49*, 9922.
(91) Milles, S.; Koehler, C.; Gambin, Y.; Deniz, A. A.; Lemke, E. A. *Mol. Biosyst.* **2012**, *8*, 2531.
(92) Nettels, D.; Gopich, I. V.; Hoffmann, A.; Schuler, B. *Proc. Natl. Acad. Sci. U.S.A.* **2007**, *104*, 2655.
(93) Nettels, D.; Hoffmann, A.; Schuler, B. *J. Phys. Chem. B* **2008**, *112*, 6137.
(94) Gopich, I. V.; Nettels, D.; Schuler, B.; Szabo, A. *J. Chem. Phys.* **2009**, *131*, 095102.
(95) Fleury, L.; Segura, J. M.; Zumofen, G.; Hecht, B.; Wild, U. P. *Phys. Rev. Lett.* **2000**, *84*, 1148.
(96) Gopich, I. V.; Szabo, A. *J. Phys. Chem. B* **2003**, *107*, 5058.
(97) Gopich, I. V.; Szabo, A. *J. Chem. Phys.* **2005**, *122*, 1.
(98) Schuler, B.; Lipman, E. A.; Eaton, W. A. *Nature* **2002**, *419*, 743.
(99) Hoffmann, A.; Kane, A.; Nettels, D.; Hertzog, D. E.; Baumgärtel, P.; Lengefeld, J.; Reichardt, G.; Horsley, D. A.; Seckler, R.; Bakajin, O.; Schuler, B. *Proc. Natl. Acad. Sci. U.S.A.* **2007**, *104*, 105.
(100) Sherman, E.; Haran, G. *Proc. Natl. Acad. Sci. U.S.A.* **2006**, *103*, 11539.
(101) Nettels, D.; Müller-Späth, S.; Küster, F.; Hofmann, H.; Haenni, D.; Rüegger, S.; Reymond, L.; Hoffmann, A.; Kubelka, J.; Heinz, B.; Gast, K.; Best, R. B.; Schuler, B. *Proc. Natl. Acad. Sci. U.S.A.* **2009**, *106*, 20740.
(102) Ziv, G.; Haran, G. *J. Am. Chem. Soc.* **2009**, *131*, 2942.
(103) Gopich, I. V.; Szabo, A. *J. Phys. Chem. B* **2007**, *111*, 12925.
(104) Schuler, B.; Lipman, E. A.; Steinbach, P. J.; Kumke, M.; Eaton, W. A. *Proc. Natl. Acad. Sci. U.S.A.* **2005**, *102*, 2754.
(105) Dale, R. E.; Eisinger, J.; Blumberg, W. E. *Biophys. J.* **1979**, *26*, 161.
(106) Merchant, K. A.; Best, R. B.; Louis, J. M.; Gopich, I. V.; Eaton, W. A. *Proc. Natl. Acad. Sci. U.S.A.* **2007**, *104*, 1528.
(107) Laurence, T. A.; Kong, X. X.; Jager, M.; Weiss, S. *Proc. Natl. Acad. Sci. U.S.A.* **2005**, *102*, 17348.
(108) Grinvald, A.; Haas, E.; Steinberg, I. *Proc. Natl. Acad. Sci. U. S. A.* **1972**, *69*, 2273.
(109) Doose, S.; Neuweiler, H.; Sauer, M. *ChemPhysChem* **2009**, *10*, 1389.
(110) Dexter, D. L. *J. Chem. Phys.* **1953**, *21*, 836.
(111) Chattopadhyay, K.; Elson, E. L.; Frieden, C. *Proc. Natl. Acad. Sci. U.S.A.* **2005**, *102*, 2385.

(112) In *Single Molecule Detection in Solution, Methods and Applications*; Zander, C., Enderlein, J., Keller, R. A., Eds.; Wiley-VCH: Berlin, 2002.
(113) Frieden, C.; Chattopadhyay, K.; Elson, E. L. *Adv. Protein Chem.* **2002**, *62*, 91.
(114) Mukhopadhyay, S.; Krishnan, R.; Lemke, E. A.; Lindquist, S.; Deniz, A. A. *Proc. Natl. Acad. Sci. U.S.A.* **2007**, *104*, 2649.
(115) Ehrenberg, M.; Rigler, R. *Chem. Phys.* **1974**, *4*, 390.
(116) Gösch, M.; Blom, H.; Holm, J.; Heino, T.; Rigler, R. *Anal. Chem.* **2000**, *72*, 3260.
(117) Arbour, T. J.; Enderlein, J. *Lab Chip* **2010**, *10*, 1286.
(118) Dittrich, P. S.; Schwille, P. *Anal. Chem.* **2002**, *74*, 4472.
(119) Wunderlich, B.; Nettels, D.; Benke, S.; Clark, J.; Weidner, S.; Hofmann, H.; Pfeil, S. H.; Schuler, B. *Nat. Protoc.* **2013**, *8*, 1459.
(120) Haustein, E.; Schwille, P. *Annu. Rev. Biophys. Biomol. Struct.* **2007**, *36*, 151.
(121) Orte, A.; Clarke, R.; Klenerman, D. *Biochem. Soc. Trans.* **2010**, *38*, 914.
(122) Lipman, E. A.; Schuler, B.; Bakajin, O.; Eaton, W. A. *Science* **2003**, *301*, 1233.
(123) Hamadani, K. M.; Weiss, S. *Biophys. J.* **2008**, *95*, 352.
(124) Pfeil, S. H.; Wickersham, C. E.; Hoffmann, A.; Lipman, E. A. *Rev. Sci. Instrum.* **2009**, *80*, 055105.
(125) Gambin, Y.; Vandelinder, V.; Ferreon, A. C.; Lemke, E. A.; Groisman, A.; Deniz, A. A. *Nat. Meth.* **2011**, *8*, 239.
(126) Orte, A.; Craggs, T. D.; White, S. S.; Jackson, S. E.; Klenerman, D. *J. Am. Chem. Soc.* **2008**, *130*, 7898.
(127) Knight, J. B.; Vishwanath, A.; Brody, J. P.; Austin, R. H. *Phys. Rev. Lett.* **1998**, *80*, 3863.
(128) Orte, A.; Birkett, N. R.; Clarke, R. W.; Devlin, G. L.; Dobson, C. M.; Klenerman, D. *Proc. Natl. Acad. Sci. U.S.A.* **2008**, *105*, 14424.
(129) Shaner, N. C.; Steinbach, P. A.; Tsien, R. Y. *Nat. Methods* **2005**, *2*, 905.
(130) Lemke, E. A. *Methods Mol. Biol.* **2011**, *751*, 3.
(131) Dawson, P. E.; Kent, S. B. *Annu. Rev. Biochem.* **2000**, *69*, 923.
(132) Muir, T. W. *Annu. Rev. Biochem.* **2003**, *72*, 249.
(133) Kapanidis, A. N.; Weiss, S. *J. Chem. Phys.* **2002**, *117*, 10953.
(134) Ratner, V.; Kahana, E.; Eichler, M.; Haas, E. *Bioconjugate Chem.* **2002**, *13*, 1163.
(135) Gambin, Y.; Deniz, A. A. *Mol. Biosyst.* **2010**, *6*, 1540.
(136) Mujumdar, R. B.; Ernst, L. A.; Mujumdar, S. R.; Lewis, C. J.; Waggoner, A. S. *Bioconjugate Chem.* **1993**, *4*, 105.
(137) Panchuk-Voloshina, N.; Haugland, R. P.; Bishop-Stewart, J.; Bhalgat, M. K.; Millard, P. J.; Mao, F.; Leung, W. Y. *J. Histochem. Cytochem.* **1999**, *47*, 1179.
(138) Deniz, A. A.; Laurence, T. A.; Beligere, G. S.; Dahan, M.; Martin, A. B.; Chemla, D. S.; Dawson, P. E.; Schultz, P. G.; Weiss, S. *Proc. Natl. Acad. Sci. U.S.A.* **2000**, *97*, 5179.
(139) Ferreon, A. C. M.; Gambin, Y.; Lemke, E. A.; Deniz, A. A. *Proc. Natl. Acad. Sci. U.S.A.* **2009**, *106*, 5645.
(140) Michalet, X.; Weiss, S.; Jäger, M. *Chem. Rev.* **2006**, *106*, 1785.
(141) Haran, G. *J. Phys.: Condens. Matter* **2003**, *15*, R1291.
(142) Haran, G. *Curr. Opin. Struct. Biol.* **2012**, *22*, 14.
(143) Dill, K. A.; Shortle, D. *Annu. Rev. Biochem.* **1991**, *60*, 795.
(144) O'Brien, E. P.; Ziv, G.; Haran, G.; Brooks, B. R.; Thirumalai, D. *Proc. Natl. Acad. Sci. U.S.A.* **2008**, *105*, 13403.
(145) Kaplon, T. M.; Michnik, A.; Drzazga, Z.; Richter, K.; Kochman, M.; Ozyhar, A. *Biochim. Biophys. Acta* **2009**, *1794*, 1616.
(146) Ferreon, A. C.; Moosa, M. M.; Gambin, Y.; Deniz, A. A. *Proc. Natl. Acad. Sci. U.S.A.* **2012**, *109*, 17826.
(147) Best, R. B.; Mittal, J. *J. Phys. Chem. B* **2010**, *114*, 14916.
(148) Hofmann, H.; Golbik, R. P.; Ott, M.; Hübner, C. G.; Ulbrich-Hofmann, R. *J. Mol. Biol.* **2008**, *376*, 597.
(149) Mao, A. H.; Crick, S. L.; Vitalis, A.; Chicoine, C. L.; Pappu, R. V. *Proc. Natl. Acad. Sci. U.S.A.* **2010**, *107*, 8183.
(150) Dobrynin, A. V.; Colby, R. H.; Rubinstein, M. *J. Pol. Sci., B: Pol. Phys.* **2004**, *42*, 3513.
(151) Elbaum-Garfinkle, S.; Rhoades, E. *J. Am. Chem. Soc.* **2012**, *134*, 16607.
(152) Choi, U. B.; Xiao, S.; Wollmuth, L. P.; Bowen, M. E. *J. Biol. Chem.* **2011**, *286*, 29904.
(153) Sevcsik, E.; Trexler, A. J.; Dunn, J. M.; Rhoades, E. *J. Am. Chem. Soc.* **2011**, *133*, 7152.
(154) Crick, S. L.; Jayaraman, M.; Frieden, C.; Wetzel, R.; Pappu, R. V. *Proc. Natl. Acad. Sci. U.S.A.* **2006**, *103*, 16764.
(155) Dima, R. I.; Thirumalai, D. *J. Phys. Chem. B* **2004**, *108*, 6564.
(156) Uversky, V. N. *Protein Sci.* **2002**, *11*, 739.
(157) Das, R. K.; Pappu, R. V. *Proc. Natl. Acad. Sci. U.S.A.* **2013**, *110*, 13392.
(158) Schneider, R.; Huang, J. R.; Yao, M.; Communie, G.; Ozenne, V.; Mollica, L.; Salmon, L.; Jensen, M. R.; Blackledge, M. *Mol. Biosyst.* **2012**, *8*, 58.
(159) Nath, A.; Sammalkorpi, M.; DeWitt, D. C.; Trexler, A. J.; Elbaum-Garfinkle, S.; O'Hern, C. S.; Rhoades, E. *Biophys. J.* **2012**, *103*, 1940.
(160) Huang, F.; Rajagopalan, S.; Settanni, G.; Marsh, R. J.; Armoogum, D. A.; Nicolaou, N.; Bain, A. J.; Lerner, E.; Haas, E.; Ying, L.; Fersht, A. R. *Proc. Natl. Acad. Sci. U.S.A.* **2009**, *106*, 20758.
(161) Neuweiler, H.; Johnson, C. M.; Fersht, A. R. *Proc. Natl. Acad. Sci. U.S.A.* **2009**, *106*, 18569.
(162) Sherman, E.; Haran, G. *ChemPhysChem* **2011**, *12*, 696.
(163) Chung, H. S.; Cellmer, T.; Louis, J. M.; Eaton, W. A. *Chem. Phys.* **2012**, *422*, 229.
(164) Gopich, I. V.; Szabo, A. *J. Phys. Chem. B* **2010**, *114*, 15221.
(165) Hoffmann, A.; Nettels, D.; Clark, J.; Borgia, A.; Radford, S. E.; Clarke, J.; Schuler, B. *Phys. Chem. Chem. Phys.* **2011**, *13*, 1857.
(166) Chung, H. S.; Gopich, I. V.; McHale, K.; Cellmer, T.; Louis, J. M.; Eaton, W. A. *J. Phys. Chem. A* **2011**, *115*, 3642.
(167) Chung, H. S.; Louis, J. M.; Eaton, W. A. *Proc. Natl. Acad. Sci. U.S.A.* **2009**, *106*, 11837.
(168) Chung, H. S.; McHale, K.; Louis, J. M.; Eaton, W. A. *Science* **2012**, *335*, 981.
(169) Rhoades, E.; Gussakovsky, E.; Haran, G. *Proc. Natl. Acad. Sci. U.S.A.* **2003**, *100*, 3197.
(170) Rhoades, E.; Cohen, M.; Schuler, B.; Haran, G. *J. Am. Chem. Soc.* **2004**, *126*, 14686.
(171) Pirchi, M.; Ziv, G.; Riven, I.; Cohen, S. S.; Zohar, N.; Barak, Y.; Haran, G. *Nat. Commun.* **2011**, *2*, 493.
(172) Kuzmenkina, E. V.; Heyes, C. D.; Nienhaus, G. U. *Proc. Natl. Acad. Sci. U.S.A.* **2005**, *102*, 15471.
(173) Doi, M.; Edwards, S. F. *The Theory of Polymer Dynamics*; Oxford University Press: New York, 1988.
(174) Khatri, B. S.; McLeish, T. C. B. *Macromolecules* **2007**, *40*, 6770.
(175) Cheng, R. R.; Hawk, A. T.; Makarov, D. E. *J. Chem. Phys.* **2013**, 138.
(176) Gast, K.; Damaschun, H.; Eckert, K.; Schulze-Forster, K.; Maurer, H. R.; Muller-Frohne, M.; Zirwer, D.; Czarnecki, J.; Damaschun, G. *Biochemistry* **1995**, *34*, 13211.
(177) Uversky, V. N.; Gillespie, J. R.; Millett, I. S.; Khodyakova, A. V.; Vasiliev, A. M.; Chernovskaya, T. V.; Vasilenko, R. N.; Kozlovskaya, G. D.; Dolgikh, D. A.; Fink, A. L.; Doniach, S.; Abramov, V. M. *Biochemistry* **1999**, *38*, 15009.
(178) Hagen, S. J.; Hofrichter, J.; Szabo, A.; Eaton, W. A. *Proc. Natl. Acad. Sci. U.S.A.* **1996**, *93*, 11615.
(179) Bieri, O.; Wirz, J.; Hellrung, B.; Schutkowski, M.; Drewello, M.; Kiefhaber, T. *Proc. Natl. Acad. Sci. U.S.A.* **1999**, *96*, 9597.
(180) Lapidus, L. J.; Eaton, W. A.; Hofrichter, J. *Proc. Natl. Acad. Sci. U.S.A.* **2000**, *97*, 7220.
(181) Neuweiler, H.; Schulz, A.; Bohmer, M.; Enderlein, J.; Sauer, M. *J. Am. Chem. Soc.* **2003**, *125*, 5324.
(182) Noe, F.; Doose, S.; Daidone, I.; Lollmann, M.; Sauer, M.; Chodera, J. D.; Smith, J. C. *Proc. Natl. Acad. Sci. U.S.A.* **2011**, *108*, 4822.
(183) Neuweiler, H.; Lollmann, M.; Doose, S.; Sauer, M. *J. Mol. Biol.* **2007**, *365*, 856.
(184) Teufel, D. P.; Johnson, C. M.; Lum, J. K.; Neuweiler, H. *J. Mol. Biol.* **2011**, *409*, 250.

(185) Neuweiler, H.; Banachewicz, W.; Fersht, A. R. *Proc. Natl. Acad. Sci. U.S.A.* **2010**, *107*, 22106.
(186) Lum, J. K.; Neuweiler, H.; Fersht, A. R. *J. Am. Chem. Soc.* **2012**, *134*, 1617.
(187) Haenni, D.; Zosel, F.; Reymond, L.; Nettels, D.; Schuler, B. *J. Phys. Chem. B* **2013**, *117*, 13015.
(188) Hofmann, H.; Hillger, F.; Pfeil, S. H.; Hoffmann, A.; Streich, D.; Haenni, D.; Nettels, D.; Lipman, E. A.; Schuler, B. *Proc. Natl. Acad. Sci. U.S.A.* **2010**, *107*, 11793.
(189) Borgia, A.; Wensley, B. G.; Soranno, A.; Nettels, D.; Borgia, M.; Hoffmann, A.; Pfeil, S. H.; Lipman, E. A.; Clarke, J.; Schuler, B. *Nat. Commun.* **2012**, *2*, 1195.
(190) Lamboy, J. A.; Kim, H.; Lee, K. S.; Ha, T.; Komives, E. A. *Proc. Natl. Acad. Sci. U.S.A.* **2011**, *108*, 10178.
(191) Lamboy, J. A.; Kim, H.; Dembinski, H.; Ha, T.; Komives, E. A. *J. Mol. Biol.* **2013**, *425*, 2578.
(192) Choi, U. B.; McCann, J. J.; Weninger, K. R.; Bowen, M. E. *Structure* **2011**, *19*, 566.
(193) Cohen, A. E.; Moerner, W. E. *Proc. Natl. Acad. Sci. U.S.A.* **2006**, *103*, 4362.
(194) Krishnan, M.; Mojarad, N.; Kukura, P.; Sandoghdar, V. *Nature* **2010**, *467*, 692.
(195) Drescher, M.; Huber, M.; Subramaniam, V. *ChemBioChem* **2012**, *13*, 761.
(196) Trexler, A. J.; Rhoades, E. *Mol. Neurobiol.* **2013**, *47*, 622.
(197) Weinreb, P. H.; Zhen, W.; Poon, A. W.; Conway, K. A.; Lansbury, P. T., Jr. *Biochemistry* **1996**, *35*, 13709.
(198) Davidson, W. S.; Jonas, A.; Clayton, D. F.; George, J. M. *J. Biol. Chem.* **1998**, *273*, 9443.
(199) Rhoades, E.; Ramlall, T. F.; Webb, W. W.; Eliezer, D. *Biophys. J.* **2006**, *90*, 4692.
(200) Ulmer, T. S.; Bax, A.; Cole, N. B.; Nussbaum, R. L. *J. Biol. Chem.* **2005**, *280*, 9595.
(201) Veldhuis, G.; Segers-Nolten, I.; Ferlemann, E.; Subramaniam, V. *ChemBioChem* **2009**, *10*, 436.
(202) Trexler, A. J.; Rhoades, E. *Biochemistry* **2009**, *48*, 2304.
(203) Nath, A.; Trexler, A. J.; Koo, P.; Miranker, A. D.; Atkins, W. M.; Rhoades, E. *Methods Enzymol.* **2010**, *472*, 89.
(204) Ducas, V. C.; Rhoades, E. *J. Mol. Biol.* **2012**, *423*, 528.
(205) Middleton, E. R.; Rhoades, E. *Biophys. J.* **2010**, *99*, 2279.
(206) Uversky, V. N.; Oldfield, C. J.; Dunker, A. K. *Annu. Rev. Biophys. Biomol. Struct.* **2008**, *37*, 215.
(207) Trexler, A. J.; Rhoades, E. *Biophys. J.* **2010**, *99*, 3048.
(208) Liang, Y.; Lynn, D. G.; Berland, K. M. *J. Am. Chem. Soc.* **2010**, *132*, 6306.
(209) Takahashi, Y.; Okamoto, Y.; Popiel, H. A.; Fujikake, N.; Toda, T.; Kinjo, M.; Nagai, Y. *J. Biol. Chem.* **2007**, *282*, 24039.
(210) Elbaum-Garfinkle, S.; Ramlall, T.; Rhoades, E. *Biophys. J.* **2010**, *98*, 2722.
(211) Ban, T.; Hoshino, M.; Takahashi, S.; Hamada, D.; Hasegawa, K.; Naiki, H.; Goto, Y. *J. Mol. Biol.* **2004**, *344*, 757.
(212) Dukes, K. D.; Rodenberg, C. F.; Lammi, R. K. *Anal. Biochem.* **2008**, *382*, 29.
(213) Ding, H.; Wong, P. T.; Lee, E. L.; Gafni, A.; Steel, D. G. *Biophys. J.* **2009**, *97*, 912.
(214) Neuman, K. C.; Nagy, A. *Nat. Methods* **2008**, *5*, 491.
(215) Zoldak, G.; Rief, M. *Curr. Opin. Struct. Biol.* **2013**, *23*, 48.
(216) Kasas, S.; Longo, G.; Dietler, G. *J. Phys. D: Appl. Phys.* **2013**, *46*, 133001.
(217) Hoffmann, T.; Dougan, L. *Chem. Soc. Rev.* **2012**, *41*, 4781.
(218) Ritzefeld, M.; Walhorn, V.; Anselmetti, D.; Sewald, N. *Amino Acids* **2013**, *44*, 1457.
(219) Heus, H. A.; Puchner, E. M.; van Vugt-Jonker, A. J.; Zimmermann, J. L.; Gaub, H. E. *Anal. Biochem.* **2011**, *414*, 1.
(220) Kienberger, F.; Ebner, A.; Gruber, H. J.; Hinterdorfer, P. *Acc. Chem. Res.* **2006**, *39*, 29.
(221) Rief, M.; Grubmuller, H. *ChemPhysChem* **2002**, *3*, 255.
(222) Janshoff, A.; Neitzert, M.; Oberdorfer, Y.; Fuchs, H. *Angew. Chem., Int. Ed.* **2000**, *39*, 3212.
(223) Hummer, G.; Szabo, A. *Proc. Natl. Acad. Sci. U.S.A.* **2001**, *98*, 3658.
(224) Evans, E.; Ritchie, K. *Biophys. J.* **1997**, *72*, 1541.
(225) Evans, E. *Annu. Rev. Biophys. Biomol. Struct.* **2001**, *30*, 105.
(226) Dudko, O. K.; Hummer, G.; Szabo, A. *Phys. Rev. Lett.* **2006**, *96*, 108101.
(227) Hanggi, P.; Talkner, P.; Borkovec, M. *Rev. Mod. Phys.* **1990**, *62*, 251.
(228) Merkel, R.; Nassoy, P.; Leung, A.; Ritchie, K.; Evans, E. *Nature* **1999**, *397*, 50.
(229) Hummer, G.; Szabo, A. *Biophys. J.* **2003**, *85*, 5.
(230) Keller, D.; Swigon, D.; Bustamante, C. *Biophys. J.* **2003**, *84*, 733.
(231) Jarzynski, C. *Phys. Rev. E: Stat. Nonlin. Soft Matter Phys* **1997**, *56*, 5018.
(232) Jarzynski, C. *Phys. Rev. Lett.* **1997**, *78*, 2690.
(233) Jarzynski, C. *Acta Phys. Pol., B* **1998**, *29*, 1609.
(234) Jarzynski, C. *Lect. Notes Phys.* **2007**, *711*, 201.
(235) Jarzynski, C. *Eur. Phys. J. B* **2008**, *64*, 331.
(236) Aioanei, D.; Samorì, B.; Brucale, M. *Phys. Rev. E: Stat. Nonlin. Soft Matter Phys.* **2009**, *80*, 061916.
(237) Butt, H. J.; Cappella, B.; Kappl, M. *Surf. Sci. Rep.* **2005**, *59*, 1.
(238) Moffitt, J. R.; Chemla, Y. R.; Smith, S. B.; Bustamante, C. *Annu. Rev. Biochem.* **2008**, *77*, 205.
(239) Bowers, C. M.; Carlson, D. A.; Shestopalov, A. A.; Clark, R. L.; Toone, E. J. *Biopolymers* **2012**, *97*, 761.
(240) Bergkvist, M.; Cady, N. C. *Methods Mol. Biol.* **2011**, *751*, 381.
(241) Kim, M.-S.; Choi, J.-H.; Kim, J.-H.; Park, Y.-K. *Measurement* **2010**, *43*, 520.
(242) Mendels, D. A.; Lowe, M.; Cuenat, A.; Cain, M. G.; Vallejo, E.; Ellis, D.; Mendels, F. *J. Micromech. Microeng.* **2006**, *16*, 1720.
(243) Michel, J. P.; Ivanovska, I. L.; Gibbons, M. M.; Klug, W. S.; Knobler, C. M.; Wuite, G. J. L.; Schmidt, C. F. *Proc. Natl. Acad. Sci. U.S.A.* **2006**, *103*, 6184.
(244) Oberhauser, A. F.; Carrion-Vazquez, M. *J. Biol. Chem.* **2008**, *283*, 6617.
(245) Brown, H. G.; Hoh, J. H. *Biochemistry* **1997**, *36*, 15035.
(246) Brown, H. G.; Troncoso, J. C.; Hoh, J. H. *J. Microsc.* **1998**, *191*, 229.
(247) Mukhopadhyay, R.; Kumar, S.; Hoh, J. H. *Bioessays* **2004**, *26*, 1017.
(248) Stevens, M. J.; Hoh, J. H. *J. Phys. Chem. B* **2011**, *115*, 7541.
(249) Mukhopadhyay, R.; Hoh, J. H. *FEBS Lett* **2001**, *505*, 374.
(250) Li, L.; Huang, H. H.-L.; Badilla, C. L.; Fernandez, J. M. *J. Mol. Biol.* **2005**, *345*, 817.
(251) Schlierf, M.; Berkemeier, F.; Rief, M. *Biophys. J.* **2007**, *93*, 3989.
(252) Carrion-Vazquez, M.; Oberhauser, A. F.; Fowler, S. B.; Marszalek, P. E.; Broedel, S. E.; Clarke, J.; Fernandez, J. M. *Proc. Natl. Acad. Sci. U.S.A.* **1999**, *96*, 3694.
(253) Rounsevell, R. W.; Steward, A.; Clarke, J. *Biophys. J.* **2005**, *88*, 2022.
(254) Carrion-Vazquez, M.; Marszalek, P. E.; Oberhauser, A. F.; Fernandez, J. M. *Proc. Natl. Acad. Sci. U.S.A.* **1999**, *96*, 11288.
(255) Oroz, J.; Hervas, R.; Carrion-Vazquez, M. *Biophys. J.* **2012**, *102*, 682.
(256) Valle, F.; Zuccheri, G.; Bergia, A.; Ayres, L.; Rowan, A. E.; Nolte, R. J. M.; Samorì, B. *Angew. Chem., Int. Ed.* **2008**, *47*, 2431.
(257) Dietz, H.; Bertz, M.; Schlierf, M.; Berkemeier, F.; Bornschlogl, T.; Junker, J. P.; Rief, M. *Nat. Protoc.* **2006**, *1*, 80.
(258) Ashkin, A.; Dziedzic, J. M.; Bjorkholm, J. E.; Chu, S. *Opt. Lett.* **1986**, *11*, 288.
(259) Neuman, K. C.; Block, S. M. *Rev. Sci. Instrum.* **2004**, *75*, 2787.
(260) Neuman, K. C.; Chadd, E. H.; Liou, G. F.; Bergman, K.; Block, S. M. *Biophys. J.* **1999**, *77*, 2856.
(261) Neuman, K. C.; Chadd, E.; Liou, G. F.; Brau, A.; Bergman, K.; Block, S. M. *Biophys. J.* **1999**, *76*, A96.
(262) Landry, M. P.; McCall, P. M.; Qi, Z.; Chemla, Y. R. *Biophys. J.* **2009**, *97*, 2128.

(263) Moffitt, J. R.; Chemla, Y. R.; Izhaky, D.; Bustamante, C. *Proc. Natl. Acad. Sci. U.S.A.* **2006**, *103*, 9006.
(264) Bustamante, C.; Chemla, Y. R.; Moffitt, J. R. *Cold Spring Harbor Protoc.* **2009**, *4*, 1266.
(265) Cecconi, C.; Shank, E. A.; Marqusee, S.; Bustamante, C. *Methods Mol. Biol.* **2011**, *749*, 255.
(266) Gittes, F.; Schmidt, C. F. *Opt. Lett.* **1998**, *23*, 7.
(267) Farre, A.; Marsa, F.; Montes-Usategui, M. *Opt. Express* **2012**, *20*, 12270.
(268) Bustamante, C.; Chemla, Y. R.; Forde, N. R.; Izhaky, D. *Annu. Rev. Biochem.* **2004**, *73*, 705.
(269) Smith, S. B.; Cui, Y.; Bustamante, C. *Science* **1996**, *271*, 795.
(270) Dietz, H.; Berkemeier, F.; Bertz, M.; Rief, M. *Proc. Natl. Acad. Sci. U.S.A.* **2006**, *103*, 12724.
(271) Jagannathan, B.; Elms, P. J.; Bustamante, C.; Marqusee, S. *Proc. Natl. Acad. Sci. U.S.A.* **2012**, *109*, 17820.
(272) Kratky, O.; Porod, G. *Recl. Trav. Chim. Pays-Bas* **1949**, *68*, 1106.
(273) Bustamante, C.; Marko, J. F.; Siggia, E. D.; Smith, S. *Science* **1994**, *265*, 1599.
(274) Aioanei, D.; Tessari, I.; Bubacco, L.; Samorì, B.; Brucale, M. *Proteins* **2011**, *79*, 2214.
(275) Aioanei, D.; Lv, S.; Tessari, I.; Rampioni, A.; Bubacco, L.; Li, H.; Samorì, B.; Brucale, M. *Angew. Chem., Int. Ed.* **2011**, *50*, 4394.
(276) Dudko, O. K.; Graham, T. G. W.; Best, R. B. *Phys. Rev. Lett.* **2011**, *107*, 208301.
(277) Woodside, M. T.; Anthony, P. C.; Behnke-Parks, W. M.; Larizadeh, K.; Herschlag, D.; Block, S. M. *Science* **2006**, *314*, 1001.
(278) Hyeon, C.; Morrison, G.; Thirumalai, D. *Proc. Natl. Acad. Sci. U.S.A.* **2008**, *105*, 9604.
(279) Gebhardt, J. C.; Bornschlogl, T.; Rief, M. *Proc. Natl. Acad. Sci. U.S.A.* **2010**, *107*, 2013.
(280) Fernandez, J.; Garcia-Manyes, S.; Dougan, L. In *Single Molecule Spectroscopy in Chemistry, Physics and Biology*; Gräslund, A., Rigler, R., Widengren, J., Eds.; Springer: Berlin, 2010; pp 317−335.
(281) Stigler, J.; Rief, M. *ChemPhysChem* **2012**, *13*, 1079.
(282) Hoffmann, A.; Woodside, M. T. *Angew. Chem., Int. Ed.* **2011**, *50*, 12643.
(283) Lang, M. J.; Asbury, C. L.; Shaevitz, J. W.; Block, S. M. *Biophys. J.* **2002**, *83*, 491.
(284) Visscher, K.; Block, S. M. *Methods Enzymol.* **1998**, *298*, 460.
(285) Cecconi, C.; Shank, E. A.; Bustamante, C.; Marqusee, S. *Science* **2005**, *309*, 2057.
(286) Capitanio, M.; Canepari, M.; Maffei, M.; Beneventi, D.; Monico, C.; Vanzi, F.; Bottinelli, R.; Pavone, F. S. *Nat. Methods* **2012**, *9*, 1013.
(287) Greenleaf, W. J.; Woodside, M. T.; Abbondanzieri, E. A.; Block, S. M. *Phys. Rev. Lett.* **2005**, 95.
(288) Getfert, S.; Evstigneev, M.; Reimann, P. *Physica A: Stat. Mech. Appl* **2009**, *388*, 1120.
(289) Friedsam, C.; Wehle, A. K.; Kuhner, F.; Gaub, H. E. *J. Phys., Condens. Matter* **2003**, *15*, S1709.
(290) Getfert, S.; Reimann, P. *Phys. Rev. E: Stat. Nonlin. Soft Matter Phys.* **2007**, *76*, 052901.
(291) Getfert, S.; Reimann, P. *Biophys. J.* **2012**, *102*, 1184.
(292) King, G. M.; Carter, A. R.; Churnside, A. B.; Eberle, L. S.; Perkins, T. T. *Nano Lett.* **2009**, *9*, 1451.
(293) Cao, Y.; Li, H. *Nat. Mater.* **2007**, *6*, 109.
(294) Gupta, A. N.; Vincent, A.; Neupane, K.; Yu, H.; Wang, F.; Woodside, M. T. *Nat Phys* **2011**, *7*, 631.
(295) Yu, J.; Malkova, S.; Lyubchenko, Y. L. *J. Mol. Biol.* **2008**, *384*, 992.
(296) Ray, C.; Akhremitchev, B. B. *J. Am. Chem. Soc.* **2005**, *127*, 14739.
(297) Lv, Z.; Condron, M. M.; Teplow, D. B.; Lyubchenko, Y. L. *J. Neuroimmune Pharmacol.* **2013**, *8*, 262.
(298) Yu, J.; Warnke, J.; Lyubchenko, Y. L. *Nanomedicine* **2011**, *7*, 146.
(299) Li, H.; Linke, W. A.; Oberhauser, A. F.; Carrion-Vazquez, M.; Kerkvliet, J. G.; Lu, H.; Marszalek, P. E.; Fernandez, J. M. *Nature* **2002**, *418*, 998.
(300) Brucale, M.; Tessari, I.; Bubacco, L.; Samorì, B. In *Intrinsically Disordered Protein Analysis*; Uversky, V. N., Dunker, A. K., Eds.; Springer: New York, 2012; Vol. *896*; pp 47−56.
(301) Brucale, M.; Sandal, M.; Di Maio, S.; Rampioni, A.; Tessari, I.; Tosatto, L.; Bisaglia, M.; Bubacco, L.; Samorì, B. *ChemBioChem* **2009**, *10*, 176.
(302) Hervas, R.; Oroz, J.; Galera-Prat, A.; Goni, O.; Valbuena, A.; Vera, A. M.; Gomez-Sicilia, A.; Losada-Urzaiz, F.; Uversky, V. N.; Menendez, M.; Laurents, D. V.; Bruix, M.; Carrion-Vazquez, M. *PLoS Biol.* **2012**, *10*, e1001335.
(303) Jonsson, S. A.; Mohanty, S.; Irback, A. *Proteins* **2012**, *80*, 2169.
(304) Hinault, M. P.; Ben-Zvi, A.; Goloubinoff, P. *J. Mol. Neurosci.* **2006**, *30*, 249.
(305) Arslan, P. E.; Mulligan, V. K.; Ho, S.; Chakrabartty, A. *J. Mol. Biol.* **2010**, *396*, 1284.
(306) Tomita, K.; Popiel, H. A.; Nagai, Y.; Toda, T.; Yoshimitsu, Y.; Ohno, H.; Oishi, S.; Fujii, N. *Bioorg. Med. Chem.* **2009**, *17*, 1259.
(307) Dougan, L.; Li, J. Y.; Badilla, C. L.; Berne, B. J.; Fernandez, J. M. *Proc. Natl. Acad. Sci. U.S.A.* **2009**, *106*, 12605.
(308) Wang, X.; Vitalis, A.; Wyczalkowski, M. A.; Pappu, R. V. *Proteins* **2006**, *63*, 297.
(309) Vitalis, A.; Wang, X.; Pappu, R. V. *Biophys. J.* **2007**, *93*, 1923.
(310) Vitalis, A.; Wang, X.; Pappu, R. V. *J. Mol. Biol.* **2008**, *384*, 279.
(311) Vitalis, A.; Lyle, N.; Pappu, R. V. *Biophys. J.* **2009**, *97*, 303.
(312) Vitalis, A.; Pappu, R. V. *J. Comput. Chem.* **2009**, *30*, 673.
(313) Wegmann, S.; Scholer, J.; Bippes, C. A.; Mandelkow, E.; Muller, D. J. *J. Biol. Chem.* **2011**, *286*, 20512.
(314) Kuzmenkina, E. V.; Heyes, C. D.; Nienhaus, G. U. *J. Mol. Biol.* **2006**, *357*, 313.
(315) Junier, I.; Ritort, F. *Proteins* **2008**, *71*, 1145.
(316) Yu, H.; Liu, X.; Neupane, K.; Gupta, A. N.; Brigley, A. M.; Solanki, A.; Sosova, I.; Woodside, M. T. *Proc. Natl. Acad. Sci. U.S.A.* **2012**, *109*, 5283.
(317) Yu, H.; Gupta, A. N.; Liu, X.; Neupane, K.; Brigley, A. M.; Sosova, I.; Woodside, M. T. *Proc. Natl. Acad. Sci. U.S.A.* **2012**, *109*, 14452.
(318) Liphardt, J.; Dumont, S.; Smith, S. B.; Tinoco, I., Jr.; Bustamante, C. *Science* **2002**, *296*, 1832.
(319) Harris, N. C.; Song, Y.; Kiang, C. H. *Phys. Rev. Lett.* **2007**, *99*, 068101.
(320) Moffitt, J. R.; Chemla, Y. R.; Bustamante, C. *Methods Enzymol.* **2010**, *475*, 221.
(321) Knight, A. E.; Veigel, C.; Chambers, C.; Molloy, J. E. *Prog. Biophys. Mol. Biol.* **2001**, *77*, 45.
(322) Watkins, L. P.; Yang, H. *J. Phys. Chem. B* **2005**, *109*, 617.
(323) Gopich, I. V.; Szabo, A. *J. Phys. Chem. B* **2009**, *113*, 10965.
(324) Blanco, M.; Walter, N. G. *Methods Enzymol.* **2010**, *472*, 153.
(325) Witkoskie, J. B.; Cao, J. *J. Chem. Phys.* **2004**, *121*, 6373.
(326) Witkoskie, J. B.; Cao, J. *J. Chem. Phys.* **2004**, *121*, 6361.
(327) Cecconi, C.; Shank, E. A.; Dahlquist, F. W.; Marqusee, S.; Bustamante, C. *Eur. Biophys. J.* **2008**, *37*, 729.
(328) Stranneheim, H.; Lundeberg, J. *Biotechnol. J.* **2012**, *7*, 1063.
(329) Maitra, R. D.; Kim, J.; Dunbar, W. B. *Electrophoresis* **2012**, *33*, 3418.
(330) Wanunu, M. *Phys. Life Rev.* **2012**, *9*, 125.
(331) Neher, E.; Sakmann, B. *Nature* **1976**, *260*, 799.
(332) Hamill, O. P.; Marty, A.; Neher, E.; Sakmann, B.; Sigworth, F. J. *Pflugers Arch.* **1981**, *391*, 85.
(333) Branton, D.; Deamer, D. W.; Marziali, A.; Bayley, H.; Benner, S. A.; Butler, T.; Di Ventra, M.; Garaj, S.; Hibbs, A.; Huang, X.; Jovanovich, S. B.; Krstic, P. S.; Lindsay, S.; Ling, X. S.; Mastrangelo, C. H.; Meller, A.; Oliver, J. S.; Pershin, Y. V.; Ramsey, J. M.; Riehn, R.; Soni, G. V.; Tabard-Cossa, V.; Wanunu, M.; Wiggin, M.; Schloss, J. A. *Nat. Biotechnol.* **2008**, *26*, 1146.
(334) Kasianowicz, J. J.; Brandin, E.; Branton, D.; Deamer, D. W. *Proc. Natl. Acad. Sci. U.S.A.* **1996**, *93*, 13770.

(335) Oukhaled, A.; Bacri, L.; Pastoriza-Gallego, M.; Betton, J. M.; Pelta, J. *ACS Chem. Biol.* **2012**, *7*, 1935.
(336) Hornblower, B.; Coombs, A.; Whitaker, R. D.; Kolomeisky, A.; Picone, S. J.; Meller, A.; Akeson, M. *Nat. Methods* **2007**, *4*, 315.
(337) Sexton, L. T.; Horne, L. P.; Sherrill, S. A.; Bishop, G. W.; Baker, L. A.; Martin, C. R. *J. Am. Chem. Soc.* **2007**, *129*, 13144.
(338) Sutherland, T. C.; Long, Y.-T.; Stefureac, R.-I.; Bediako-Amoa, I.; Kraatz, H.-B.; Lee, J. S. *Nano Lett.* **2004**, *4*, 1273.
(339) Payet, L.; Martinho, M.; Pastoriza-Gallego, M.; Betton, J.-M.; Auvray, L.; Pelta, J.; Mathé, J. *Anal. Chem.* **2012**, *84*, 4071.
(340) Miles, B. N.; Ivanov, A. P.; Wilson, K. A.; Dogan, F.; Japrung, D.; Edel, J. B. *Chem. Soc. Rev.* **2013**, *42*, 15.
(341) Bahrami, A.; Dogan, F.; Japrung, D.; Albrecht, T. *Biochem. Soc. Trans.* **2012**, *40*, 624.
(342) Madampage, C.; Tavassoly, O.; Christensen, C.; Kumari, M.; Lee, J. S. *Prion* **2012**, *6*, 116.
(343) Li, J.; Stein, D.; McMullan, C.; Branton, D.; Aziz, M. J.; Golovchenko, J. A. *Nature* **2001**, *412*, 166.
(344) Storm, A. J.; Chen, J. H.; Ling, X. S.; Zandbergen, H. W.; Dekker, C. *Nat. Mater.* **2003**, *2*, 537.
(345) Firnkes, M.; Pedone, D.; Knezevic, J.; Döblinger, M.; Rant, U. *Nano Lett.* **2010**, *10*, 2162.
(346) Howorka, S.; Siwy, Z. *Chem. Soc. Rev.* **2009**, *38*, 2360.
(347) Bayley, H.; Martin, C. R. *Chem. Rev.* **2000**, *100*, 2575.
(348) Oukhaled, G.; Mathé, J.; Biance, A. L.; Bacri, L.; Betton, J. M.; Lairez, D.; Pelta, J.; Auvray, L. *Phys. Rev. Lett.* **2007**, *98*, 158101.
(349) Rosenstein, J. K.; Wanunu, M.; Merchant, C. A.; Drndic, M.; Shepard, K. L. *Nat. Methods* **2012**, *9*, 487.
(350) Meller, A. *J. Phys., Condens. Matter* **2003**, *15*, R581.
(351) Talaga, D. S.; Li, J. L. *J. Am. Chem. Soc.* **2009**, *131*, 9287.
(352) Oukhaled, A.; Cressiot, B.; Bacri, L.; Pastoriza-Gallego, M.; Betton, J. M.; Bourhis, E.; Jede, R.; Gierak, J.; Auvray, L.; Pelta, J. *ACS Nano* **2011**, *5*, 3628.
(353) Freedman, K. J.; Jurgens, M.; Prabhu, A.; Ahn, C. W.; Jemth, P.; Edel, J. B.; Kim, M. J. *Anal. Chem.* **2011**, *83*, 5137.
(354) Pastoriza-Gallego, M.; Rabah, L.; Gibrat, G.; Thiebot, B.; Goot, F. G.; Auvray, L.; Betton, J. M.; Pelta, J. *J. Am. Chem. Soc.* **2011**, *133*, 2923.
(355) Merstorf, C.; Cressiot, B.; Pastoriza-Gallego, M.; Oukhaled, A.; Betton, J. M.; Auvray, L.; Pelta, J. *ACS Chem. Biol.* **2012**, *7*, 652.
(356) Raffy, S.; Sassoon, N.; Hofnung, M.; Betton, J. M. *Protein Sci.* **1998**, *7*, 2136.
(357) Baran, C.; Smith, G. S. T.; Bamm, V. V.; Harauz, G.; Lee, J. S. *Biochem. Biophys. Res. Commun.* **2010**, *391*, 224.
(358) Japrung, D.; Dogan, J.; Freedman, K. J.; Nadzeyka, A.; Bauerdick, S.; Albrecht, T.; Kim, M. J.; Jemth, P.; Edel, J. B. *Anal. Chem.* **2013**, *85*, 2449.
(359) Stefureac, R. I.; Lee, J. S. *Small* **2008**, *4*, 1646.
(360) Stefureac, R. I.; Madampage, C. A.; Andrievskaia, O.; Lee, J. S. *Biochem. Cell Biol.* **2010**, *88*, 347.
(361) Madampage, C. A.; Andrievskaia, O.; Lee, J. S. *Anal. Biochem.* **2010**, *396*, 36.
(362) Tavassoly, O.; Lee, J. S. *FEBS Lett.* **2012**, *586*, 3222.
(363) Wang, H.-Y.; Ying, Y.-L.; Li, Y.; Kraatz, H.-B.; Long, Y.-T. *Anal. Chem.* **2011**, *83*, 1746.
(364) Tran, E. J.; Wente, S. R. *Cell* **2006**, *125*, 1041.
(365) Denning, D. P.; Patel, S. S.; Uversky, V.; Fink, A. L.; Rexach, M. *Proc. Natl. Acad. Sci. U.S.A.* **2003**, *100*, 2450.
(366) Patel, S. S.; Belmont, B. J.; Sante, J. M.; Rexach, M. F. *Cell* **2007**, *129*, 83.
(367) Jovanovic-Talisman, T.; Tetenbaum-Novatt, J.; McKenney, A. S.; Zilman, A.; Peters, R.; Rout, M. P.; Chait, B. T. *Nature* **2009**, *457*, 1023.
(368) Yamada, J.; Phillips, J. L.; Patel, S.; Goldfien, G.; Calestagne-Morelli, A.; Huang, H.; Reza, R.; Acheson, J.; Krishnan, V. V.; Newsam, S.; Gopinathan, A.; Lau, E. Y.; Colvin, M. E.; Uversky, V. N.; Rexach, M. F. *Mol. Cell. Proteomics* **2010**, *9*, 2205.
(369) Milles, S.; Lemke, E. A. *Biophys. J.* **2011**, *101*, 1710.
(370) Tu, L. C.; Musser, S. M. *Biochim. Biophys. Acta* **2011**, *1813*, 1607.
(371) Yang, W.; Gelles, J.; Musser, S. M. *Proc. Natl. Acad. Sci. U.S.A.* **2004**, *101*, 12887.
(372) Yang, W.; Musser, S. M. *Methods* **2006**, *39*, 316.
(373) Nevo, R.; Stroh, C.; Kienberger, F.; Kaftan, D.; Brumfeld, V.; Elbaum, M.; Reich, Z.; Hinterdorfer, P. *Nat. Struct. Biol.* **2003**, *10*, 553.
(374) Nevo, R.; Brumfeld, V.; Elbaum, M.; Hinterdorfer, P.; Reich, Z. *Biophys. J.* **2004**, *87*, 2630.
(375) Nevo, R.; Brumfeld, V.; Kapon, R.; Hinterdorfer, P.; Reich, Z. *EMBO Rep.* **2005**, *6*, 482.
(376) Rangl, M.; Ebner, A.; Yamada, J.; Rankl, C.; Tampe, R.; Gruber, H. J.; Rexach, M.; Hinterdorfer, P. *Angew. Chem., Int. Ed.* **2013**, *52*, 10356.
(377) Lim, R. Y.; Fahrenkrog, B.; Koser, J.; Schwarz-Herion, K.; Deng, J.; Aebi, U. *Science* **2007**, *318*, 640.
(378) Otsuka, S.; Iwasaka, S.; Yoneda, Y.; Takeyasu, K.; Yoshimura, S. H. *Proc. Natl. Acad. Sci. U.S.A.* **2008**, *105*, 16101.
(379) Kowalczyk, S. W.; Kapinos, L.; Blosser, T. R.; Magalhaes, T.; van Nies, P.; Lim, R. Y.; Dekker, C. *Nat. Nanotechnol.* **2011**, *6*, 433.
(380) Turjanski, A. G.; Gutkind, J. S.; Best, R. B.; Hummer, G. *PLoS Comput. Biol.* **2008**, *4*, e1000060.
(381) Click, T. H.; Ganguly, D.; Chen, J. *Int. J. Mol. Sci.* **2010**, *11*, 5292.
(382) O'Brien, E. P.; Morrison, G.; Brooks, B. R.; Thirumalai, D. *J. Chem. Phys.* **2009**, *130*, 124903.
(383) Levy, Y.; Onuchic, J. N. *Acc. Chem. Res.* **2006**, *39*, 135.
(384) Knott, M.; Best, R. B. *PLoS Comput. Biol.* **2012**, *8*, e1002605.
(385) Kim, Y. C.; Hummer, G. *J. Mol. Biol.* **2008**, *375*, 1416.
(386) Vuzman, D.; Levy, Y. *Mol. BioSyst.* **2012**, *8*, 47.
(387) Jensen, M. R.; Ruigrok, R. W. H.; Blackledge, M. *Curr. Opin. Struct. Biol.* **2013**, *23*, 426.
(388) Bernado, P.; Svergun, D. I. *Mol. BioSyst.* **2012**, *8*, 151.
(389) Chakraborty, A.; Wang, D.; Ebright, Y. W.; Ebright, R. H. *Methods Enzymol.* **2010**, *472*, 19.
(390) Gopich, I. V.; Szabo, A. *Proc. Natl. Acad. Sci. U.S.A.* **2012**, *109*, 7747.
(391) Gopich, I. V.; Szabo, A. In *Single-Molecule Biophysics: Experiment and Theory*; Komatsuzaki, T., Kawakami, M., Takahashi, S., Yang, H., Silbey, R. J., Eds.; John Wiley & Sons, Inc.: New York, 2011; Vol. *146*; pp 245−297.
(392) Gopich, I. V. *Chem. Phys.* **2012**, *396*, 53.
(393) Kalinin, S.; Valeri, A.; Antonik, M.; Felekyan, S.; Seidel, C. A. M. *J. Phys. Chem. B* **2010**, *114*, 7983.
(394) Schuetz, P.; Wuttke, R.; Schuler, B.; Caflisch, A. *J. Phys. Chem. B* **2010**, *114*, 15227.
(395) Eid, J.; Fehr, A.; Gray, J.; Luong, K.; Lyle, J.; Otto, G.; Peluso, P.; Rank, D.; Baybayan, P.; Bettman, B.; Bibillo, A.; Bjornson, K.; Chaudhuri, B.; Christiansqq, F.; Cicero, R.; Clark, S.; Dalal, R.; Dewinter, A.; Dixon, J.; Foquet, M.; Gaertner, A.; Hardenbol, P.; Heiner, C.; Hester, K.; Holden, D.; Kearns, G.; Kong, X.; Kuse, R.; Lacroix, Y.; Lin, S.; Lundquist, P.; Ma, C.; Marks, P.; Maxham, M.; Murphy, D.; Park, I.; Pham, T.; Phillips, M.; Roy, J.; Sebra, R.; Shen, G.; Sorenson, J.; Tomaney, A.; Travers, K.; Trulson, M.; Vieceli, J.; Wegener, J.; Wu, D.; Yang, A.; Zaccarin, D.; Zhao, P.; Zhong, F.; Korlach, J.; Turner, S. *Science* **2009**, *323*, 133.
(396) Zappa, F.; Tisa, S.; Tosi, A.; Cova, S. *Sens. Actuators, A: Phys.* **2007**, *140*, 103.
(397) Kamagata, K.; Kawaguchi, T.; Iwahashi, Y.; Baba, A.; Fujimoto, K.; Komatsuzaki, T.; Sambongi, Y.; Goto, Y.; Takahashi, S. *J. Am. Chem. Soc.* **2012**, *134*, 11525.
(398) Ha, T.; Tinnefeld, P. *Annu. Rev. Phys. Chem.* **2012**, *63*, 595.
(399) Acuna, G. P.; Moller, F. M.; Holzmeister, P.; Beater, S.; Lalkens, B.; Tinnefeld, P. *Science* **2012**, *338*, 506.
(400) Sakon, J. J.; Weninger, K. R. *Nat. Methods* **2010**, *7*, 203.
(401) Uphoff, S.; Reyes-Lamothe, R.; de Leon, F. G.; Sherratt, D. J.; Kapanidis, A. N. *Proc. Natl. Acad. Sci. U.S.A.* **2013**, *110*, 8063.
(402) Weiss, S. *Science* **1999**, *283*, 1676.

(403) Hugel, T.; Holland, N. B.; Cattani, A.; Moroder, L.; Seitz, M.; Gaub, H. E. *Science* **2002**, *296*, 1103.
(404) Sarkar, A.; Robertson, R. B.; Fernandez, J. M. *Proc. Natl. Acad. Sci. U.S.A.* **2004**, *101*, 12882.
(405) Ishijima, A.; Kojima, H.; Funatsu, T.; Tokunaga, M.; Higuchi, H.; Tanaka, H.; Yanagida, T. *Cell* **1998**, *92*, 161.
(406) Hohng, S.; Zhou, R.; Nahas, M. K.; Yu, J.; Schulten, K.; Lilley, D. M.; Ha, T. *Science* **2007**, *318*, 279.
(407) Tarsa, P. B.; Brau, R. R.; Barch, M.; Ferrer, J. M.; Freyzon, Y.; Matsudaira, P.; Lang, M. J. *Angew. Chem., Int. Ed.* **2007**, *46*, 1999.
(408) Zhou, R.; Schlierf, M.; Ha, T. In *Methods Enzymol.*; Nils, G. W., Ed.; Academic Press, 2010; pp 405−426.
(409) Smith, S.; Finzi, L.; Bustamante, C. *Science* **1992**, *258*, 1122.
(410) Bustamante, C.; Smith, S. B.; Liphardt, J.; Smith, D. *Curr. Opin. Struct. Biol.* **2000**, *10*, 279.
(411) Seol, Y.; Li, J.; Nelson, P. C.; Perkins, T. T.; Betterton, M. D. *Biophys. J.* **2007**, *93*, 4360.
(412) Brau, R. R.; Tarsa, P. B.; Ferrer, J. M.; Lee, P.; Lang, M. J. *Biophys. J.* **2006**, *91*, 1069.
(413) Comstock, M. J.; Ha, T.; Chemla, Y. R. *Nat. Methods* **2011**, *8*, 335.
(414) Abbondanzieri, E. A.; Greenleaf, W. J.; Shaevitz, J. W.; Landick, R.; Block, S. M. *Nature* **2005**, *438*, 460.
(415) Carter, A. R.; Seol, Y.; Perkins, T. T. *Biophys. J.* **2009**, *96*, 2926.
(416) Long, X.; Parks, J. W.; Bagshaw, C. R.; Stone, M. D. *Nucleic Acids Res.* **2013**, *41*, 2746.
(417) Liu, R.; Garcia-Manyes, S.; Sarkar, A.; Badilla, C. L.; Fernandez, J. M. *Biophys. J.* **2009**, *96*, 3810.
(418) Borisenko, V.; Lougheed, T.; Hesse, J.; Fureder-Kitzmuller, E.; Fertig, N.; Behrends, J. C.; Woolley, G. A.; Schutz, G. J. *Biophys. J.* **2003**, *84*, 612.
(419) Aouani, H.; Mahboub, O.; Bonod, N.; Devaux, E. s.; Popov, E.; Rigneault, H.; Ebbesen, T. W.; Wenger, J. r. m. *Nano Lett.* **2011**, *11*, 637.
(420) Chansin, G. A. T.; Mulero, R.; Hong, J.; Kim, M. J.; deMello, A. J.; Edel, J. B. *Nano Lett.* **2007**, *7*, 2901.
(421) McNally, B.; Singer, A.; Yu, Z.; Sun, Y.; Weng, Z.; Meller, A. *Nano Lett.* **2010**, *10*, 2237.
(422) Zwolak, M.; Di Ventra, M. *Nano Lett.* **2005**, *5*, 421.